UNIVERSITÀ DEGLI STUDI DI PARMA

Dottorato di ricerca in "Matematica"

Ciclo XXXV

Algorithms on braids and links in 3-manifolds

Coordinatore: Prof.ssa Alessandra Lunardi
Relatore: Prof.ssa Alessia Cattabriga
Tutor: Prof.ssa Paola Cristofori

Candidato: Cavicchioli Paolo

Anni Accademici 2019/2020 – 2021/2022

Acknowledgements

I would like to deeply thank the following people:

- Prof. Paola Cristofori and Prof. Alessia Cattabriga for the passion for low dimensional geometry and knot theory that they conveyed me, and for the huge support that they gave me during these three years of Ph.D.;
- Prof. Sofia Lambropoulou for her enlightening remarks and ideas, and for her huge support during my stay in Athens;
- My parents and my brother that supported me in my very long trip to reach for the Ph.D.;
- My fiancée, this achievement is just the first of many victories that we will accomplish together in our lifetime.

Introduction

Knot theory has always been an object of research interest among mathematicians, the subject having many connections to other mathematical theories, such as the theory of 3- and 4-manifolds [31], quantum group theory [40] and graph theory [16]. It has also interesting connections with chemistry, physics and biology [50]. The aim of the thesis is to study relations between knots, links and 3-manifolds, analyzing also the algorithmic part of certain solutions that we produce.

A classical result by Brunn and Alexander states that any oriented link in $\mathbb{R}^3$ is isotopic to the standard closure of a braid; moreover a theorem by Markov establishes a bijection between isotopy classes of oriented links and equivalence classes of braids under a fixed set of moves, called *Markov moves*. By considering *mixed link diagrams* [43], the extension of the same result is achieved for links in 3-manifolds described by Dehn surgery [42].

Another representation of links that uses braids is the plat closure of braids with an even number of strands, that goes back to the work of Birman [13], who proved in 1976 that any link in $\mathbb{R}^3$ could be represented as the plat closure of a braid and described a set of moves that connects braids having isotopic plat closures. It is also important to mention that all rational knots can be represented, via plat closure, by braids with four strands, leaving the last strand as the identity one [8]. In [13], Birman also proved an equivalence theorem for braids with isotopic plat closures. Since her initial article, a lot of work has been done using the plat representation for links. For instance, in [11] Bigelow studied the possibility of computing the Jones polynomial of a link in terms of the action of a braid, having the link as plat closure, over a homological pairing defined on a covering of the configuration space of n points into the $2n$-punctured disc. This result was analyzed in recent years also from a computational point of view [39, 30] and in order to compute further link invariants, such as the Conway potential function [62] and other polynomial invariants [29]. By using Heegaard surfaces, in [23] Doll introduced the notion of (g,b)-decomposition or *generalized bridge decomposition* for links in a closed, connected and orientable 3-manifold, opening the way to the study of links in 3-manifolds via surface braid groups and their plat closure [10, 17]. The study of links in handlebodies and closed, connected and orientable 3-manifolds is now a fertile soil of research, with many researchers at work in generalizing the results obtained in $\mathbb{R}^3$ to the more general setting of 3-manifolds (see [59, 6, 54]).

In particular, in [17] Cattabriga and Gabrovšek studied the equivalence of links in 3-manifolds, obtaining a Markov-like theorem: the bijection between isotopy classes of oriented links and equivalence classes of braids is now obtained under braid isotopy moves, *M-moves, plat slide moves* and *dual plat slide moves.* Given a handle decomposition of a 3-manifold and a link in it, the slide moves can be described as isotopy moves that pass a small arc of the link around a handle in the handle decomposition of the 3-manifold. If we pass around a 2-handle (resp 1-handle) we obtain the plat (resp. dual plat) slide move. Since the description of a 3-manifold via handle decomposition can be very challenging, obtaining an algorithmic way of representing these plat slide moves is an important step forward in understanding the equivalence between links in 3-manifolds. A representation is indeed obtained by describing the attaching curve of the involved handle (which is a knot on the Heegaard surface) as the plat closure of an element of the braid group of the Heegaard surface. In the cited paper the authors give a nice presentation of the braid isotopy moves and the *M*-moves, which depend only on the number of strands of the braids and the Heegaard genus of the 3-manifold. At the same time, they provide a general construction of the plat and dual plat slide moves, and give a formula for constructing the words in the braid group of the Heegaard surface associated to the plat and dual plat slide moves in the case of genus one 3-manifolds, that is $S^2 \times S^1$ and lens spaces.

In this thesis, the result will be generalized to the case of (i) genus two 3-manifolds and (ii) Dunwoody and Takahashi manifolds, two infinite classes of arbitrary large Heegaard genus manifolds.

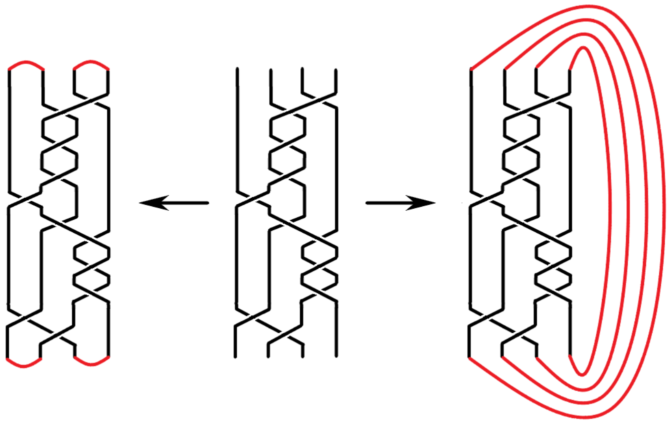

Figure 1: An example of a braid closed via plat closure (on the left) and standard closure (on the right). Note that, usually, the two obtained links are not isotopic.

A further problem addressed in the thesis is that of passing from the representation of a link in a 3-manifold through plat closure of a braid to representation through standard closure (see Fig. 1). We solve it in the case of $\mathbb{R}^3$, handlebodies and thickened surfaces.

All results will be accompanied by C++ programs, implementing the algorithmic solutions of the described problems.

Chapter 1 contains a description of the representation of 3-manifolds by Heegaard diagrams and Dehn surgery. We will also give some basic definitions and notions of graph theory which will be necessary in Chapter 2 to make use of the representation theory of PL manifolds by *crystallizations*. We recall that a crystallization of a 3-manifold is a particular 4-regular edge colored graph dual to a triangulation of the manifold. Moreover, each crystallization gives rise to three Heegaard splittings of the manifold (see Section 1.3.1 for a more complete dissertation). In particular, a 3-manifolds of Heegaard genus two can always be represented by a crystallization whose combinatorial structure is encoded by a 6-tuple of integers satisfying particular conditions (see [16]).

In Chapter 2 we will introduce the representations of knots and links via standard and plat closure of braids in the four settings of $\mathbb{R}^3$, handlebodies, thickened surfaces and, more generally, 3-manifolds.

Chapter 3 contains the first original part of the thesis, concerning the problem of finding equivalence between braids representing links in 3-manifolds. More precisely, the algorithmic result allows us to explicitly describe plat slide moves in the case of genus two 3-manifolds:

Theorem 0.0.1. *Let f be a 6-tuple representing a crystallization of a genus two 3-manifold. There exists an algorithm depending only on f that computes the psl-slide moves corresponding to the Heegaard splitting associated to f.*

In Chapter 4 we will consider the case of Dunwoody and Takahashi manifolds, giving a detailed description of the plat slide moves also for these two classes of manifolds.

In Chapter 5 we will address the problem of finding the braid representatives of a link via plat and standard closure, and we will give an algorithmic procedure which describes, given a link in $\mathbb{R}^3$, a handlebody or a thickened surface, how to pass from one representation to the other:

Theorem 0.0.2. *Let X be $\mathbb{R}^3$ (or S^3), a handlebody H_g of genus g or a thickened closed, connected and orientable surface $N(\Sigma_g)$. Given a link L in X represented by a braid B with plat closure, it is algorithmically possible to generate a braid B' which represents an equivalent link in X but with standard closure. The algorithm has a computational complexity of $O(N')$ where N' is the sum of the number of crossings, a_i and b_i type generators present in the braid B.*

Contents

Chapter 1

Preliminaries on 3-manifolds

In this chapter we will give the theoretical background necessary to have a deeper understanding of our work on links in 3-manifolds.

In what follows, if not otherwise specified, we will suppose that all manifolds are closed, connected and oriented. Diffeomorphisms between oriented manifolds will be assumed to be orientation preserving. In order to identify a manifold M with the opposite orientation we will use the notation $\overline{M}$. Furthermore, D^n and S^n will denote an n-dimensional ball and an n-dimensional sphere respectively. Finally, as in Peano definition of $\mathbb{N}$, zero is considered a natural number.

1.1 Heegaard decompositions and Heegaard diagrams

We recall some basic definitions concerning handles and handle decompositions of manifolds, in order to define the Heegaard diagram of a 3-manifold. For further details, we refer to [31].

Definition 1.1.1. Let X_1, X_2 be compact, oriented, smooth n-dimensional manifolds, and let Z_i be a compact submanifolds of the boundaries of X_i, $i = 1, 2$. Let $\phi : Z_1 \to Z_2$ be an orientation reversing diffeomorphism. By identifying Z_1 with Z_2 via ϕ we get a new oriented manifold, denoted by $X_1 \cup_\phi X_2$ or by $X_1 \cup_Z X_2$, if $Z = Z_1 = \overline{Z_2}$ and $\phi = id_Z$.

Two special cases of this definition are:

- when both Z_1 and Z_2 are $(n-1)$-dimensional balls then the result is the *boundary sum* of X_1 and X_2;

- when $X_i = M_i - \text{int}(D_i^n)$ and $Z_i = \partial D_i^n$, $i = 1, 2$, where M_i is a oriented, smooth n-dimensional manifold, the result is the *connected sum* of M_1 and M_2.

We denote by # the *connected sum* operator.

Definition 1.1.2. Given two integers $0 \leq k \leq n$, an n-dimensional k-handle (or *handle of index k*) H^k is a copy of $D^k \times D^{n-k}$ attached to the boundary of a smooth n-manifold X along $\partial D^k \times D^{n-k}$ via an embedding

$$\phi : \partial D^k \times D^{n-k} \to \partial X$$

that is called *attaching map*.

We will call the discs $D^k \times \{0\}$ and $\{0\} \times D^{n-k}$ respectively the *core* and *cocore* of the handle. Their boundaries will be called respectively the *attaching sphere* and the *belt sphere*. For

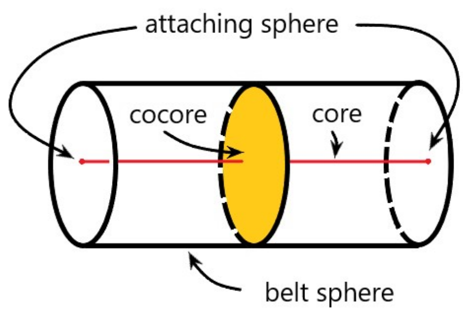

Figure 1.1: A 3-dimensional 1-handle.

example, in dimension three, a 1-handle on X is a copy of $D^1 \times D^2$ attached along $\partial D^1 \times D^2$ (see Fig.1.1), while a 2-handle on X is a copy of $D^2 \times D^1$ attached along $\partial D^2 \times D^1$. Here we will call *handlebody of genus g* the union of D^3 with g 1-handles.

Definition 1.1.3. Let X be a compact, oriented, smooth n-manifold with boundary ∂X decomposed as a disjoint union $\partial_+ X \coprod \partial_- X$ of two compact submanifolds (either of which may be empty). Orient $\partial_\pm X$ so that $\partial X = \partial_+ X \coprod \overline{\partial_- X}$ is the boundary orientation. A *handle decomposition* of X (relative to $\partial_- X$) is an identification of X with a manifold obtained from $I \times \partial_- X$ by attaching handles, such that $\partial_- X$ corresponds to $\{0\} \times \partial_- X$ in the obvious way. We will say that two handle decompositions $(X, \partial_- X)$ and $(X, \partial'_- X)$ of the same n-manifold X are equivalent if there exists an automorphism of X that transforms one decomposition into the other.

It is shown in [47] that every smooth, compact manifold pair $(X, \partial_- X)$ as above admits a handle decomposition.

It is important to note that we can always create a *cancelling pair* of handles with indices $k-1$ and k, for $1 \leq k \leq n$. Write ∂D^k as $S^{k-1} = D^{k-1}_+ \cup_\partial D^{k-1}_-$, glued along their common boundary $\partial = \partial D^{k-1}_+ = \partial D^{k-1}_-$. If we form the boundary sum of X with $D^n = D^k \times D^{n-k}$ by gluing along $D^{k-1}_- \times D^{n-k}$, the diffeomorphism type of X is not changed. Now, considering a slightly smaller D^k_0 contained in D^k such that:

$$D^k = D^k_0 \cup_{D^{k-1}_+} \left(D^{k-1}_+ \times D^1\right)$$

Then we can slice a neighbourhood of D^{k-1}_+ off D^k, and $D^{k-1}_+ \times \left(D^1 \times D^{n-k}\right)$ is the $(k-1)$-handle attached to ∂X, and $D^k_0 \times D^{n-k}$ is the cancelling k-handle. This procedure is also reversible, provided that the attaching sphere of the k-handle intersects the belt sphere of the $k-1$-handle in a single point. For examples in dimension 2 and 3, see Fig. 1.2.

There is also another move that can help us to obtain an handle decomposition with the smallest number of handles:

Definition 1.1.4. Given two k-handles H^k_1 and H^k_2 $(0 < k < n)$, attached to ∂X, a *handle slide* of H^k_1 over H^k_2 is given by taking the attaching sphere A of H^k_1 and pushing it through the belt sphere B of H^k_2 (see Fig.1.3).

A result of [20] ensures that handle sliding and elimination of cancelling pairs of handles form a complete set of moves for determining equivalent handle decompositions.

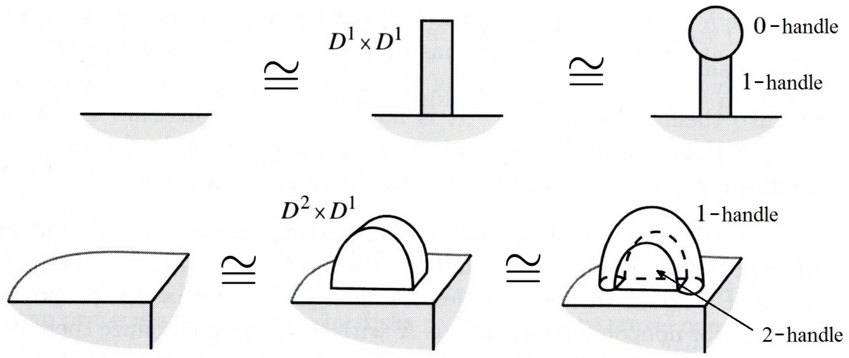

Figure 1.2: An example of handle creation in dimension 2 and 3, reproduced from [31].

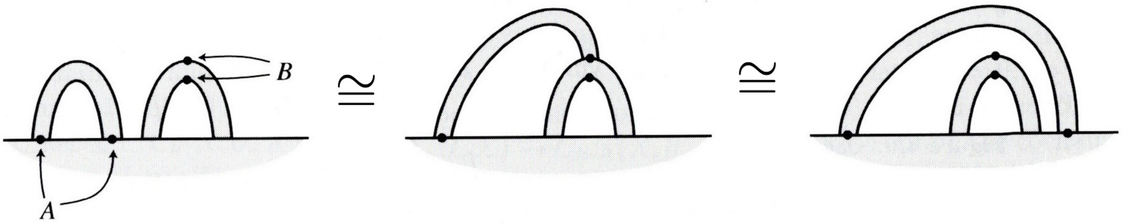

Figure 1.3: Example of handle slide, reproduced from [31].

Let us consider a handle decomposition of a closed oriented 3-manifold M. By [31] we know that M admits a handle decomposition with only one 0-handle and one 3-handle.

The union of the 0-handle with the g 1-handles of the decomposition is diffeomorphic to a genus g handlebody H_1. Once we specify the attaching circles of the 2-handles we have completely determined the resulting 3-manifold M since there is only one way to attach the 3-handle [31]. By turning the decomposition upside down, we notice that the union of the k 2-handles with the 3-handle is again diffeomorphic to a genus k handlebody H_2. Since $\{0-\text{handle}\} \cup \{1-\text{handles}\}$ and $\{3-\text{handle}\} \cup \{2-\text{handles}\}$ must have the same boundary, we have $g = k$. We have obtained a decomposition of M into two handlebodies H_1, H_2 of the same genus, glued together along their boundary. This kind of decomposition given by the triple (Σ_g, H_1, H_2) is called a *Heegaard splitting of* M, the common surface $\Sigma_g = H_1 \cap H_2$ is called *Heegaard surface* and g is the genus of the splitting. Two Heegaard splittings (Σ_g, H_1, H_2), $({\Sigma_g}', {H_1}', {H_2}')$ of a 3-manifold M are *equivalent* if there exists an automorphism of M that transforms Σ_g into ${\Sigma_g}'$ and H_i into ${H_i}'$, $i = 1, 2$.

The *Heegaard genus* of M is the minimum g such that M admits a Heegaard splitting of genus g. It is proven that each 3-manifold admits at least one Heegaard splitting [35]. In general, a manifold may admit non isotopic Heegaard surfaces of the same genus (see for example the case of small Seifert manifolds in [14]).

If we add a cancelling pair to M, we obtain a new pair of 1-handle and 2-handle to add to the correspondent handlebodies H_1 and H_2. In this way we increase their genus by one, and consequently also the genus of their common surface and the one of the Heegaard splitting. We call this procedure *stabilization*. The opposite action is called *destabilization*, and it can be done if and only if there are two properly embedded discs $D_i \subset H_i, i = 1, 2$ so that ∂D_1 and ∂D_2 intersect in only one point [58]. These two operations lead to the following result by Reidemeister and Singer:

Theorem 1.1.1 ([58]). *Given two Heegaard splittings of a closed* 3*-manifold there is a sequence of stabilizations and destabilizations that transforms the first into the second and vice versa.*

We say that M is *prime* if the equation $M = M_1 \# M_2$ implies that M_1 or M_2 is homeomorphic to S^3. A 3-manifold M is called *irreducible* if every 2-sphere in M bounds a 3-ball. Irreducibility implies primeness. However, $S^2 \times S^1$ is prime, but not irreducible: this is the only closed orientable 3-manifold with this property.

We recall that a *set of meridians* of a handlebody H_g of genus g is a collection of simple closed curves $u = \{u_1, \dots, u_g\}$ bounding properly embedded disjoint discs $D_1, \dots, D_g$ such that $H_g \backslash \{D_1, \dots, D_g\}$ is a 3-ball. We can then give the definition of a Heegaard diagram for M, a much more graphic way to encode the information of a Heegaard splitting for a closed 3-manifold:

Definition 1.1.5. A genus *g (closed) Heegaard diagram* for a Heegaard splitting (Σ_g, H_1, H_2) of a 3-manifold M is a triple $(\Sigma_g, \alpha, \beta)$, where α and β are sets of meridians for H_1 and H_2 respectively.

Given a closed Heegaard diagram $(\Sigma_g, \alpha, \beta)$, by cutting the surface Σ_g along one of the sets of meridians, say α, we obtain a 2-dimensional disc with $2g$ holes, say $D_1, \dots, D_{2g}$, distinct and paired, each pair corresponding to a certain α_i. Therefore, the meridians β_i will be naturally cut into arcs joining the holes in various ways, yielding a graph on the sphere with $2g$ holes called an *open Heegaard diagram* of $(\Sigma_g, \alpha, \beta)$.

Every Heegaard diagram produces a single Heegaard splitting, while every Heegaard splitting gives rise to infinitely many distinct Heegaard diagrams [37]. These are related to each other by the following result:

Theorem 1.1.2 ([31])**.** *Two Heegaard diagrams $(\Sigma_g, \alpha, \beta)$ and $(\Sigma_g, \alpha', \beta')$ determine the equivalent splittings if and only if there is at least one sequence of handle slides that transforms α to α' and β to β'.*

Moreover, if we have a surface Σ_g and two sets of mutually disjoint simple closed curves $\alpha = \{\alpha_1, \dots, \alpha_g\}$ and $\beta = \{\beta_1, \dots, \beta_g\}$ on it, a necessary and sufficient condition for the triple $(\Sigma_g, \alpha, \beta)$ to represent a 3-manifold is that neither the α's nor the β's split the surface (in other words, both $\Sigma_g - \alpha$ and $\Sigma_g - \beta$ are connected).

1.1.1 The cases of genus one and two

Clearly, from the definition of Heegaard genus, we can say that the 3-sphere S^3 has genus zero, moreover, it can be proved that no other 3-manifold has genus zero [4]. Analogously, a 3-manifold has Heegaard genus one if and only if it can be obtained by gluing together two solid tori by some homeomorphism of their boundaries, and cannot be obtained by gluing together two balls in any way.

Following the procedure described in [46], it can be proven that only $S^2 \times S^1$ and lens spaces have Heegaard genus one. For example, following [57], if we take two copies of the solid torus $D^2 \times S^1$ and glue them on their boundary $S^1 \times S^1$ using the identity map, we obtain $S^2 \times S^1$. On the other hand, if we glue the two solid tori in such a way that the two copies of S^1 are interchanged, then we obtain S^3; this is the Heegaard decomposition of genus one of the 3-sphere.

We recall the definition of lens space:

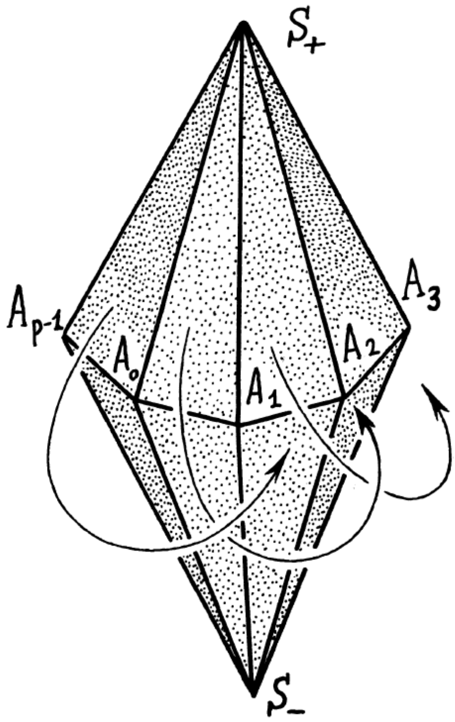

Figure 1.4: An example of construction of lens space, reproduced from [26].

Definition 1.1.6. Let $p > q > 0, p \geq 3$ be a pair of coprime integers. In $\mathbb{R}^3$ consider the bipyramid made by the union of two cones over a regular p sided polygon. Denote the vertices of this polygon with $A_0, A_1, \dots, A_{p-1}$ and the vertices of the two cones by S_+, S_- (see Fig. 1.4). For each $i \in 0, \dots, p-1$ we glue the face $A_i S_+ A_{i+1}$ with the face $A_{i+q} S_- A_{i+q+1}$ (where the indices are taken modulo p, and the vertices are glued in the order in which they are written). The closed 3-manifold obtained is the lens space $L_{p,q}$.

We could formally set $S^3 = L(1,0)$, $S^2 \times S^1 = L(0,1)$ and $\mathbb{R}P^3 = L(2,1)$, but since regular bigons, 1- and 0-gons are not well defined, it is not straightforward to describe these manifolds by using Definition 1.1.6. For this reason, we will usually omit these cases when considering lens spaces, unless otherwise stated. It is well known that lens spaces $L_{p,q}$ and $L_{p',q'}$ are homeomorphic if and only if $p = p'$ and $q \equiv \pm q'^{\pm 1} \mod p$ (see for example [37]). We also recall another construction for lens spaces [46]: let $D^2 \times S^1$ be a solid torus, and on its boundary choose a simple closed (q,p) type curve[1] l. Glue a handle of index 2 to the torus along l, to obtain a 3-dimensional manifold with boundary. Gluing a ball to the boundary sphere gives us

[1]Given a pair meridian-longitude on the boundary torus $S^1 \times S^1$, we recall that, for p and q coprime, a simple closed curve (q,p) on a torus is a curve obtained going q times along the meridian $S^1 \times \{*\}$ and p times along the longitude $\{*\} \times S^1$ of the torus, see Fig. 1.5.

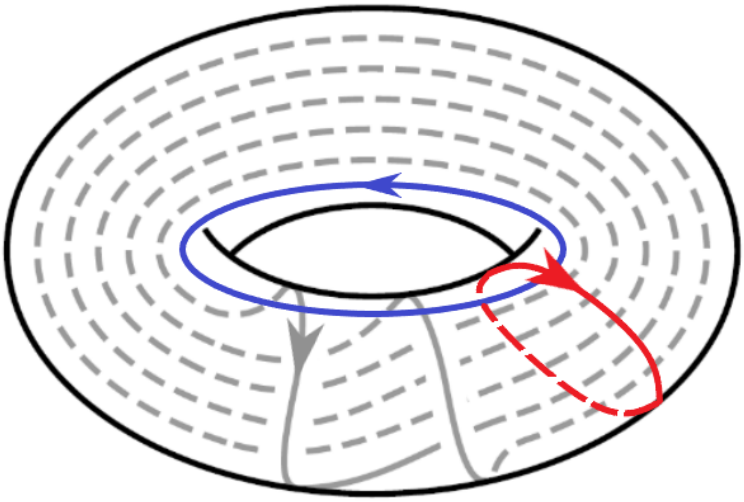

Figure 1.5: The Heegaard diagram for the lens space $L(5, 2)$.

the lens space $L_{p,q}$.

This proves that lens spaces admit a genus one Heegaard decomposition. The fact that only S^3 has Heegaard genus 0 prove that any lens space has genus exactly 1. Moreover, from the previous construction, we can easily obtain a Heegaard diagram for the lens space $L_{p,q}$. Take α_1 as a meridian on the torus T^2 and β_1 as a (q, p) curve on T^2. Then the triple (T^2, α_1, β_1) is a Heegaard diagram for the lens space $L_{p,q}$ (see Fig. 1.5 for $L_{5,2}$).

Let us now focus on the problem of genus two Heegaard manifolds. In literature there is no classification of genus two 3-manifolds, anyway there is a good result concerning their possible Heegaard diagrams, described in [46]. First, we need to give the definition of α-wave.

Definition 1.1.7. Let $(\Sigma_g, \alpha, \beta)$ be a closed Heegaard diagram such that $\alpha \cap \beta$ does not create bigons (polygons with two vertices and two sides) on Σ_g. Then a simple curve $l \subset \Sigma_g$ is an α-wave if (see Fig.1.6 for an example):

- the end-points of l lie on one of the meridians α_i and l has no points in common with any other curve of α or β;
- the end-points belong to different arcs into which the meridians β divide α_i, but l approaches these two arcs from the same side in Σ_g.

The notion of α-waves is very useful in the theory of Heegaard diagrams because it provides an equivalence move called *wave transformation* that is defined as follows. Let $\alpha =$

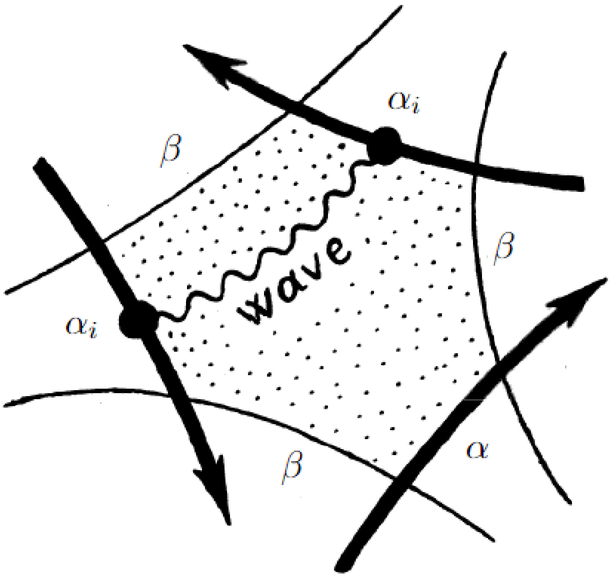

Figure 1.6: An example of α-wave, reproduced and relabeled from [26].

$\{\alpha_1, \dots, \alpha_i, \dots, \alpha_g\}$, be a set of meridians and let $\alpha_i{}'$ be the union of a α-wave l and one of the parts of the meridian α_i into which α_i is split by the ends of the arc l. The new triple $(\Sigma_g, \alpha', \beta)$, with $\alpha' = \{\alpha_1, \dots, \alpha_i{}', \dots, \alpha_g\}$, is equivalent to the initial Heegaard diagram.
Now we are ready to state the result:

Theorem 1.1.3 ([26]). *A genus two open Heegaard diagram $(\Sigma_2, \alpha, \beta)$ such that $\alpha \cap \beta$ does not create bigons on Σ_2 can always be depicted as the diagrams in Fig.1.7, where an arc with label k denotes k parallel arcs.*

A diagram of type III will always present an α-wave [46]. Moreover, any diagram of type II will admit a wave under the condition that either $a = 0$ or $d = 0$. If $c = d = 0$, then a diagram of type I also contains a wave. In diagrams of type I and II, when we have $b = d = 0$, $a = b = 0$ or $a = c = 0$, we do not get anything new since a can be replaced by d and b by c by a transposition of the first and second holes or the third and fourth holes. Provided we are interested only in manifolds and not in their diagrams, we can disregard diagrams with waves, because they can be simplified by wave transformations.

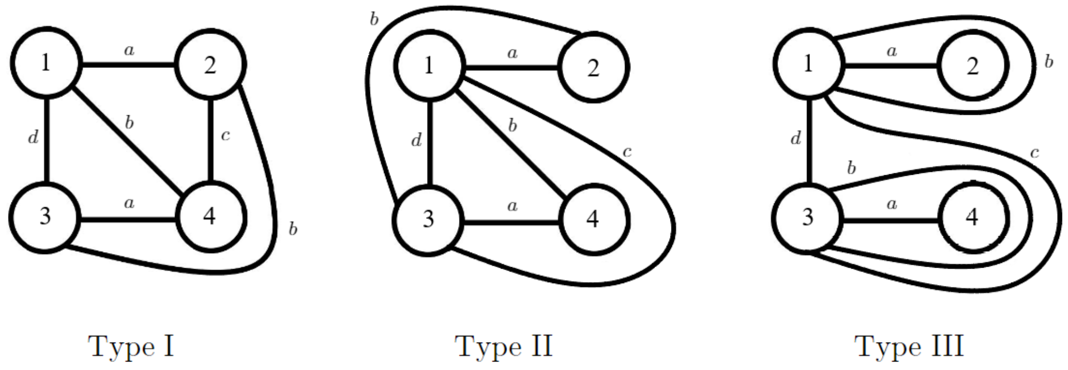

Figure 1.7: The three possible types of genus two Heegaard diagrams. Here the identification that produces the closed Heegaard diagram is between discs $1-3$ and $2-4$.

1.1.2 A genus n example: Dunwoody manifolds

In this section we will describe briefly the construction of the Dunwoody manifolds introduced in [24] and recall some of their properties.

Let $a, b, c, n \in \mathbb{N}$, with $n > 0$ and $a + b + c > 0$. Let $\Gamma = \Gamma(a, b, c, n)$ be the regular, trivalent, planar graph depicted in figure Fig. 1.8, where, an arc with label k represents k parallel arcs. The graph contains n top and n bottom circles, each one having $d = 2a + b + c$ vertices. We denote them with $C_1^u, \dots, C_n^u$ and $C_1^d, \dots, C_n^d$ respectively. All indexes will be considered mod n.

For each $i = 1, \dots, n$, we have a parallel arcs connecting C_i^u (resp. C_i^d) with C_{i+1}^u (resp C_{i+1}^d), b parallel arcs connecting C_i^u to C_{i+1}^d and c parallel arcs connecting C_i^u to C_i^d. From now on we will set $\mathbf{C}^u = \{C_1^u, \dots, C_n^u\}, \mathbf{C}^d = \{C_1^d, \dots, C_n^d\}$.

The one-point compactification of the plane brings Γ onto S^2. The diagram Γ is invariant under a rotation ρ_n of the sphere by $\frac{2\pi}{n}$ radians around an axis passing through the center of the sphere and non intersecting Γ. Obviously ρ_n sends C_i^u to C_{i+1}^u and C_i^d to C_{i+1}^d.

Now, let r, s be two given integers. We give a clockwise (resp. counterclockwise) orientation to the C_i^u's (resp. C_i^d's), and we enumerate the vertices as in figure Fig. 1.9. All numbers are to be considered mod d.

For $i = 1, \dots, n$ we cut off from S^2 the interiors of the $2n$ discs bounded by the C_i^u's and C_i^d's, which don't contain any arc of Γ, and glue the circle C_i^u with C_{i-s}^d so that vertices having the same labelling correspond. In this way we obtain a regular graph of degree four on an orientable surface Σ_n of genus n. Of course, by construction, we can always consider r mod d and s mod n.

By the identification, the nd arcs of Γ connect via their end-points creating m closed curves, $e_1, \dots, e_m$. Now, denote by c_i the closed curve coming from the identification of C_i^u and C_{i-s}^d and set $(\mathbf{C} = \{c_1, \dots, c_n\}, \mathcal{E} = \{e_1, \dots, e_m\})$.

Clearly, if we cut Σ_n along $\mathbf{C}$ we don't disconnect the surface. If $m = n$ and even cutting Σ_n along $\mathcal{E}$ has the result of not disconnecting the surface, then the triple $(\Sigma_n, \mathbf{C}, \mathcal{E})$ is a Heegaard diagram of genus n of a 3-manifold, completely determined by the 6-tuple (a, b, c, n, r, s). Such manifold is called a *Dunwoody manifold*.

We will denote by S the set of 6-tuples $(a, b, c, n, s, r) \in \mathbb{Z}^6$ with $n > 0$, $a, b, c \geq 0$ that are *admissible*, which means that:

- the set $\mathcal{E}$ contains exactly n closed curves;
- the surface Σ_n is not disconnected by cutting along the curves of $\mathcal{E}$.

Given an admissible 6-tuple $\sigma \in S$, we denote the open Heegaard diagram and the 3-manifold associated to σ by $H(\sigma)$ and $M(\sigma)$, respectively.

1.2 Dehn surgery on a manifold along a link

Before giving the definition of Dehn surgery on a 3-manifold M along a link L, we first need to recall the definition of link: we call a *k-component link* in $\mathbb{R}^3$ (resp. S^3 or a 3-manifold M) the embedding of a collection of disjoint circles into $\mathbb{R}^3$ (resp. S^3 or M). Usually we will refer to links in $\mathbb{R}^3$ and S^3 indifferently, seeing S^3 as the 1-point compactification of $\mathbb{R}^3$. We recall that two links $L_1, L_2 \subset X = \mathbb{R}^3$, S^3 or a 3-manifold M are equivalent if there exists an ambient isotopy of the space that transforms one into the other, i.e. if there exists an isotopy

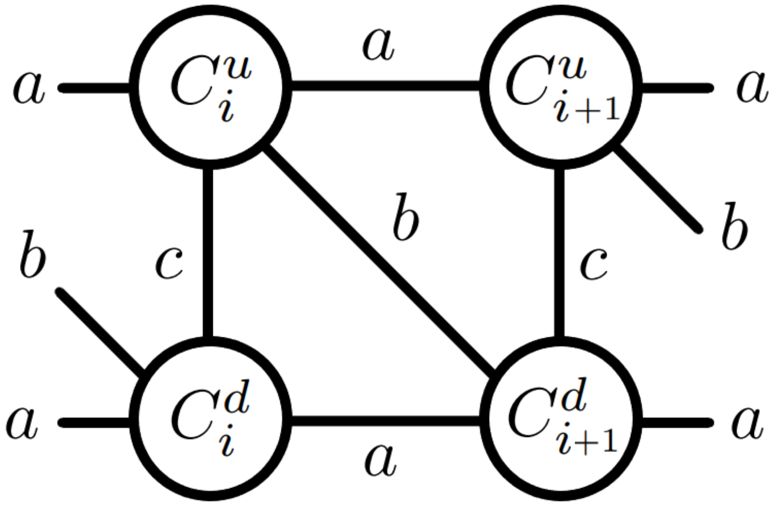

Figure 1.8: The graph $\Gamma(a, b, c, n, s, r)$.

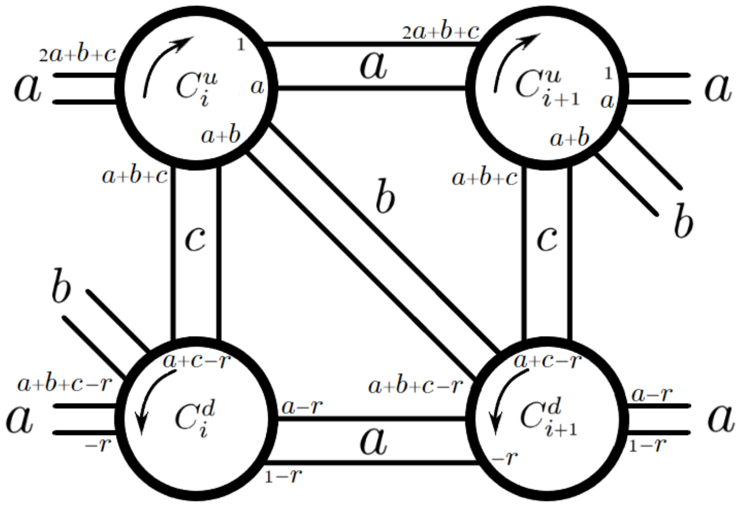

Figure 1.9: The labelling of vertices of $\Gamma(a, b, c, n, s, r)$.

$h : X \times [0,1] \to X$ such that $h(t,0)$ is the identity and $h(L_1, 1) = L_2$. We call *knot* a 1-component link. Remember also that a *trivial knot* is one ambient isotopic to a geometrically round circle, in other terms, the unknot.

Now, suppose that we are given a 3-manifold M and a link $L = L_1 \cup L_2 \cup \dots \cup L_n$ in M. Let $N = N_1 \cup N_2 \cup \dots \cup N_n$ be a set of disjoint closed tubular neighbourhoods N_i of L_i s.t. $N_i \subset \operatorname{int}(M)$, $i = 1, \dots, n$. Let also $J = J_1 \cup J_2 \cup \dots \cup J_n$ be a set of specified simple closed curves $J_i \subset \partial N_i$.
The *Dehn surgery* on M along L is the 3-manifold:

$$M' = (M \setminus \operatorname{int}(N)) \bigcup_h N$$

where h is a collection of homeomorphisms $h_i : \partial N_i \to \partial N_i$, each of which takes a meridian curve μ_i of N_i onto the specified J_i.
Therefore, we have two steps: the drilling part, which depends only on the link, and the filling part. Each component L_i of L has a preferred framing for the tubular neighbourhood N_i: the longitude λ_i is oriented coherently with L_i and the meridian μ_i has linking number $= +1$ with L_i. Then we may write the homology class of J_i in terms of this basis:

$$[J_i] = a_i \lambda_i + b_i \mu_i$$

If we take the ratio $r_i = b_i/a_i$ we will obtain the *surgery coefficient* associated with the component L_i. If for each $i = 1, \dots, n$ we have $r_i \in \mathbb{Z}$ then the surgery will be called *integral*.

For example, Figure 1.10 shows two possible representations of the Poincaré sphere as Dehn surgery on S^3 along two different links.

Dehn surgery on S^3 provides a useful representation of 3-manifolds according to the following result:

Theorem 1.2.1 ([44]). *Every closed, orientable, connected 3-manifold may be obtained by surgery on S^3 along a link. Moreover, one may always find such a surgery presentation where the surgery coefficients are all ± 1 and each component of the link is unknotted.*

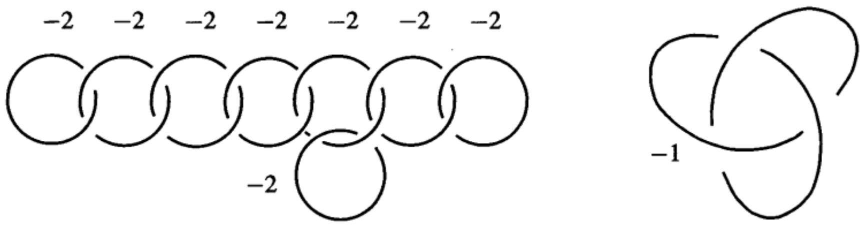

Figure 1.10: Two possible Dehn surgeries on S^3 resulting in the Poincaré sphere, reproduced from [57].

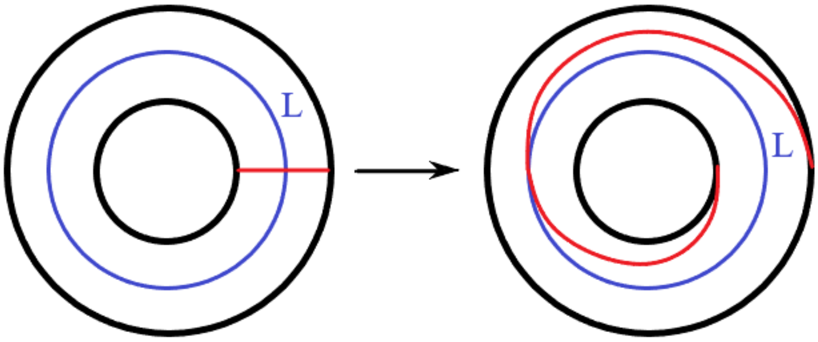

Figure 1.11: The action of a Dehn twist in the annulus of L.

We point out that the proof of this theorem, by Likorish, contains a construction of a Dehn surgery representation of a 3-manifold starting from a given Heegaard splitting.

Therefore, for the purpose of our research, it is really useful to give a brief sketch of the proof, after giving a couple more clarifications.

Definition 1.2.1. A *Dehn twist* along a simple closed curve L in a 2-manifold is a map which is the identity outside an annular neighbourhood of L and acts like in Fig. 1.11 inside the neighbourhood.

It was proven, by Lickorish, that it is possible to determine every possible orientation preserving homeomorphism of a 2-manifold in terms of Dehn twists over a specific set of curves in the surface:

Theorem 1.2.2 ([44]). *Let Σ_g be a closed orientable 2-manifold of genus g. Then every orientation-preserving homeomorphism of Σ_g is isotopic to a product of Dehn twists along the $3g-1$ curves depicted in Fig. 1.12.*

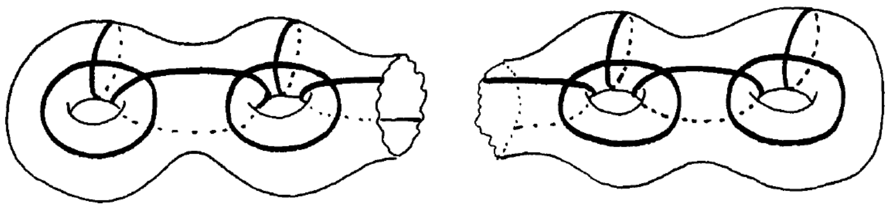

Figure 1.12: The family of curves used by Theorem 1.2.2, reproduced from [55].

Now we can give a quick sketch of the proof of Theorem 1.2.1.

Let (M, H_1, H_2) be a Heegaard splitting of a 3-manifold M. We have:

$$M = H_1 \cup_h H_2$$

with h, a diffeomorphism, mapping ∂H_1 to ∂H_2. Since H_1 and H_2 are two equal genus handlebodies, there exists a diffeomorphism $\phi : \partial H_1 \to \partial H_2$ such that $S^3 = H_1 \cup_\phi H_2$. Theorem 1.2.2 guarantees that there exist ψ, a product of Dehn twists on ∂H_1, and m, a diffeomorphism of the surface that is isotopic to the identity, such that $h \circ m \circ \psi = \phi$.

Now we can perform an operation on H_1 translating a Dehn twist along a closed curve C in ∂H_1: following Fig. 1.13 we can cut open the surface along C, carving then a solid torus out of $\mathrm{int}(H_1)$, twisting by 2π and gluing back the surface ∂H_1. We have performed a Dehn twist over ∂H_1 at the only expense of cutting a solid torus out of the interior of H_1, and having to sew it back differently (with a ± 1 twist). We can repeat this operation for all the twist needed to generate ψ, arranging the toral holes in such a way that they are all disjoint and all included in $\mathrm{int}(H_1)$.

Since ∂H_1 is not affected by the carving in $int(H_1)$, there exists a diffeomorphism h of H_1 to itself, such that h restricted to ∂H_1 is m^{-1}. Now we can apply the previous operations on hH_1 in order to perform ψ^{-1} on ∂H_1, and then glue this newly modified hH_1 onto H_2 to obtain M. Now, any point $P \in \partial H_1$ is identified with the point $h \circ m \circ \psi(P) \in \partial H_2$. Thus P is identified with $\phi(P)$. But ϕ is the map such that $H_1 \cup_\phi H_2 = S^3$, so M is diffeomorphic to S^3 from which disjoint solid tori have been carved, twisted and sewn back.

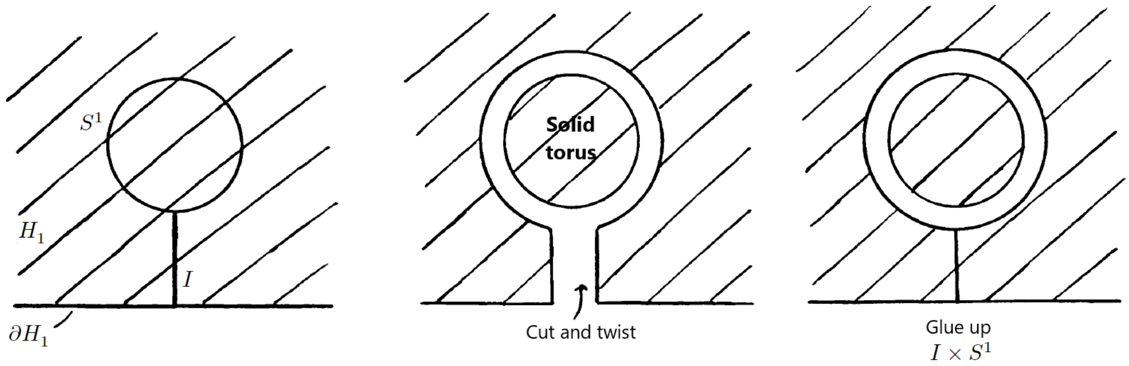

Figure 1.13: The cut-twist-glue operation in H_1, reproduced and relabeled from [44].

1.2.1 Another genus n example: Takahashi manifolds

Takahashi manifolds are closed orientable 3-manifolds introduced in [60] and obtained by Dehn surgery with rational coefficients on $\mathbf{S}^3$, along the $2n$-component link L_n of Fig.1.14, which is a closed chain of $2n$ unknotted components. These manifolds have been intensively studied in [41, 48, 56, 61].

A Takahashi manifold is said to be *periodic* when the surgery coefficients have the same cyclic symmetry of order n of the link L_n, i.e. the coefficients are $p_k/q_k = p/q$ and $r_k/s_k = r/s$ alternately, for $k = 1, \ldots, n$. Several important classes of 3-manifolds, such as (fractional) Fibonacci manifolds [36, 61] and Sieradski manifolds [19], represent notable examples of periodic Takahashi manifolds.

In this section, following the work of [49], we define a family of manifolds which generalizes Takahashi manifolds. For any pair of positive integers m and n, we consider the link $L_{n,m} \subset S^3$ with $2mn$ components presented in Fig. 1.15. All its components $c_{i,j}$, $1 \leq i \leq 2n$, $1 \leq j \leq m$, are unknotted circles and they form $2n$ subfamilies of m unlinked circles $c_{i,j}$, $1 \leq j \leq m$, with a common center. We observe that $L_{n,1}$ is the link L_n discussed above. The link $L_{n,m}$ has a cyclic symmetry of order n which permutes these $2n$ subfamilies of circles.

Let us consider the manifold obtained by Dehn surgery on S^3, along the link $L_{n,m}$, such that the surgery coefficients $p_{k,j}/q_{k,j}$ correspond to the components $c_{2k-1,j}$ and $r_{k,j}/s_{k,j}$ correspond to the components $c_{2k,j}$, where $1 \leq k \leq n$ and $1 \leq j \leq m$ (see Fig. 1.15). Without loss of generality, we can always suppose $\gcd(p_{k,j}, q_{k,j}) = 1$, $\gcd(r_{k,j}, s_{k,j}) = 1$ and $p_{k,j}, r_{k,j} \geq 0$.

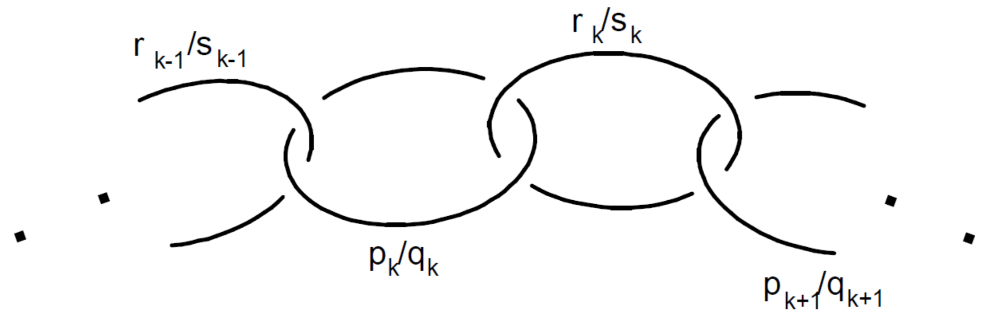

Figure 1.14: Presentation via Dehn surgery for standard Takahashi manifolds, reproduced from [48].

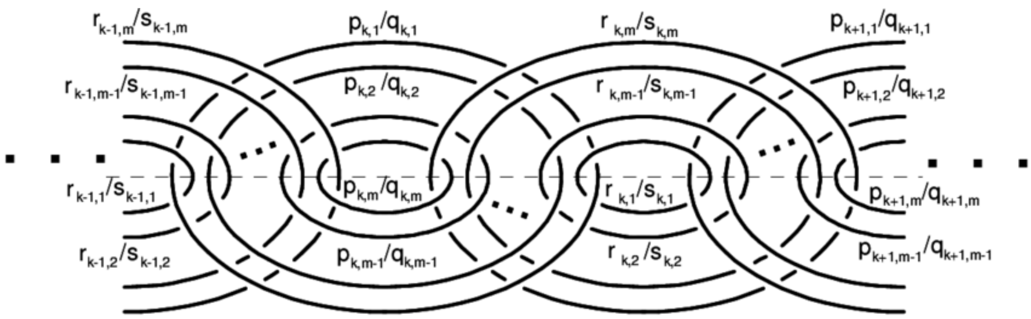

Figure 1.15: Presentation via Dehn surgery for generalized Takahashi manifolds, reproduced from [21].

We will denote the resulting 3-manifold by $T_{n,m}(p_{k,j}/q_{k,j}; r_{k,j}/s_{k,j}), j = 1, \dots, n$. This manifold will be referred to as a *generalized Takahashi manifold*, since for $m = 1$ we get the Takahashi manifolds introduced in [60].

In [21, Proposition 7] a description of a Heegaard diagram for a periodic generalized Takahashi manifold is given. The diagram, depending on the parameters p, q, r, s, is shown in Fig. 1.16. Here the identifications are C_i with $C_i{}'$ and D_i with $D_i{}'$, for $i = 1, \dots, n$.

If we deform the sphere where the open Heegaard diagram is embedded, we can redraw the diagrams in Fig. 1.16 as in Fig. 1.17.

1.3 Graph theory and crystallizations

In this section we give the basic definitions and some results about colored graphs and crystallizations. We will always consider a graph Γ, with vertices $V(\Gamma)$ and edges $E(\Gamma)$, where we

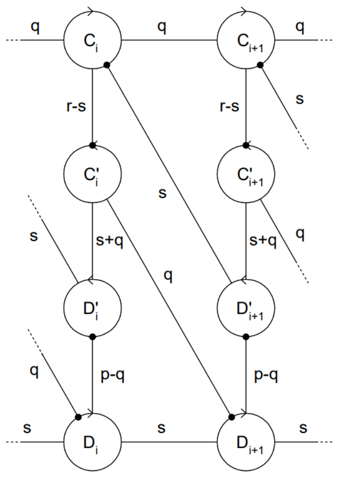

(a) $p > q, r > s$.

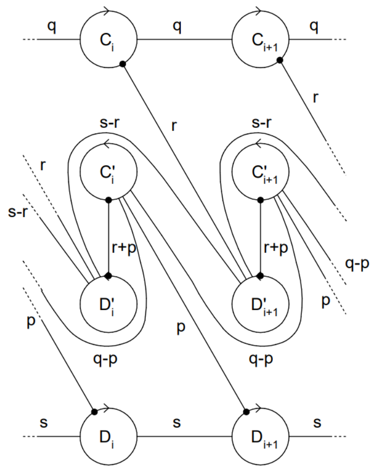

(b) $p < q, r < s$.

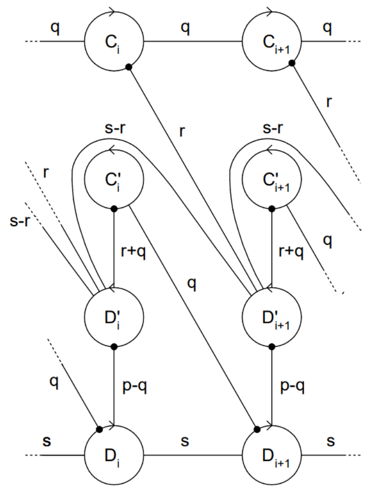

(c) $p > q, r < s$.

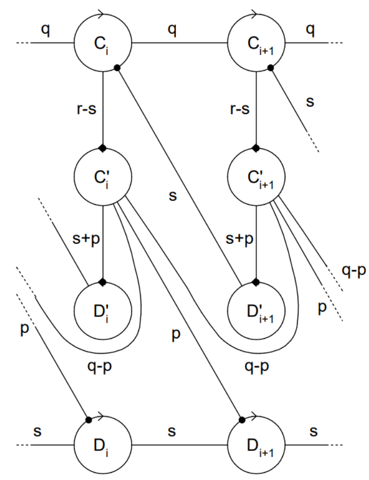

(d) $p < q, r > s$.

Figure 1.16: Four open Heegaard diagrams describing, depending on the parameters p, q, r, s, the general periodic Takahashi manifold $T_{n,m}(p, q, r, s)$, reproduced from [21].

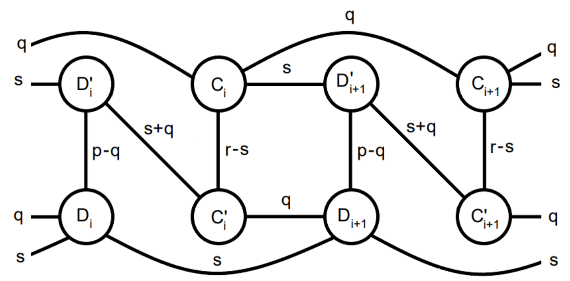

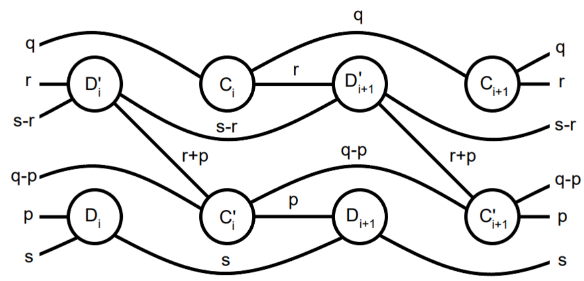

(a) $p > q, r > s$. (b) $p < q, r < s$.

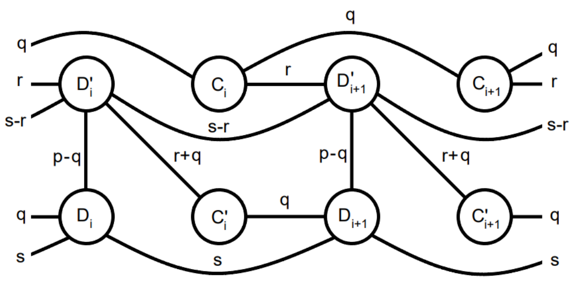

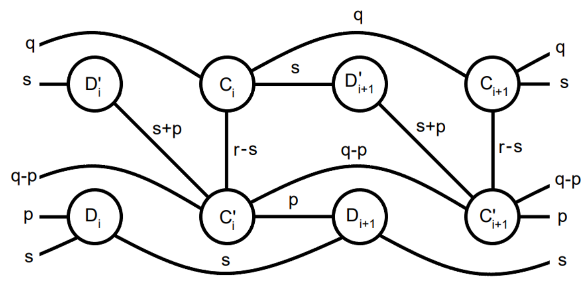

(c) $p > q, r < s$. (d) $p < q, r > s$.

Figure 1.17: The diagrams of Fig. 1.16 redrawn in order to have only one row of handles.

can have multiple edges having the same end-points but no loops.

Definition 1.3.1. Given a set $\mathcal{C} = \{1, 2, \dots, n\}$ of *colors*, we call *edge coloring* of a graph Γ a map $\gamma : E(\Gamma) \to \mathcal{C}$ such that $\gamma(e) \neq \gamma(f)$ for all e, f that are adjacent. Two vertices are said to be *c-adjacent* (with $c \in \mathcal{C}$) if they are the end-points of a c-colored edge.

The pair (Γ, γ) is called an *h-colored graph (without boundary)* if Γ is regular of degree $h \geq 2$ and if γ is an edge coloring of Γ with $|\mathcal{C}| = h$. From now on, we will often identify (Γ, γ) with Γ.

Let Γ be an h-colored graph and $\mathcal{B}$ a subset of $\mathcal{C}$ with cardinality k. We call $\mathcal{B}$-residue (or k-residue) every connected component of the $(h-k)$-colored graph obtained from Γ by deleting edges whose colors are not in $\mathcal{B}$ and we denote by $\rho_{\mathcal{B}}$ the number of $\mathcal{B}$-residues of Γ. Note that if $\mathcal{B} = \{i_1, i_2\}$ then $\rho_{i_1 i_2}$ is the number of cycles whose edges are alternatively colored by i_1, i_2. Given $c \in \mathcal{C}$ we denote by $\hat{c}$ the set $\mathcal{C} \setminus \{c\}$.

We recall that K, a finite collection of closed PL balls whose union is denoted by $|K|$, is a *pseudocomplex* if and only if:

- $|K|$ is the disjoint union of the interiors of the balls in K;
- if $A, B \in K$, then $A \cap B$ is a union of balls of K;
- for any n-ball $A \in K$ there exists a bijection preserving inclusions among faces, between the set $\{B \in K | B \subseteq A\}$ and the simplicial complex Σ_n consisting of the standard n-simplex and all its faces.

Given an $(n+1)$-colored graph, we can construct an n-colored pseudocomplex $K(\Gamma)$ in the following way:

1. we associate every vertex $v \in V(\Gamma)$ to a n-simplex $\sigma(v)$ and label the vertices of $\sigma(v)$ with colors $\{0, 1, \ldots, n\}$;
2. for every pair v, w of c-adjacent vertices in Γ, we glue the correspondent n-simplices, $\sigma(v), \sigma(w)$, along the $(n-1)$-faces opposite to vertices labelled c, identifying vertices labelled with the same color.

In [25] it is proven that every $(n+1)$-coloured graph Γ gives rise to an n-dimensional pseudomanifold[2] $|K(\Gamma)|$. Moreover, $|K(\Gamma)|$ is orientable if and only if Γ is bipartite. Now we can give the definition of crystallization:

Definition 1.3.2. A *crystallization* Γ is an $(n+1)$-coloured graph such that $\Gamma_{\hat{c}}$ is connected, for every $c \in \Delta_{n+1}$, and $M(\Gamma) = |K(\Gamma)|$ is an n-manifold.

Every n-manifold admits a crystallization [51], in particular we can represent every 3-manifold with a 4-colored crystallization.

[2] A pseudomanifold without boundary (respectively with boundary) is the support of a connected simplicial complex where every simplex is face of at least one n-simplex, every $(n-1)$-dimensional simplex is face of exactly (resp. at most) two n-dimensional simplices and every two n-simplexes can be connected by means of a series of alternating n- and $(n-1)$-simplexes, each of which is incident with its successor.

1.3.1 From crystallizations to Heegaard diagrams

Given a crystallization of a 3-manifold, it is possible to recover from it the Heegaard diagrams of the manifold. Let Γ be a 4-coloured graph, and let c, d be distinct colors of $\{0, 1, 2, 3\}$. Set $\{c', d'\} = \{0, 1, 2, 3\} - \{c, d\}$.

Remark 1 ([28]). If Γ is a crystallization of a 3-manifold then $\rho_{cd} = \rho_{c'd'}$.

In [28] the following result is proven:

Theorem 1.3.1 ([28]). *If Γ is a crystallization of a 3-manifold M, for any choice of a couple of colors c, d, there exists an embedding $\mathbf{i}$ of Γ into a surface F_{cd} of genus $\rho_{cd} - 1$ that is a Heegaard surface for M.*

More precisely, the procedure to obtain a Heegaard diagram from a crystallization Γ of M is the following.

Let $\xi^0, \dots, \xi^n$ be the components of $\Gamma_{c,d}$ and $\xi^{0\prime}, \dots, \xi^{n\prime}$ the ones of $\Gamma_{c',d'}$. Set $x^i = \mathbf{i}(\xi^i)$ and $y^i = \mathbf{i}(\xi^{i\prime})$ for $i = 0, \dots, n$ and consider the sets $\mathbf{x} = \{x^0, \dots, x^n\}$, $\mathbf{y} = \{y^0, \dots, y^n\}$; furthermore, let us define $\mathbf{x}(\hat{j}) = \mathbf{x} \backslash \{x^j\}$, $\mathbf{y}(\hat{j}) = \mathbf{y} \backslash \{y^j\}$. Then, for each $j = 0, \dots, n$ the triple $(F_{c,d}, \mathbf{x}(\hat{j}), \mathbf{y}(\hat{j}))$ is a Heegaard diagram for the 3-manifold M.

In Fig. 1.18 we can see an example of a crystallization representing the Poincaré sphere (see [7]).

1.3.2 6-tuples of integers and 4-colored graphs

In [16, 32] it is described a way of representing all 3-manifolds of genus $g \leq 2$ via crystallizations defined by 6-tuples of integers.

Let $\mathcal{F}$ be the set of the 6-tuples $f = (h_0, h_1, h_2, q_0, q_1, q_2)$ of integers satisfying the following conditions (index i is considered mod2):

1. $h_i + h_{i+1} = 2l_{i+1}$ (i.e. an even integer) for $i = 0, 1, 2$;

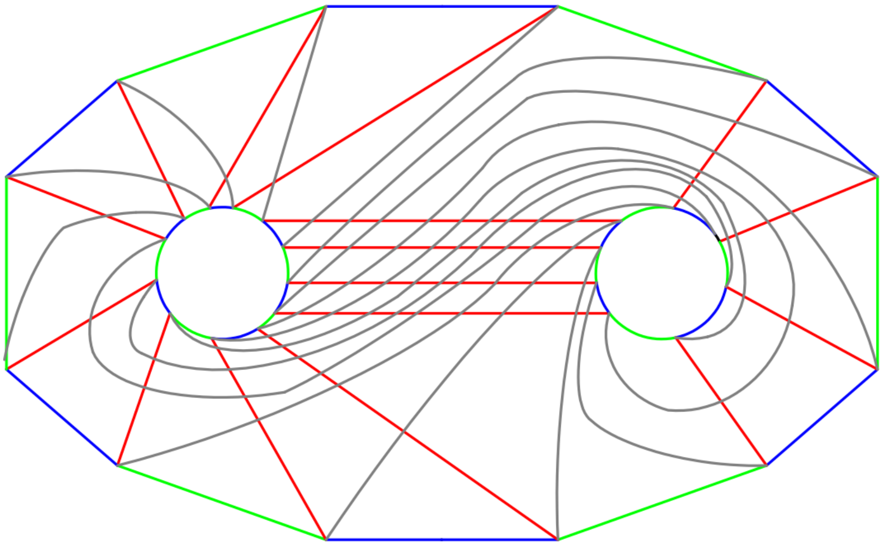

Figure 1.18: A crystallization representing the Poincaré sphere.

2. $0 \leq q_i < 2l_i$, for $i = 0, 1, 2$;

3. all q_i's have the same parity;

4. $h_i + q_i$ is odd for $i = 0, 1, 2$;

5. there exists at most one j such that $h_j = 0$.

The parameter q_i will be considered mod $2l_i$ for $i = 0, 1, 2$.

Let $\mathcal{G} = \{\Gamma(f) | f \in \mathcal{F}\}$ be the class of 4-coloured graphs $\Gamma(f)$ whose vertices are the elements of the set

$$V(f) = \bigcup_{i=0,1,2} \{i\} \times \mathbb{Z}_{2l_i},$$

and such that there exists a c-edge, with $c = 0, 1, 2, 3$, connecting the vertices (i, j) and (i', j') if and only if $(i', j') = \tau_c(i, j)$ where τ_c is the fixed-point-free involution defined as follows:

$$\begin{array}{rcl} \tau_0(i,j) & = & (i, j + (-1)^j) \\ \tau_1(i,j) & = & (i, j - (-1)^j) \\ \tau_2(i,j) & = & \left\{ \begin{array}{ll} (i+1, 2l_{i+1} - j - 1) & \text{if } j = 0, \dots, h_i - 1 \\ (i-1, 2l_i - j - 1) & \text{if } j = h_i, \dots, 2l_i - 1 \end{array} \right. , \\ \tau_3(i,j) & = & \rho\tau_2\rho^{-1}(i,j) \end{array} \tag{1.1}$$

and $\rho : V(f) \to V(f)$ is the bijection defined by $\rho(i,j) = (i, j+q_i)$.

Clearly, $\Gamma(f)$ is regular and is also bipartite because of condition 3, so that the polyhedron triangulated by the associated pseudocomplex is indeed a closed orientable 3-pseudomanifold. Moreover, note that $\Gamma(f)$ has exactly three $\{0,1\}$-residues, that is $\rho_{01} = 3$. We denote them by C_0, C_1, C_2, where C_i has as vertices the elements with i as first coordinate.

In [16], it is proven that $\Gamma(f) \in \mathcal{G}$ is a crystallization of a 3-manifold if and only if $\rho_{23} = 3$. We call *admissible* a 6-tuple belonging to $\mathcal{F}$ and satisfying this last condition, and we denote by D_0, D_1 and D_2 the three {2,3}-residues of $\Gamma(f)$ and by M_f the 3-manifold associated to f.

As recalled before, the manifold M_f has genus $\rho_{01} - 1 = 3 - 1 = 2$.

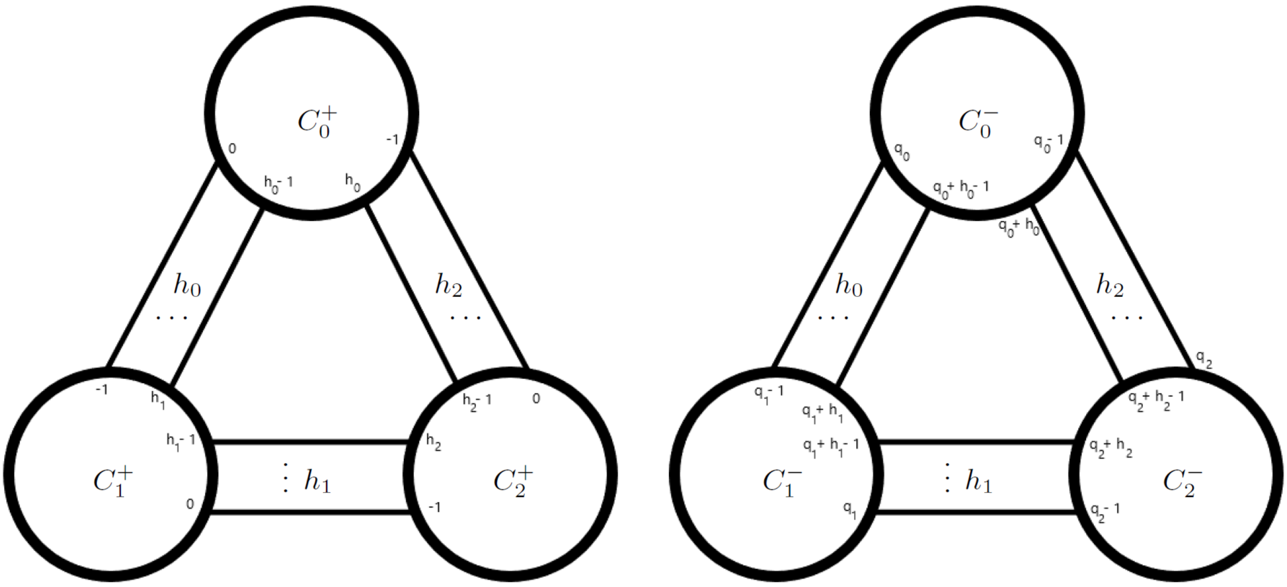

Figure 1.19: The residues $\Gamma(f)_{\hat{3}}$, $\Gamma(f)_{\hat{2}}$. All C_i's have a counterclockwise orientation.

Let us give an example to understand better the actual construction. Let $f = (4, 6, 10, 1, 1, 1)$ be the 6-tuple representing the Poincaré sphere [7]. Start considering the planar representation of the two 3-residues $\Gamma(f)_{\hat{3}}$ and $\Gamma(f)_{\hat{2}}$. Referring to Fig.1.19, denote by C_0^+, C_1^+, C_2^+ (resp. C_0^-, C_1^-, C_2^-) the copy of C_0, C_1, C_2 belonging to $\Gamma(f)_{\hat{3}}$ (resp. $\Gamma(f)_{\hat{2}}$). Following Fig.1.20 we can embed $\Gamma(f)_{\hat{3}}$ and $\Gamma(f)_{\hat{2}}$ in a genus two surface, that is F_{01}, so that:

- C_0, C_1, C_2 are the curves belonging to the intersection with the horizontal plane of symmetry of the surface
- $\Gamma(f)_{\hat{3}}$ is embedded in the front part of the surface (and represented by using violet arcs)

- $\Gamma(f)_{\hat{2}}$ is embedded in the back part (and represented by using green arcs)

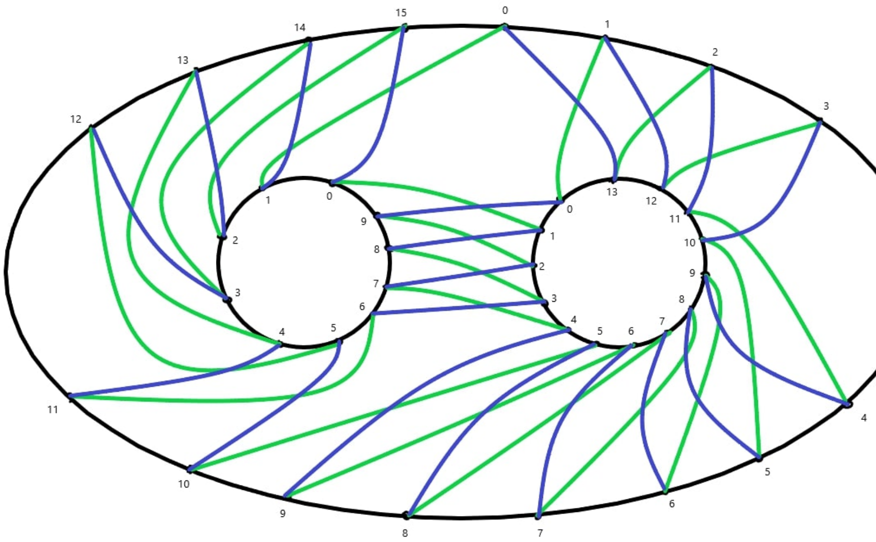

Figure 1.20: A genus two embedding of $f = (4, 6, 10, 1, 1, 1)$.

So, as recalled in Section 1.3.1, the choice of a couple of curves C_i's and a couple of curves D_i's gives a closed Heegaard diagram for M_f. We call *rich Heegaard diagram*, and denote it by R_f, the colored graph obtained by removing the cycle C_2, cutting the genus two surface along C_0 and C_1 and coloring with the same color the arcs belonging to the same D_i. See Fig.1.21 for an example with the 6-tuple $(4, 6, 10, 1, 1, 1)$. The name is due to the fact that, if we remove the arcs of any of the three D_i's we get an open Heegaard diagram for M_f (in all figures an arc with label k denotes k parallel arcs). Therefore, it is possible to obtain from a rich Heegaard diagram three open Heegaard diagrams of the same manifold all coming from one crystallization.

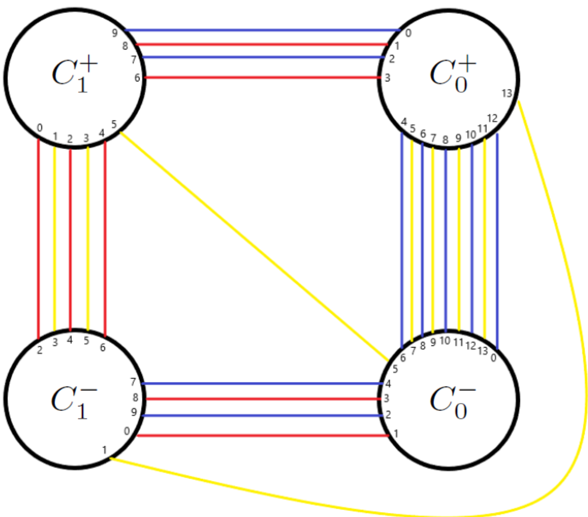

Figure 1.21: The rich Heegaard diagram obtained from $(4, 6, 10, 1, 1, 1)$.

Chapter 2

Preliminaries on braids and links

We have already given the definition of link in the previous chapter. Now we will focus mainly on the algebraic approach to knots and links, starting from the definition of the braid group.

2.1 Links as the standard closure of braids

2.1.1 The Artin's braid group and the (standard) closure in $\mathbb{R}^3$

Following the construction in [52], consider $2n$ points in $\mathbb{R}^3$: $A_i = (i, 0, 1), B_i = (i, 0, 0), i = 1, \dots, n$. A *braid* in n strands is a set of pairwise non-intersecting descending polygonal lines joining points $A_1, \dots, A_n$ to the points $B_1, \dots, B_n$ in any order. The equivalence between braids is defined by using the Δ-move, represented in Fig. 2.1: we can substitute a piece of braid $[a, b]$ with the two pieces $[a, c]$ and $[c, b]$ if we have no other strands in the triangle abc. If, equivalently, we consider braids composed by smooth strands, Δ-equivalence corresponds to ambient isotopy [15, Theorem 1.10]. In the following we will use the word "braid" to refer to the equivalence class of a braid.

To the set of braids in n strands a group structure naturally can be given. By defining the product as the concatenation of braids and the unit element as the braid consisting of n parallel strands we obtain what is called by Artin *the braid group*. We denote it with $\mathcal{B}_n$.

Using the results by Reidemeister [53], Artin proved [5] that the braid group is isomorphic to the abstract group generated by $\sigma_1, \dots, \sigma_{n-1}$ (σ_i being the elementary exchange of the strands i and $i+1$, see Fig.2.2) with the "braid relations":

$$\begin{aligned} \sigma_i \sigma_{i+1} \sigma_i &= \sigma_{i+1} \sigma_i \sigma_{i+1}, && i \leq n-2 \\ \sigma_i \sigma_j &= \sigma_j \sigma_i && |i-j| \geq 2 \end{aligned} \tag{2.1}$$

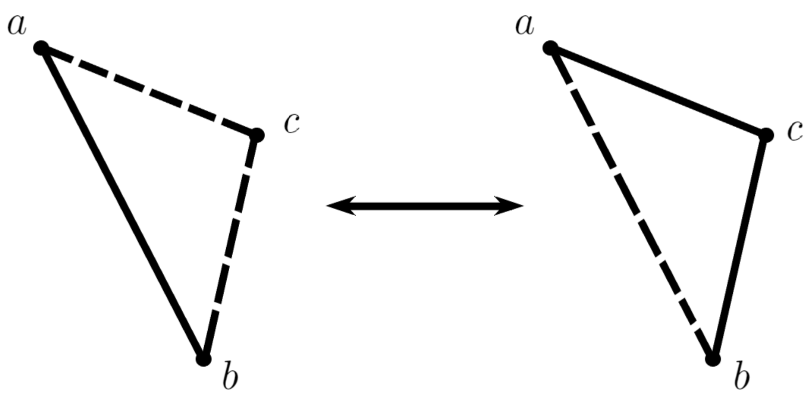

Figure 2.1: An example of Δ-move.

The relationship between braids and links arises from the closure operation. It can be done in multiple ways, but in this section we will deal with the so called *standard closure* of braids.

The standard closure of a braid $b \in \mathcal{B}_n$ is the link $\beta(b)$ obtained joining the points A_i to the B_i's, as in Fig. 2.3. The obtained link inherits the orientation from the one we gave to the braid (going from the top to the bottom of the braid): the closure arcs are oriented upward and the overall orientation is still coherent.

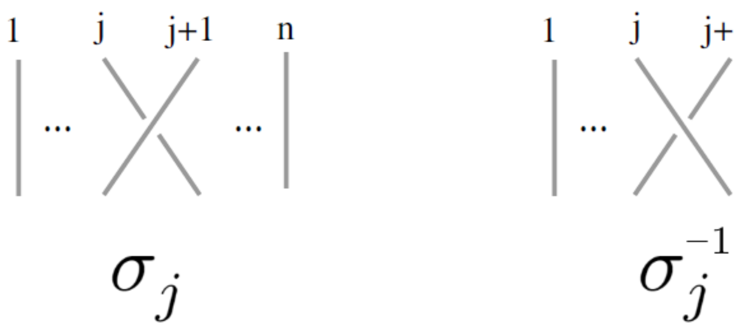

Figure 2.2: The generator σ_j and its inverse.

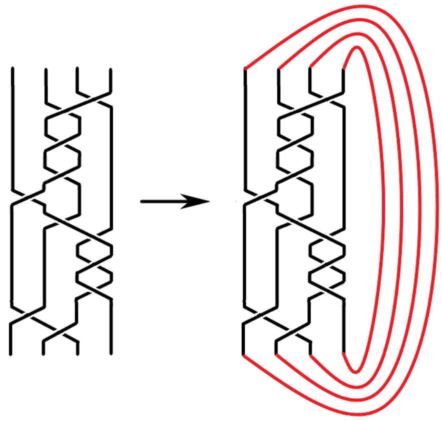

Figure 2.3: An example of standard closure of a braid.

A classic theorem by Alexander [3] states that this closure map is surjective, i.e., any link is the (standard) closure of some braid. The proof is analogue to the one sketched in Section 2.1.2 for $g = 0$. Discussing how different braids can have isotopic closures, we have as a first result the following one by Markov:

Theorem 2.1.1 ([45]). *The closures of two braids are isotopic if and only if one differs from the other by braid relations and a finite sequence of the following two moves (see Fig. 2.4)*

1. *First Markov move (conjugation):* $b \leftrightarrow aba^{-1}$, *where* $a, b \in \mathcal{B}_n$*;*

2. *Second Markov move (stabilization):* $b \leftrightarrow b\sigma_n^{\pm 1}$, *where* $b \in \mathcal{B}_n$*;*

Note that the rightmost braid in the figure is a braid in $\mathcal{B}_{n+1}$.

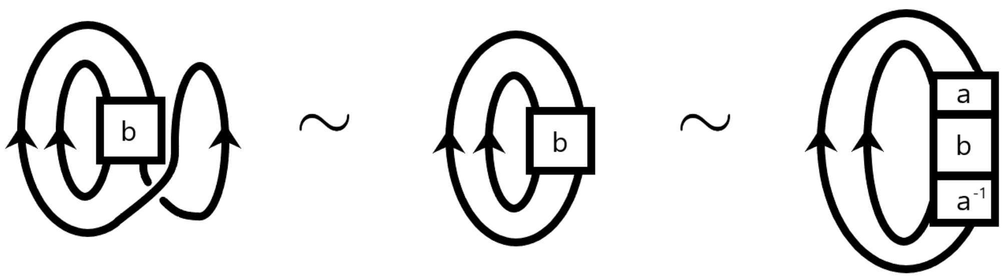

Figure 2.4: The two Markov moves; from the center to the right there is the first one, on the left the second one.

In [42] Lambropoulou and Rourke proved an analogous result but only by using a single equivalence move, the "L-move". The L–move consists in cutting a strand of the braid at a point,

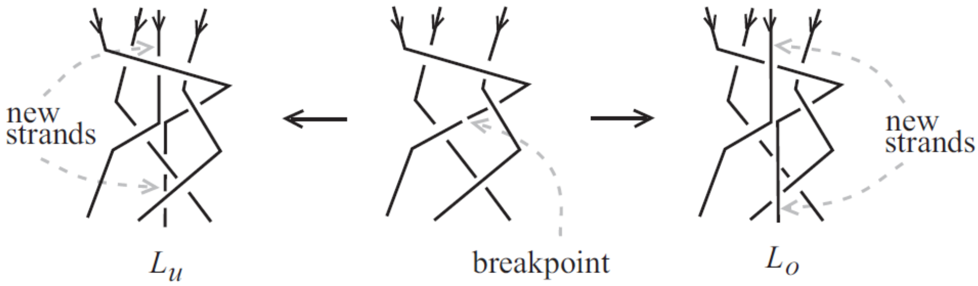

Figure 2.5: The L-moves, reproduced from [43].

then pulling the two ends of the cut, the upper downward and the lower upward, both running entirely *over* the braid or entirely *under* it, and keeping them aligned so as to obtain a new pair of corresponding braid strands.

Following the definition there are two types of L–moves, an "under" L–move, or L_u–move, and an "over" L–move, or L_o–move (see Fig. 2.5).

Fig.2.5 shows the local effects of the two moves.

Theorem 2.1.2 ([42])**.** *Two oriented links in $\mathbb{R}^3$ are isotopic if and only if any two corresponding braids differ by braid relations and L-moves.*

2.1.2 The mixed braid group and links in handlebodies and 3-manifolds

Now, consider a handlebody H_g of genus g: it can be represented as

$$H_g = S^3 \setminus \text{open tubular neighbourhood of } I_g$$

where I_g denotes the identity braid on g indefinitely extended strands, all meeting at the point at infinity. A link L in H_g will wind around these g holes, like the one represented in Fig. 2.6.

We can braid L as follows. Orient the link, then take any up-arc:

- cut the arc at any point;

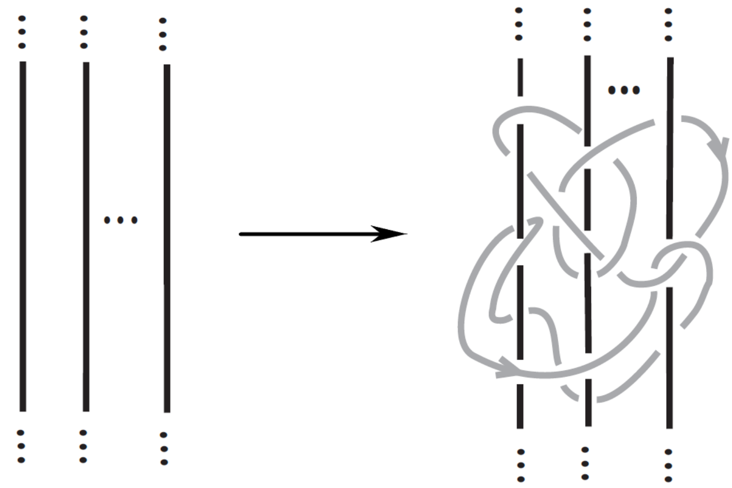

Figure 2.6: A link in a handlebody, by courtesy of Prof. Sophia Lambropoulou.

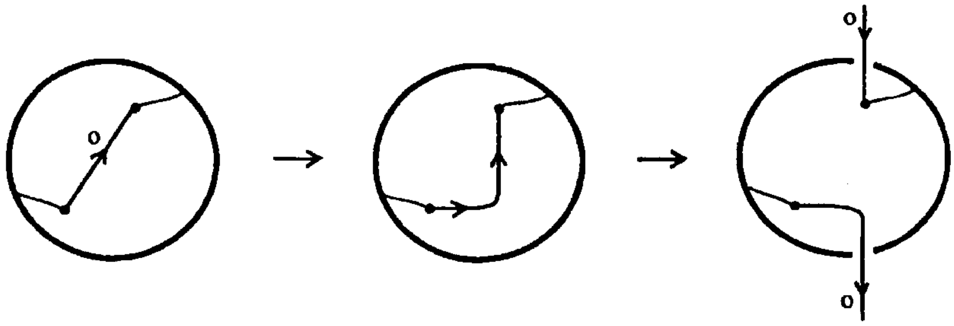

Figure 2.7: The standard braiding operation for the case of an over-arc, reproduced from [42].

- pull the two open ends upward and downward (see Fig. 2.7), keeping them aligned, obtaining a pair of corresponding braid strands, both running entirely over the previously constructed tangle[1] or entirely under it (depending if and how the up-arc goes through crossings, see [42] for details).

The tangle which we obtain is isotopic to the original one, but with one less up-arc. Applying this operation to all up-arcs, we will obtain a new braid in n strings, winding around I_g, the identity braid representing the holes of the handlebody.

Following the construction of [34] we can perform a *parting* operation to our braid. *Parting* a mixed braid means to separate its end-points into two different sets, so that the resulting braids have isotopic closures (see Fig.2.8). The operation has to be done bringing all the strands of the

[1]Here we will use the term *tangle* to refer to a link with some braided open strands, but still not completely braided.

second set on the right, passing on top of the strands of the first set. We will call the resulting braid a *parted mixed braid*. In our case, we can redraw our braid as one in $\mathcal{B}_{g+n}$ having our first g strands as the identity braid, the fixed part of the braid (the first set of end-points), and the other n strands representing the moving part of the braid (the second set of end-points).

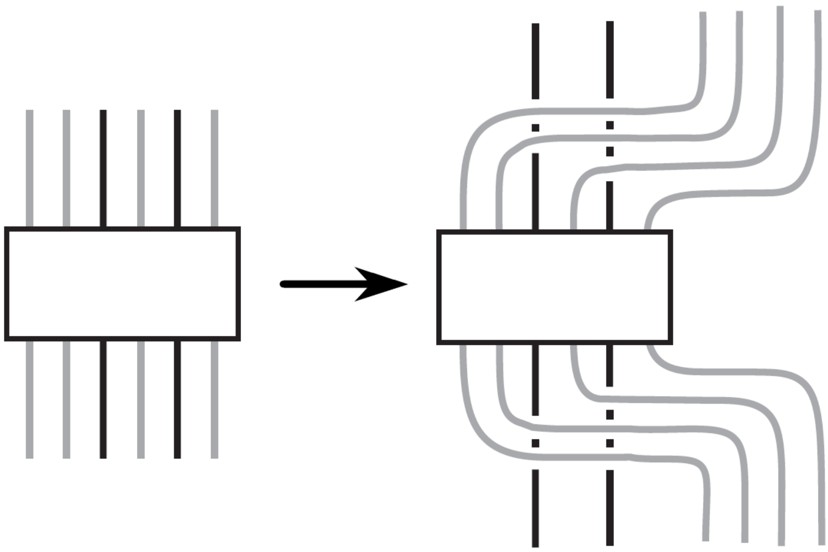

Figure 2.8: The mixed braid after the parting operation in the case of handlebodies.

We define $\mathcal{B}_{g,n}$ the *mixed braid group* as the set of all elements of $\mathcal{B}_{g+n}$ for which, if we remove the last n strands, we are left with the identity braid on g strands.
Following the construction in [34], we are led to the presentation of $\mathcal{B}_{g,n}$ as:

$$\left\langle \begin{array}{c} a_1, \dots, a_g \\ \sigma_1, \dots, \sigma_n \end{array} \left| \begin{array}{ll} \sigma_k\sigma_j = \sigma_j\sigma_k, & |k-j|>1,\ k,j=1,\dots,n \\ \sigma_k\sigma_{k+1}\sigma_k = \sigma_{k+1}\sigma_k\sigma_{k+1}, & 1 \leq k \leq n-1 \\ a_i\sigma_k = \sigma_k a_i, & 2 \leq k \leq n, 1 \leq i \leq g \\ a_i\sigma_1 a_r \sigma_1 = \sigma_1 a_r \sigma_1 a_i, & 1 \leq r \leq i \leq g \end{array} \right. \right\rangle$$

with the a_i and σ_i generators defined as in Fig.2.9.

Using also in this handlebody setting the same approach as in $\mathbb{R}^3$, Lambropoulou obtained an analogous result for mixed braids:

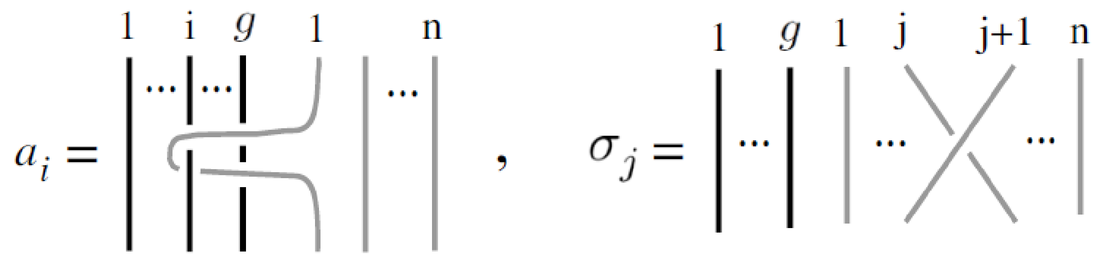

Figure 2.9: The generators of $\mathcal{B}_{g,n}$.

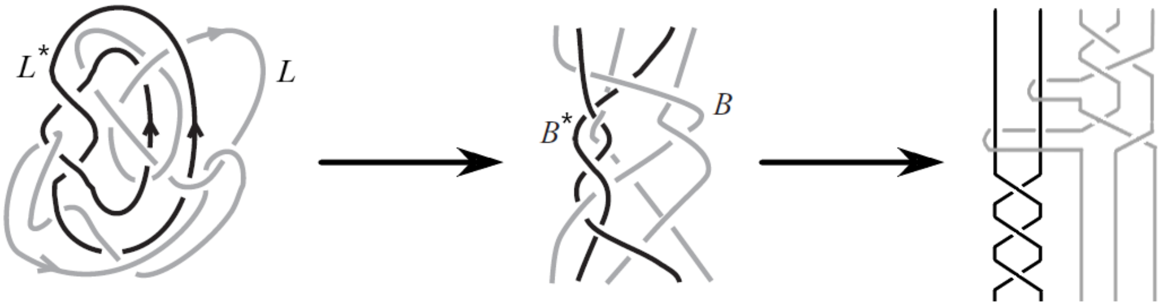

Figure 2.10: The mixed braid after the parting and combing operation in the case of 3-manifolds.

Theorem 2.1.3 ([34]). *The closures of two mixed braids $B_1, B_2 \in \mathcal{B}_{g,n}$ are equivalent if and only if they are related by braid isotopy and L-moves that do not affect the common fixed part.*

Finally, let us consider a 3-manifold M represented via Dehn surgery on a link L^* in $\mathbb{R}^3$. The way of representing a link L in M as the closure of a mixed braid uses in a similar way the previous braiding algorithm with the only difference being that it should be applied also to L^*. In this way L^* is represented as the closure of a braid $B^* \in \mathcal{B}_m$, while our link L is represented as the closure of a braid $B \in \mathcal{B}_n$.

These two braids wind around each other, so the resulting braid will belong to $\mathcal{B}_{n+m}$, with B^* being the fixed part of our mixed braid. After performing a parting and *combing*[2] operation [43] (see Fig. 2.10), we will obtain a braid in which the top part is an element from the mixed braid group, while the bottom part contains B^* on the left and I_n on the right. We will call this kind of element a *combed mixed braid*.

Before stating the equivalence theorem for links in 3-manifolds, we need the definition of link

[2]Combing a parted mixed braid means to separate the fixed sub-braid from the moving part, using mixed braid isotopy.

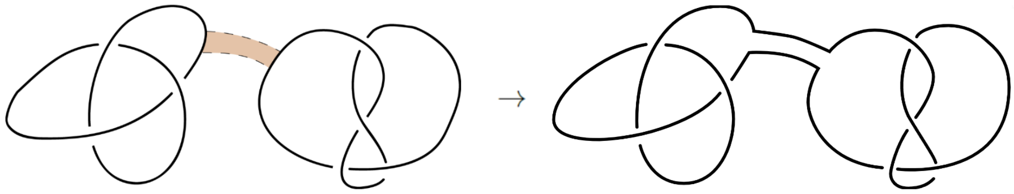

Figure 2.11: An example of link band sum, by courtesy of Prof. Boštjan Gabrovšek.

band sum:

Definition 2.1.1. Let L_1 and L_2 be two disjoint links in M and let $b = I \times I$ be an embedded band in M, such that $b \cap L_1 = e_1 = I \times 0$ and $b \cap L_2 = e_2 = I \times 1$. The *band connected sum* $L_1 \# L_2$ of L_1 and L_2 along b is the link

$$(L_1 - e_1) \cup (L_2 - e_2) \cup \overline{(\partial b - e_1 - e_2)}.$$

An example can be seen in Fig.2.11. It can be shown that the link band sum does not depend on the choice of the band b when L_2 is an unknot contained inside a 3-ball, that is disjoint from L_1, and b does not intersect the open disk which L_2 bounds [17].
Now, consider a manifold M represented via Dehn surgery of a link L^* in $\mathbb{R}^3$. Let $L_1 \cup L^*$ and $L_2 \cup L^*$ be two mixed links in M, and give an orientation to L_1, L_2 and L^*. We want to chose L_1 and L_2 so that the second is the link band sum over a band b of a component c of L_1 and the specified (from the surgery coefficient) longitude of a surgery component of L^*, in such a way that the orientation of the link band sum is coherent with the orientation of the surgery component of L^*. This is not an isotopy between the mixed links in $\mathbb{R}^3$ but it reflects isotopy between the two links L_1 and L_2 in M and we call it *band move* between the two mixed links (throughout literature, the band move is often referred to also as the *slide move*). Since c and L^* are oriented, there are two types of band moves according to the orientation of the arcs replacing the little band edges, see Figure 2.12 for an example with integral surgery p. A *braid band move* is a move between mixed braids that upon closure is a band move between the exploited mixed links.

The extension of the Theorem 2.1.3 to the case of 3-manifolds is the following:

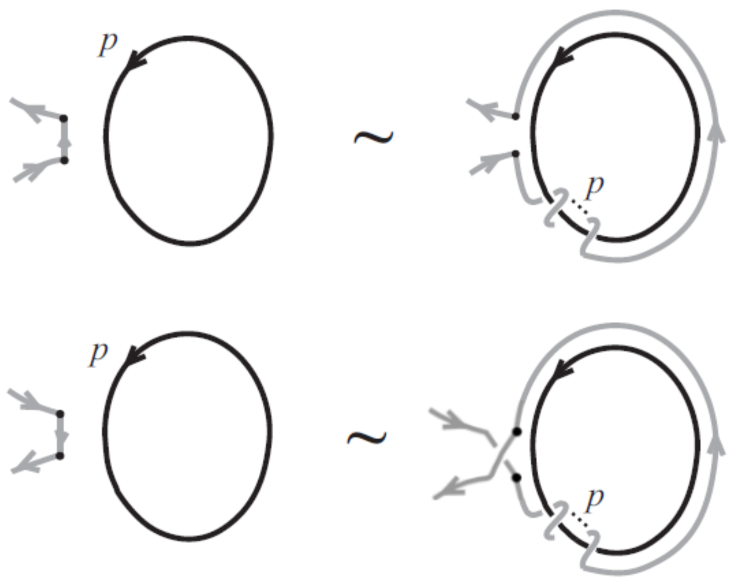

Figure 2.12: The two possible band moves.

Theorem 2.1.4 ([43]). *Let L_1, L_2 be two links in a 3-manifold M, and let $B_1 \cup B^*, B_2 \cup B^*$ be the two corresponding mixed braids in $\mathbb{R}^3$. Then L_1 is isotopic to L_2 if and only if $B_1 \cup B^*$ is equivalent to $B_2 \cup B^*$ in $\mathbb{R}^3$ by a finite sequence of braid isotopies, braid band moves and L-moves that do not affect B^*.*

2.2 Links as the plat closure of braids

There is another way of closing the free edges of a braid in order to obtain a link. Let $B \in \mathcal{B}_{2n}$ be a braid with an even number of strands. We can close it using small arcs connecting at the top and at the bottom of the braid the free edges of strands $2i-1$ and $2i$, $i = 1, \dots, n$ (see Fig. 2.13). Birman extensively studied this different *plat closure of braids* [13], proving that every link in $\mathbb{R}^3$ can be represented by the plat closure of a braid in $\mathcal{B}_{2n}$.

Let us now remember how to obtain a representation of a given link as the plat closure of a braid. The setting of Birman is the following. Let $\mathbb{R}^3_+$ denote the subset of $\mathbb{R}^3$ defined by $\{(x, y, z) \mid z \geq 0\}$, and let $A = A_1 \cup \cdots \cup A_n$ denote the union of the set of n line segments $[(i-0.25, 0, 0), (i-0.25, 0, 1)], [(i+0.25, 0, 0), (i+0.25, 0, 1)]$ and the half circles $\{(x, 0, z) \mid (x-i)^2 + (z-1)^2 = (0.25)^2, z \geq 1\}$ (see Fig.2.14). Let $\mathbb{R}^3_-$ denote

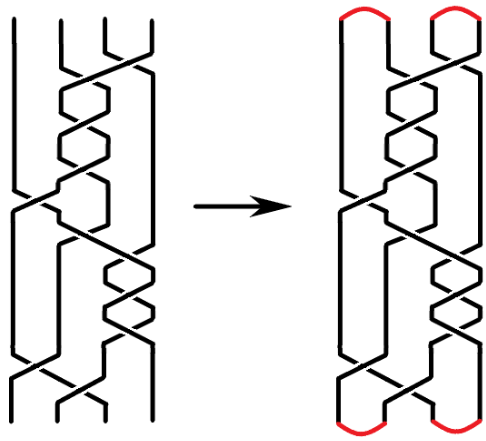

Figure 2.13: An example of plat closure of a braid.

the lower half-space (with $z \leq 0$), and let $A' = {A_1}' \cup \cdots \cup {A_n}'$ denote the half circles $\{(x, 0, z) \mid (x-i)^2 + z^2 = (0.25)^2, z \leq 0\}$. Let $\rho : \mathbb{R}^3_+ \to \mathbb{R}^3_- : \rho(x, y, z) = (x, y, -z)$.

The group of isotopy classes $\Phi = [\phi]$ of orientation-preserving homeomorphisms $\phi : (\partial\mathbb{R}^3_+, \partial A) \to$

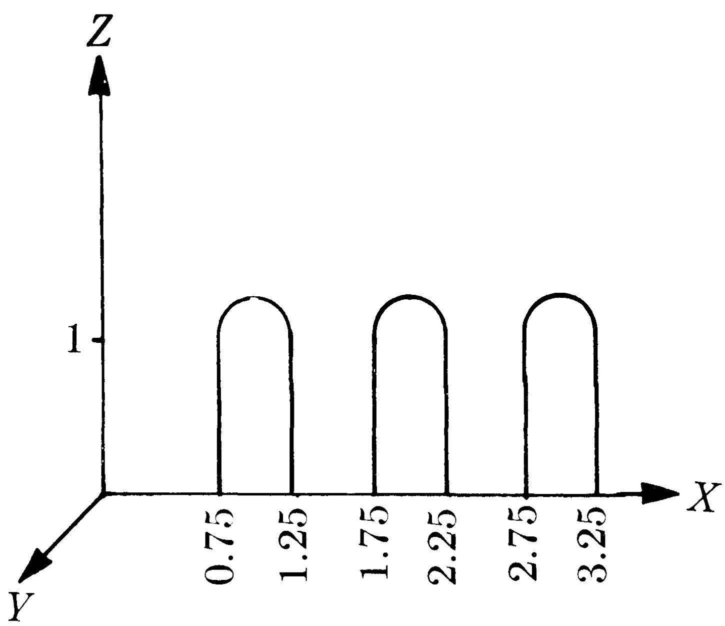

Figure 2.14: An example of the setting for $n = 3$, reproduced from [13].

$(\partial\mathbb{R}^3_+, \partial A)$ is the classical braid group $\mathcal{B}_{2n}$ [12, Corollary 1.1].

By these definitions, $L = A \cup_{\rho\phi} A'$ is a link in $\mathbb{R}^3$ (in plat closure), and every link L in $\mathbb{R}^3$ can be represented in this way [13]. Assume L to be polygonal and contained in the subset of $\mathbb{R}^3$

represented by the inequalities $0.25 \leq z \leq 0.75$. We can also consider that no edge lies in a plane parallel to the xy plane and also that for any three consecutive vertices b_{j-1}, b_j, b_{j+1} of L the line parallel to the z axis through b_j has a neighbourhood which meets the link only in the edges $[b_{j-1}, b_j]$ and $[b_j, b_{j+1}]$.

Now, starting from a vertex of L, let us consider three consecutive vertices b_{k-1}, b_k, b_{k+1}. The two segments $[b_{k-1}, b_k], [b_k, b_{k+1}]$ may form a local maxima or minima. Consider a vertical neighbourhood of b_k, which intersects only in two points ${b_k}'$ and ${b_k}''$, one in the first segment and the other in the second. Now, in the local maxima (resp. local minima) case let b_k^* the vertical projection of b_k on the plane $z = 1$ (resp $z = 0$). We substitute the two arcs $[{b_k}', b_k], [b_k, {b_k}'']$ with the arcs $[{b_k}', b_k^*]$ and $[b_k^*, {b_k}'']$ (see Fig. 2.15). Now the link intersects the planes $z = 0, z = 1$ in the same number of points, say n, and the planes $z = i)$ with $i \in (0, 1)$ in exactly $2n$ points. Points on planes $z = 0, z = 1$ will be called *boundary points*, while points on planes $z = i)$ with $i \in (0, 1)$ will be called *interior points.*

What we obtain is the representation of the link in plat closure.

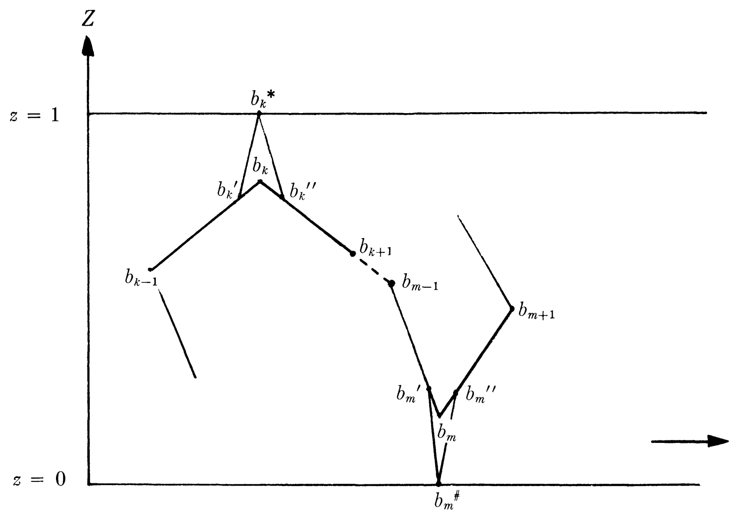

Figure 2.15: An example of braiding move, reproduced from [13].

After showing this braiding algorithm, Birman [13] proves the equivalence theorem starting from geometric moves and then passing to the algebraic setting. The two main moves are the *spike* move and the *stabilization* move (see also [17] for the definition in the 3-manifold setting):

- *Spike* move: let c', r, c'' be consecutive vertices of our link in polygonal form, with r a boundary point. Let $s \neq r$ be a second boundary point, on the same boundary component as r, and let d', d'' be interior points like in Fig.2.16. We define the spike move as retracting the *spike* at r to the base c', c'', shooting out a new spike at s with new base d', d''. In other words, we substitute $[c', r], [r, c'']$ with $[c', d'], [d', s], [s, d''], [d'', c'']$.

- *Stabilization* move: let a, b, c be consecutive vertices of our link in polygonal form. Let b', b'' be the projections of b onto the planes $z = 0, z = 1$, and b_1, b_2 the intersection of a small neighbourhood of b with the segments $[a, b]$ and $[b, c]$. The stabilization is the substitution of $[a, b]$ and $[b, c]$ with the segments $[a, b_1], [b_1, b'], [b', b''], [b'', b_2]$ and $[b_2, c]$, see Fig. 2.17.

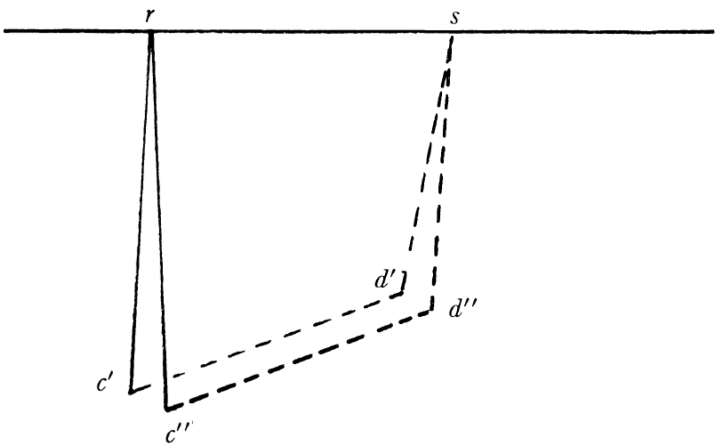

Figure 2.16: An example of spike move, reproduced and relabeled from [13].

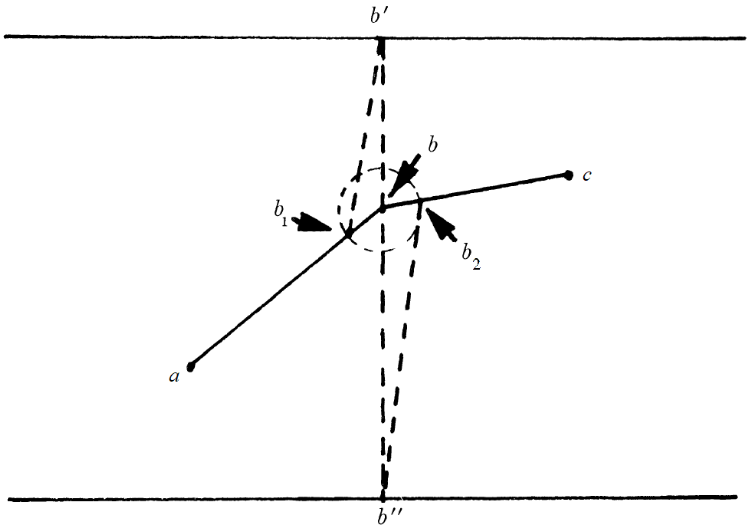

Figure 2.17: An example of stabilization move, reproduced and relabeled from [13].

In order to describe the algebraic equivalence of links represented by plat closure of braids, we need to define the subgroup K_{2n} of $\mathcal{B}_{2n}$. It is defined to be the set of those mapping classes $\Phi \in \mathcal{B}_{2n}$ which have a representative $\phi : (\partial\mathbb{R}^3_+, \partial A) \to (\partial\mathbb{R}^3_+, \partial A)$ which extends to a map $\hat{\phi} : (\mathbb{R}^3_+, A) \to (\mathbb{R}^3_+, A)$. Hilden found the generators of this subgroup:

Theorem 2.2.1 ([38]). *The group K_{2n} is generated by $\{\sigma_1, \sigma_2\sigma_1^2\sigma_2,$ and $\sigma_{2i}\sigma_{2i-1}\sigma_{2i+1}\sigma_{2i}, 1 \leq i \leq n-1\}$.*

Now we are ready to state the result for links in $\mathbb{R}^3$:

Theorem 2.2.2 ([13]). *Let L_1, L_2 be two links represented by $b_1 \in \mathcal{B}_{2n_1}$ and $b_2 \in \mathcal{B}_{2n_2}$ respectively as plat closures. Then the two links are equivalent if and only if there exists an integer $t \geq max\{n_1, n_2\}$ such that, $\forall n \geq t$ the elements:*

$$b_i{}' = b_i \sigma_{2n_i} \sigma_{2n_i+2} \dots \sigma_{2n-2} \in \mathcal{B}_{2n}, \qquad i = 1, 2$$

are in the same double coset of $\mathcal{B}_{2n}$ modulo K_{2n}.

Before going into the case of links in 3-manifolds, let us recall the definition of generalized bridge position for links in 3-manifolds [23]. First, we define:

Definition 2.2.1. Let H_g be a handlebody of genus g. A set of n properly embedded disjoint arcs $\{A_1, \dots, A_n\}$ in H_g is a *trivial system* of arcs if there exist n mutually disjoint embedded discs, called *trivializing discs*, $D_1, \dots, D_n$ properly embedded in H_g such that $A_i \cap D_i = A_i \cap \partial D_i = A_i$, $A_i \cap D_j = \emptyset$ and $\partial D_i - A_i \subset \partial H_g$ for all $i, j = 1, \dots, n$ and $i \neq j$.

In this case, we say that the arc A_i *projects* onto the arc $\partial D_i - \text{int}(A_i) \subset \partial H_g$ via D_i.

Let Σ_g be a Heegaard surface of genus g for M. We say that a link L in M is in *bridge position* with respect to Σ_g if:

1. L intersects Σ_g transversally and

2. the intersection of L with both handlebodies, obtained by splitting M along Σ_g, is a trivial system of arcs.

The decomposition for L into these two trivial systems of arcs is called a *(g,n)-decomposition* or *n-bridge decomposition of genus g* of L, where g is the genus of Σ_g and n is the cardinality of the trivial systems.

The minimal n such that L admits a (g,n)-decomposition is called the *genus g bridge number* of L. If $g = 0$, the manifold M is the 3-sphere and we get the usual notion of bridge decomposition and bridge number of links in the 3-sphere (or in $\mathbb{R}^3$). Following [17] we describe a way to represent links in 3-manifolds via braids closed in a plat way. Let $\mathcal{P}_{2n} = \{P_1, \dots, P_{2n}\}$ be a set of $2n$ distinct points on Σ_g and let us denote by $\mathcal{B}_{\Sigma_g,2n}$, the *surface braid group* on $2n$-strands of Σ_g, i.e, the fundamental group of the configuration space of the $2n$ points in Σ_g.

Bellingeri studied this group, obtaining in [9] the presentation of $\mathcal{B}_{\Sigma_g,n}$; given the generators (see Fig.2.18):

- σ_i, which exchanges points P_i and P_{i+1}, and keeps fixed all other points, for $i = 1, \dots, n-1$;
- a_i, which keeps fixed all points but P_1, which goes around the longitude of the i-th hole, for $i = 1, \dots, g$;
- b_i, which keeps fixed all points but P_1, which goes around the meridian of the i-th hole, for $i = 1, \dots, g$.

The relations are the following:

- Braid relations:
  - $\sigma_i \sigma_{i+1} \sigma_i = \sigma_{i+1} \sigma_i \sigma_{i+1}, \qquad i = 1, \dots, 2n-2$
  - $\sigma_i \sigma_j = \sigma_j \sigma_i, \qquad i, j = 1, \dots, 2n-1, \ \ |i-j| \geq 2$

- Mixed relations:

  - $a_r\sigma_i = \sigma_i a_r, \qquad 1 \le r \le g, i \ne 1$
  - $b_r\sigma_i = \sigma_i b_r, \qquad 1 \le r \le g, i \ne 1$
  - $\sigma_1^{-1}a_r\sigma_1^{-1}a_r = a_r\sigma_1^{-1}a_r\sigma_1^{-1}, \qquad 1 \le r \le g$
  - $\sigma_1^{-1}b_r\sigma_1^{-1}b_r = b_r\sigma_1^{-1}b_r\sigma_1^{-1}, \qquad 1 \le r \le g$
  - $\sigma_1^{-1}a_s\sigma_1 a_r = a_r\sigma_1^{-1}a_s\sigma_1, \qquad 1 \le s < r \le g$
  - $\sigma_1^{-1}b_s\sigma_1 b_r = b_r\sigma_1^{-1}b_s\sigma_1, \qquad 1 \le s < r \le g$
  - $\sigma_1^{-1}a_s\sigma_1 b_r = b_r\sigma_1^{-1}a_s\sigma_1, \qquad 1 \le s < r \le g$
  - $\sigma_1^{-1}b_s\sigma_1 a_r = a_r\sigma_1^{-1}b_s\sigma_1, \qquad 1 \le s < r \le g$
  - $\sigma_1^{-1}a_r\sigma_1^{-1}b_r = b_r\sigma_1^{-1}a_r\sigma_1, \qquad 1 \le s < r \le g$
  - $[a_1, b_1^{-1}] \dots [a_g, b_g^{-1}] = \sigma_1\sigma_2 \dots \sigma_{2n-1}^2 \dots \sigma_2\sigma_1$

where $[a, b^{-1}] = ab^{-1}a^{-1}b$.

Now we will describe how to represent a link L in M with an element of this group in our setting. Fix a set of n arcs $\gamma_1, \dots, \gamma_n$ embedded into Σ_g, with Σ_g being a genus g Heegaard surface for M, such that $\gamma_i \cap \gamma_j = \emptyset$ if $i \ne j$ and $\partial\gamma_i = \{P_{2i-1}, P_{2i}\}$, for $i, j = 1, \dots, n$. Given an element $\beta \in \mathcal{B}_{g,2n}$, realize it as a geometric braid, that is, as a set of $2n$ disjoint paths in $\Sigma_g \times [0, 1]$ connecting $\mathcal{P}_{2n} \times \{0\}$ to $\mathcal{P}_{2n} \times \{1\}$. The *plat closure* $\hat{\beta} \subseteq M$ of β is the link obtained "closing" β by connecting $P_{2i-1} \times \{0\}$ with $P_{2i} \times \{0\}$ through $\gamma_i \times \{0\}$ and $P_{2i-1} \times \{1\}$ with $P_{2i} \times \{1\}$ through $\gamma_i \times \{1\}$, for $i = 1, \dots, n$. Clearly, $\hat{\beta}$ is in bridge position with respect to Σ_g and so it has genus g bridge number at most n. For each link L in a 3-manifold M, there exists a braid $\beta \in \cup_{n\in\mathbb{N}}\mathcal{B}_{g,2n}$ such that $\hat{\beta}$ is isotopic to L [17].

It is possible to prove an Alexander representation theorem:

Theorem 2.2.3 ([10])**.** *Every link L in a 3-manifold M having Heegaard genus at most g, may be braided to a geometric braid in $\mathcal{B}_{g,2n}$, the plat closure of which is equivalent to L.*

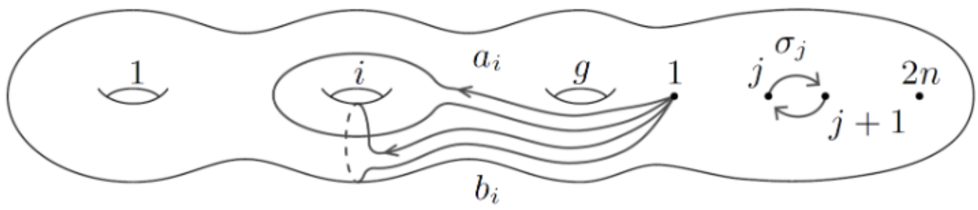

Figure 2.18: The generators of $\mathcal{B}_{g,2n}$ on Σ_g, reproduced from [17].

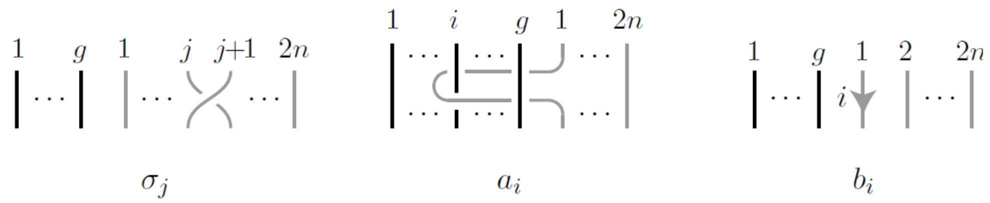

Figure 2.19: The generators of $\mathcal{B}_{g,2n}$ represented in braid form.

Moreover, as proved in [17], two braids $\beta_1, \beta_2 \in \bigcup_{n\in\mathbb{N}} \mathcal{B}_{g,2n}$ have isotopic plat closure if and only if β_1 and β_2 differ by braid isotopy, a finite sequence of the following moves (see Fig.2.20):

$(M1)$ $\quad \sigma_1\beta \longleftrightarrow \beta \longleftrightarrow \beta\sigma_1$

$(M2)$ $\quad \sigma_{2i}\sigma_{2i+1}\sigma_{2i-1}\sigma_{2i}\beta \longleftrightarrow \beta \longleftrightarrow \beta\sigma_{2i}\sigma_{2i+1}\sigma_{2i-1}\sigma_{2i}$

$(M3)$ $\quad \sigma_2\sigma_1^2\sigma_2\beta \longleftrightarrow \beta \longleftrightarrow \beta\sigma_2\sigma_1^2\sigma_2$

$(M4)$ $\quad a_j\sigma_1^{-1}a_j\sigma_1^{-1}\beta \longleftrightarrow \beta \longleftrightarrow \beta a_j\sigma_1^{-1}a_j\sigma_1^{-1}$ for $j = 1, \dots, g$

$(M5)$ $\quad b_j\sigma_1^{-1}b_j\sigma_1^{-1}\beta \longleftrightarrow \beta \longleftrightarrow \beta b_j\sigma_1^{-1}b_j\sigma_1^{-1}$ for $j = 1, \dots, g$

$(M6)$ $\quad \beta \longleftrightarrow T_k(\beta)\sigma_{2k}$

where $T_k : \mathcal{B}_{g,2n} \to \mathcal{B}_{g,2n+2}$ is defined by $T_k(a_i) = a_i,\ T_k(b_i) = b_i$ and

$$T_k(\sigma_i) = \begin{cases} \sigma_i & \text{if } i < 2k \\ \sigma_{2k}\sigma_{2k+1}\sigma_{2k+2}\sigma_{2k+1}^{-1}\sigma_{2k}^{-1} & \text{if } i = 2k \\ \sigma_{i+2} & \text{if } i > 2k \end{cases} .$$

and two sets of moves called *plat slide moves* and *dual plat slide moves* that depend on the Heegaard decomposition of M. If $(\Sigma_g, \mathbf{c}, \mathbf{c}^*)$ is a Heegaard diagram for M, we define these two moves as the band connected sum between the link and the curves c_i and c_i^* respectively.

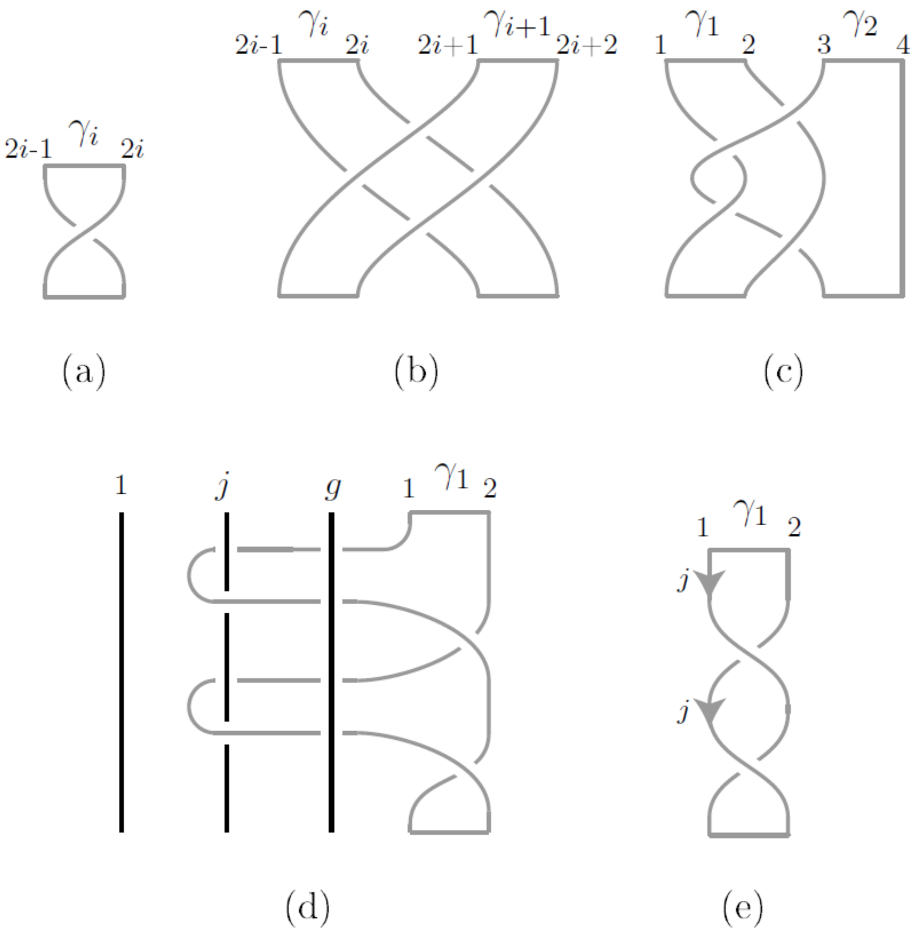

Figure 2.20: The five M-moves $(M1) - (M5)$, reproduced from [17]. Note that $(M6)$ is indeed the stabilization move.

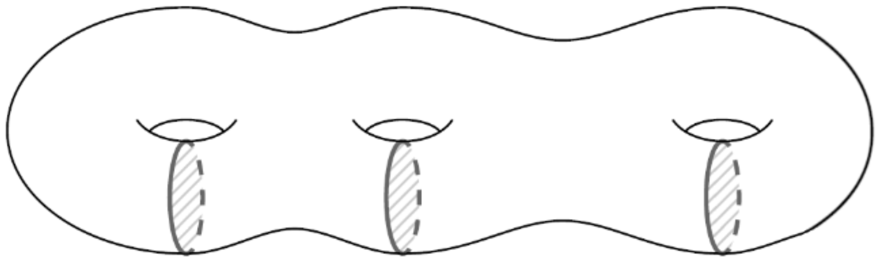

Figure 2.21: The standard decomposition of a genus g handlebody.

Since all c_i and c_i^* bound meridian disks in M and thus are trivial knots in M, they can be represented in $\mathcal{B}_{g,2}$ [17]. We can then describe the plat connected sum in braid form: if $\beta \in \mathcal{B}_{g,2n}$ is a braid representative of L and $\bar{c}_i, \bar{c}_i^*$ are braid representatives of c_i, c_i^* then

$$psl_i : \beta \longrightarrow \bar{c}_i \# \beta \in \mathcal{B}_{g,2n},\ i = 1, \dots, g$$

$$psl_i^* : \beta \longrightarrow \beta \# \bar{c}_i^* \in \mathcal{B}_{g,2n},\ i = 1, \dots, g$$

which are called the *i-th plat slide* and *i-th dual plat slide move.* We recall that we denote with $L_1 \# L_2$ the band sum between L_1 and L_2. If we assume that $\mathbf{c}^*$ is the system corresponding to the standard decomposition of a genus g handlebody (see Fig. 2.21), then we have $c_i^* = \widehat{b_i}$ and so the dual plat slide move psl_i^* is

$$psl_i^* : \beta \longrightarrow \beta \# b_i = \beta b_i$$

In [17] an explicit formula for plat slide moves in lens spaces $L(p, q)$ (i.e., the case of genus one) can be found as:

$$psl_{p,q} :\ \beta \longrightarrow \alpha_{p,q} \# \beta = \alpha_{p,q}\, \beta,$$

where

$$\alpha_{p,q} = \prod_{i=1}^{r} b_1^{-1} a_1^{\lceil \frac{p}{q} \rceil} \cdot \prod_{i=1}^{q-r} b_1^{-1} a_1^{\lfloor \frac{p}{q} \rfloor} \in \mathcal{B}_{1,2}.$$

An example of this result can be seen in Fig.2.22 for $L(5, 2)$.

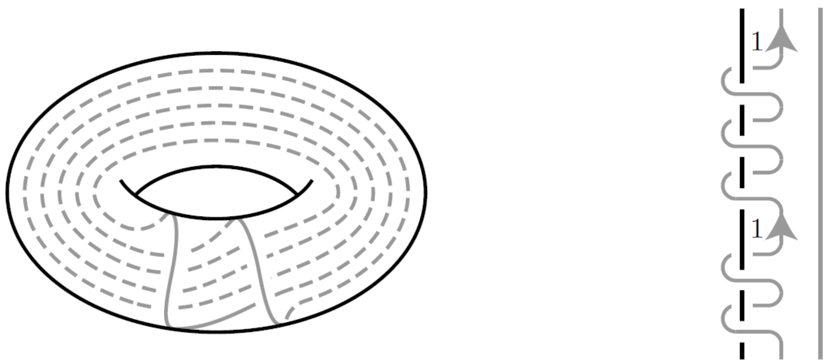

Figure 2.22: The example for $L(5, 2)$, reproduced from [17].

Chapter 3

An algorithmic method to compute plat-like Markov moves for genus two 3-manifolds

As seen in Section 2.2, the equivalence of links in 3-manifolds, under isotopy, has been described in terms of (g, b)-decomposition: we reported a finite set of moves that connect braids in $\mathcal{B}_{g,2n}$ having isotopic plat closures. In the result, some moves are explicitly described as elements in $\mathcal{B}_{g,2n}$, while others, called plat slide moves, depend on a Heegaard surface of the manifold and are explicitly described only for the case of Heegaard genus at most 1, that is for S^3, lens spaces and $S^2 \times S^1$. The goal of this chapter is to determine plat slide moves for links in 3-manifolds of genus 2. Our approach uses the representation described in Section 1.3.2 connected with crystallization theory. To sum up, every 3-manifold of Heegaard genus 2 can be represented using a 4-colored graph depending on a 6-tuple of integer numbers that determines some of its Heegaard splittings. Starting from the 6-tuple, we will construct an algorithm (also implemented on the computer) that allows to describe the plat slide moves associated to the Heegaard surface of a particular Heegaard splitting in terms of elements in $\mathcal{B}_{2,2n}$ and so to determine explicitly the moves realizing the equivalence of links in plat form in the associated 3-manifold.

Let us take an admissible 6-tuple $f = (h_0, h_1, h_2, q_0, q_1, q_2)$. Our goal is to precisely draw the open Heegaard diagram representing the 3-manifold encoded by f relying only on the values of the 6-tuple. Let Γ be a crystallization of a 3-manifold, let C_0, C_1, C_2, D_0, D_1, D_2 and Σ_2 the two sets of bicolored cycles and the genus two surface from the construction of Theorem 1.3.1; we recall from Section 1.3.2 the definition of rich Heegaard diagram as the colored graph obtained by removing the cycle C_2, cutting the Σ_2 along C_0 and C_1 and coloring with the same color the arcs belonging to the same D_i.

Here we will use edges with labels in order to describe blocks; for example in Fig. 3.1a there are a parallel edges from C_1^+ to C_0^+, and we denote them with a single edge with label a.

We are ready to prove the first theorem of this chapter.

Theorem 3.0.1. *Let $f = (h_0, h_1, h_2, q_0, q_1, q_2)$ be an admissible 6-tuple.*

1. *If $q_2 < h_1, h_2$ then the rich Heegaard diagram R_f is the one depicted in Fig. 3.1a, with $a = h_0,\ b = q_2,\ c = h_2 - q_2,\ d = h_1 - q_2$;*

2. *If $h_2 \leq q_2 \leq h_1$ then the rich Heegaard diagram R_f is the one depicted in Fig. 3.1b, with $a = h_0, b = h_2, c = q_2 - h_2, d = h_1 - q_2$;*

3. *If $h_1 < q_2 < h_2$ then the rich Heegaard diagram R_f is the one depicted in Fig. 3.1c, with $a = h_0, b = h_1, c = q_2 - h_1, d = h_2 - q_2$;*

4. *If $q_2 > h_1, h_2$ then the rich Heegaard diagram R_f is the one depicted in Fig. 3.1d, with $a = h_0, b = h_1 + h_2 - q_2, c = q_2 - h_1, d = q_2 - h_2$;*

and vertices are labeled as in Fig. 3.3.

Proof. Following the construction in Section 1.3.2, let Γ be a 4-colored crystallization and consider $\Gamma_{\hat{3}}$ and $\Gamma_{\hat{2}}$, with $C_i^{\pm}$ as in Fig. 1.19. Now we "flip horizontally" $\Gamma_{\hat{2}}$, then we glue together C_2^+ with C_2^- and "cut it open" as follows: by cutting the genus 2 surface $F_{\{0,1\}}$ along C_0 and C_1 we get a diagram on the sphere with four holes with C_2 as the equator and the two halves of C_1 and C_0 on opposite emispheres (see Fig. 3.2). For $i = 0, 1$ we give a standard clockwise orientation to C_i^-, a standard counterclockwise orientation to C_i^+, and an orientation

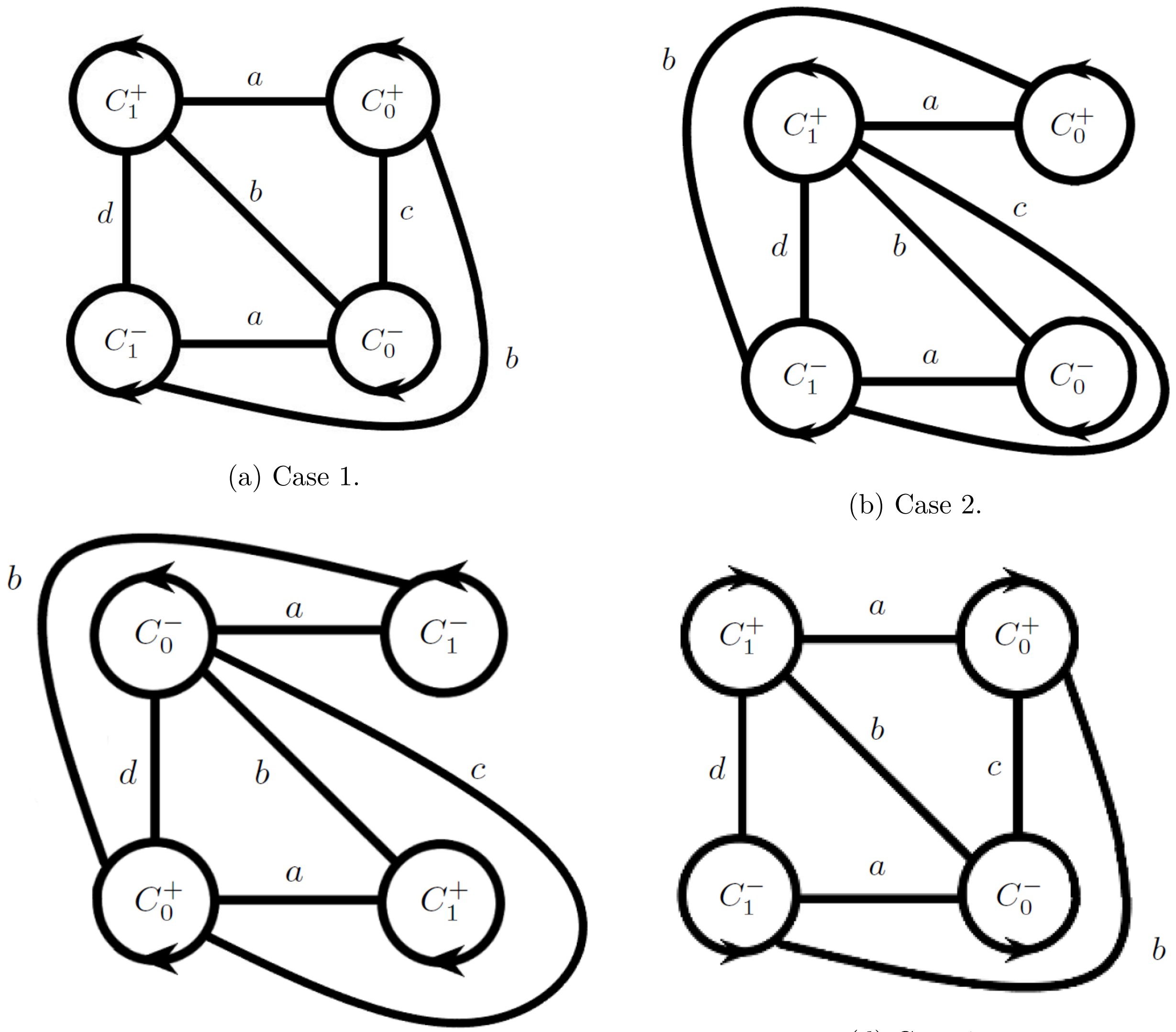

(a) Case 1.

(b) Case 2.

(c) Case 3.

(d) Case 4.

Figure 3.1: The four possible cases.

from right to left to C_2.

According to the definition of the involutions τ_c, for $c = 0, 1, 2, 3$, the labelling of the vertices of $C_0^{\pm}, C_1^{\pm}$ is as follows (see Fig. 3.3). First, check the orientation of $C_i^{\pm}$. In C_0^+ (resp. C_0^-), the first vertex adjacent to a vertex of C_1^+ (resp. C_1^-) with respect to the orientation is labelled '0' (resp. 'q_0'). This vertex is connected to the vertex of C_1^+ (resp. C_1^-) labelled '$h_0 + h_1 - 1$' (resp. '$q_1 - 1$').

We can then label all the vertices of C_0^+ and C_1^+ according to the orientation.

It is important to note that in case 4, where we have a different orientation, the labeling is the

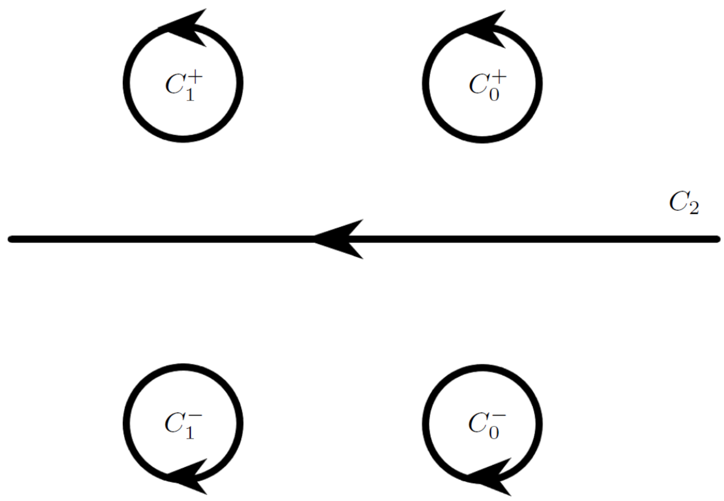

Figure 3.2: The standard orientation.

same.

From now on, C_2 will only be useful in term of the construction of the $\{2,3\}$-residues via τ_c.

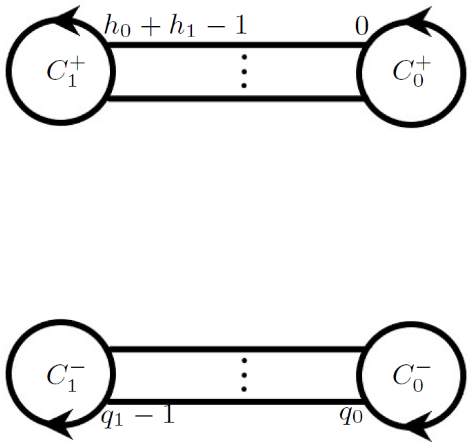

Figure 3.3: The labelling of $C_0^{\pm}$, $C_1^{\pm}$.

Following the definition of τ_2 and τ_3, we observe that (see Fig. 3.4a):

- exactly h_0 arcs go from $C_0^{\pm}$ to $C_1^{\pm}$ and so $a = h_0$;
- exactly h_2 arcs go from $C_0^{\pm}$ to C_2;
- exactly h_1 arcs go from $C_1^{\pm}$ to C_2.

The involution τ_3 on the vertices of C_2 differs from τ_2 by a "circular shifting" of q_2 steps that connects C_2 to C_0^- and C_1^-. The shifting is exactly q_2 in the positive direction according to the fixed orientation (as depicted in Fig. 3.4b).

When we remove C_2 in order to obtain the open rich Heegaard diagram, all we have to do is to merge the connecting arcs, obtaining:

- an arc from C_0^+ to C_0^- if both arcs come from the h_2 arcs;
- an arc from C_1^+ to C_1^- if both arcs come from the h_1 arcs;
- an arc from C_1^+ to C_0^- if the upper arc comes from the h_1 arcs and the lower one comes from the h_2 arcs;
- an arc from C_0^+ to C_1^- if the upper arc comes from the h_2 arcs and the lower one comes from the h_1 arcs;

The two last kind of arcs are in the same quantity: indeed, when we shift an h_2 lower arc so that it is connected to an upper h_1 one, we obtain an arc from C_1^+ to C_0^- and at the same time an h_1 lower arc is connected to an upper h_2 one.

Now, depending on the values of h_1, h_2 and q_2 we can have four different cases:

1. If $q_2 < h_1, h_2$, we are in the situation depicted in Fig. 3.4b: here q_2 arcs of the h_1 lower ones are moved to the right. So we obtain a graph like the one in Fig. 3.1a. We have exactly q_2 arcs from upper h_1 to lower h_2, so $b = q_2$. Since the remaining lower arcs from h_2 go into upper h_2 ones, we have $c = h_2 - q_2$. Lastly, in order to balance the accounts for the lower h_1 arcs, we get $d = h_1 - q_2$.

2. If $h_2 \leq q_2 \leq h_1$, we are in the situation depicted in Fig. 3.4c: as before, all the h_2 lower arcs go into upper h_1 ones and q_2 arcs of the h_1 lower ones are moved to the right. So we obtain a graph like the one in Fig. 3.5a. We have all the lower h_2 arcs going to upper h_1 ones, so $b = h_2$. To determine c and d we need to count how many arcs are there on the right and on the left. Keeping track of q_2 and of the hypothesis $h_2 \leq q_2 \leq h_1$, on the

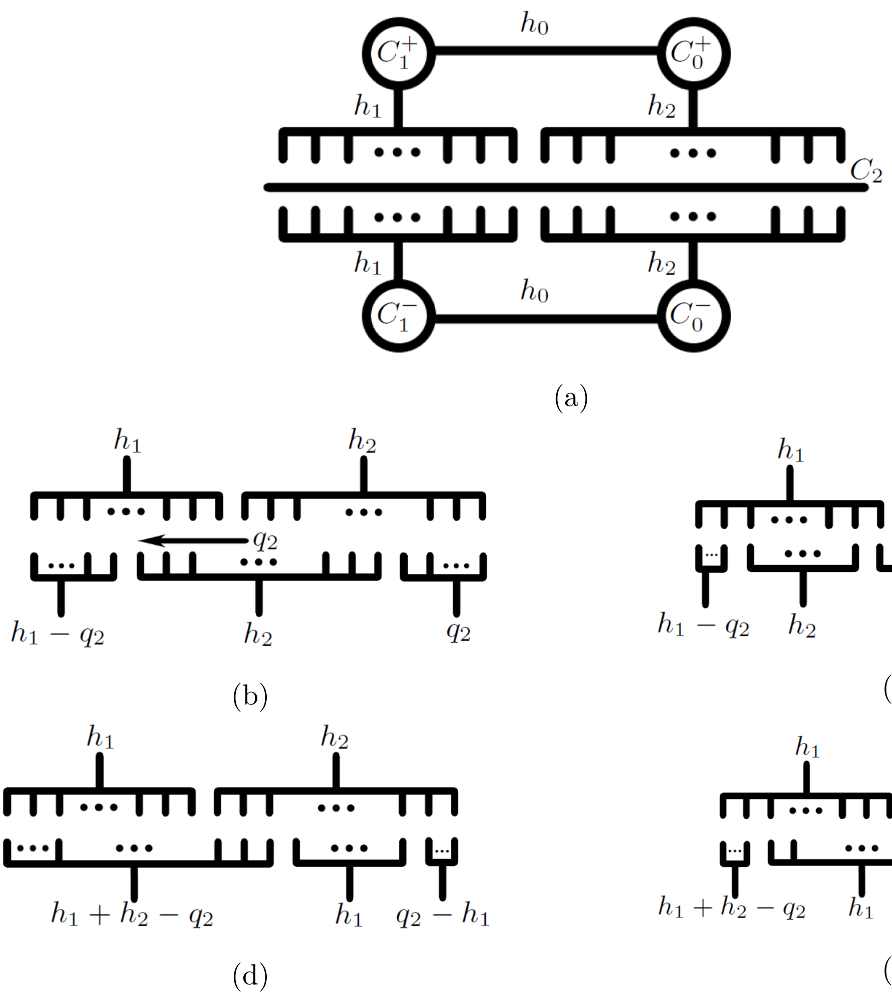

Figure 3.4: The starting position and the four possible arcs positions.

right there are $q_2 - h_2 = c$ arcs while on the left there are $h_1 - q_2 = d$ arcs.

Using a homeomorphism of the sphere invariant on the set of vertices, we can transform the diagram of Fig. 3.5a into the one of Fig. 3.1b, passing the right b arcs onto the left.

3. If $h_1 < q_2 < h_2$, we are in the situation depicted in Fig. 3.4d: here all the h_1 lower arcs and $q_2 - h_1$ lower h_2 arcs are moved to the right. So, we obtain a graph like the one in Fig. 3.5b. We have all the h_1 lower arcs going to upper h_2 ones, so $b = h_1$. As before, to determine c and d we need to count how many arcs are there on the right and on the left. Keeping track of q_2 and of the hypothesis $h_1 < q_2 < h_2$, on the right there are $q_2 - h_1 = c$ arcs while on the left there are $h_2 - q_2 = d$ arcs.

   Using a homeomorphism of the sphere invariant on the set of vertices, we can transform the diagram of Fig. 3.5b into the one of Fig. 3.1c, passing the right d arcs onto the left and flipping the diagram horizontally and vertically.

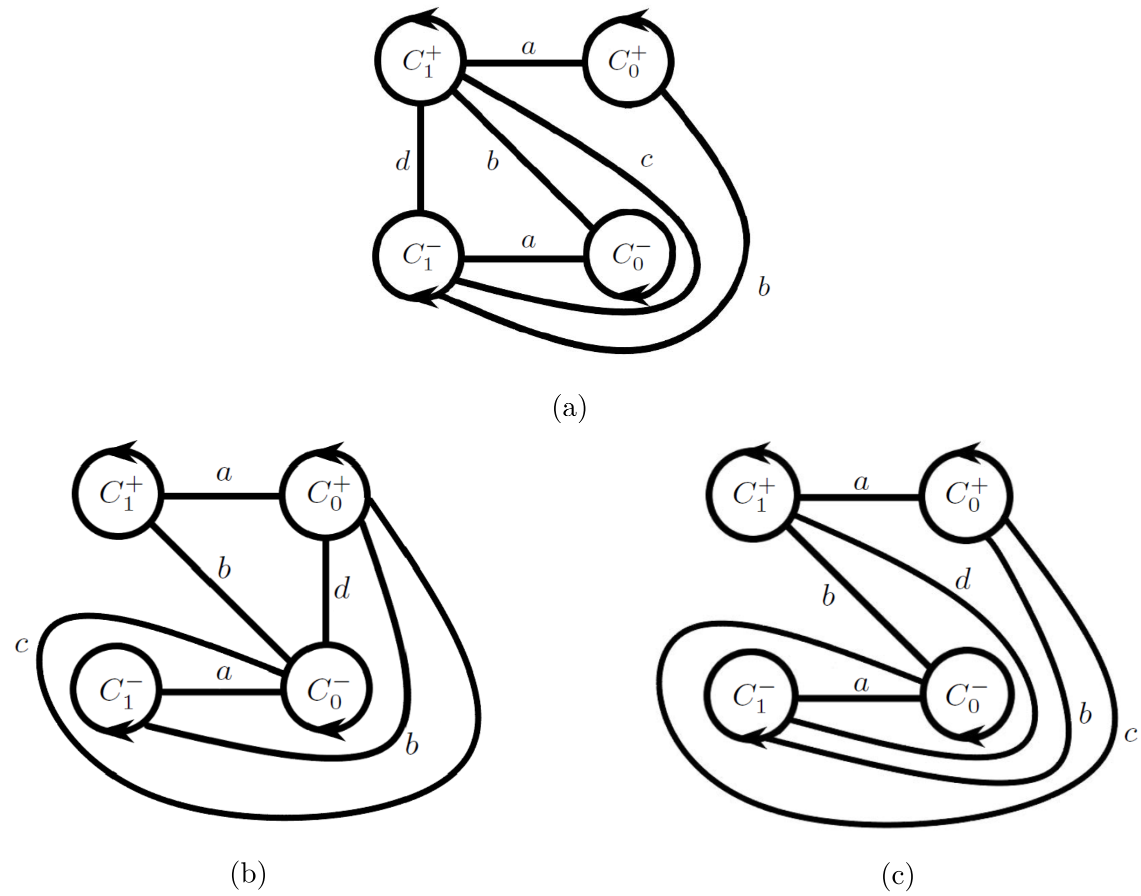

Figure 3.5: The three unrefined configurations.

4. If $q_2 > h_1, h_2$, we are in the situation depicted in Fig. 3.4e: as before, all h_1 lower arcs and $q_2 - h_1$ lower h_2 arcs are moved to the right. So, we obtain a graph like the one in Fig. 3.5c, where $b = h_1 + h_2 - q_2$, $d = h_1 - (h_1 + h_2 - q_2) = q_2 - h_2$ and $c = q_2 - h_1$. Using a homeomorphism of the sphere invariant on the set of vertices, we can transform the diagram of Fig. 3.5c into the one of Fig. 3.6a, passing the right c arcs onto the left. Then, following the red arrows, we can shift both C_0^+ and C_0^- on the left of $C_1^\pm$ (see Fig. 3.6b). The diagram of Fig. 3.1d is obtained flipping it horizontally.

This ends the proof. □

In Fig. 1.21 it is depicted the rich Heegaard diagram obtained from the 6-tuple $f = (4, 6, 10, 1, 1, 1)$; the manifold M_f is the Poincaré sphere.

Remark 2. The normalization of the diagrams that we apply by using homeomorphisms of the

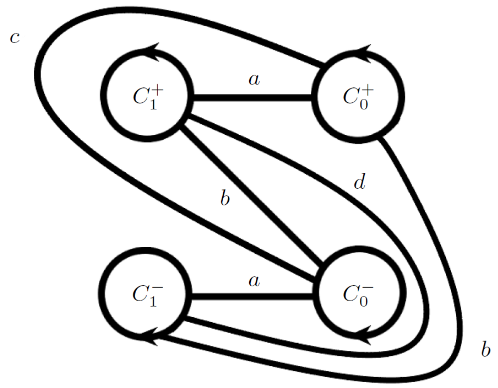

(a)

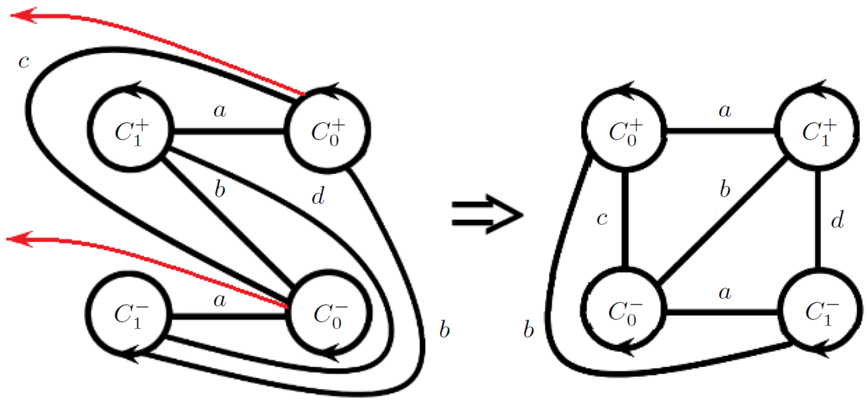

(b)

Figure 3.6: Dealing with the fourth case.

sphere in all cases different from the first one are not essential, but they are done in order to obtain a normalized diagram in the sense of Section 1.1.1. As we saw before, there are three possible classes of genus 2 open Heegaard diagrams. Since we are interested only in manifolds (and not in their splittings), the class III is not necessary (for the certain presence of α-waves). Indeed, the diagrams that we obtain in the previous result belong to the classes I and II.

3.1 The algorithmic construction of plat moves

In this section, starting from the 6-tuple f, we construct an algorithm that allows to describe, in terms of elements in $\mathcal{B}_{2,2n}$, the plat slide moves in M_f associated to the Heegaard diagram obtained from R_f.

First of all, we need to fix some notation on the genus 2 surface. Referring to Fig. 3.7, we denote with $b_l, b_r, a_l, a_r, \sigma$ the standard generators of $\mathcal{B}_{2,2}$, where "l" and "r" stand for left and right. Moreover, we identify the boundary circles of the 4-holed sphere containing R_f with the meridians $C_{Tr}, C_{Tl}, C_{Br}, C_{Bl}$, where "$T$" stands for top and "$B$" for bottom, so that C_{Tl} is identified with C_1^+ in case 1, 2, 4 of Proposition 3.0.1 (corresponding to pictures 3.1a, 3.1b, 3.1d respectively) and with C_0^- in case 3 (corresponding to picture 3.1c). The four meridians are oriented as depicted in the figure in cases 1, 2, 3, while we take the opposite orientation for all of them in case 4.

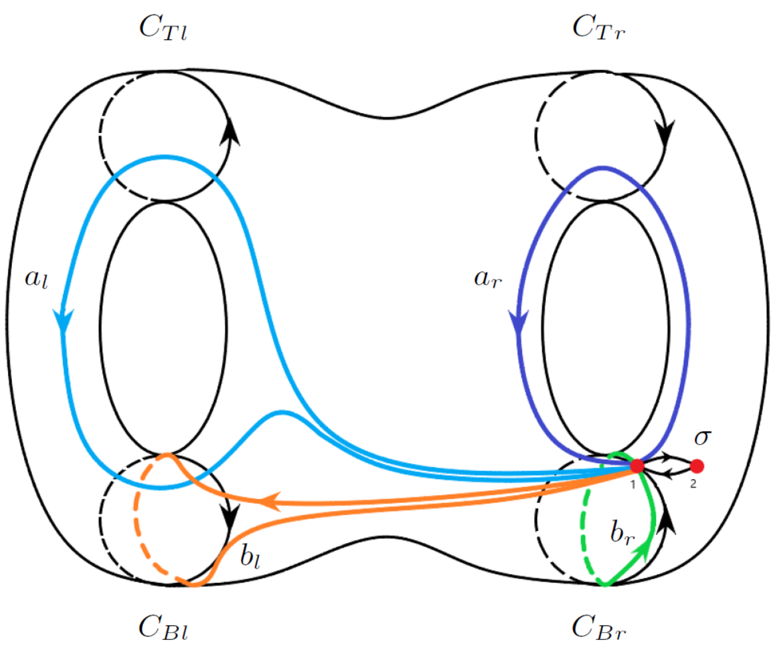

Figure 3.7: The genus 2 surface.

We represent in red the arcs of R_f on this surface (see Fig. 3.8a for an example). Clearly, according to these identifications, some (or part of) arcs, as well as some vertices, are contained in the "back part" of the surface (and so are dashed in figures) while some others are in the "front one" (and are not dashed in figures); more precisely:

- all the labelled b arcs of figure 3.1 connecting C_{Tr} and C_{Bl} are as depicted in Fig. 3.11h, that is, their end-points are in the back part;
- the labelled c arcs of figure 3.1 connecting C_{Tl} and C_{Bl} are as depicted in Fig. 3.11j, that is, their end-points on C_{Tl} are in the front while those on C_{Bl} are in the back;

All the remaining vertices and arcs are in the front part.

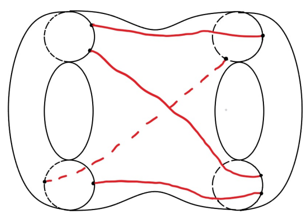

(a) $(3,3,3,2,2,2)$ only red arcs.

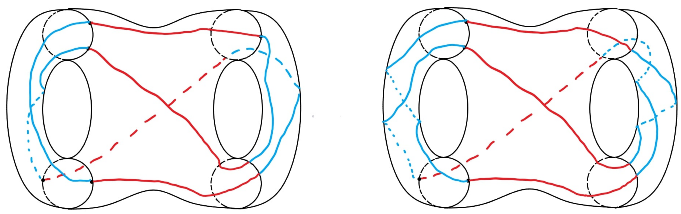

(b) Two ways to connect the arcs of the $(3,3,3,2,2,2)$.

Figure 3.8: The $(3,3,3,2,2,2)$ case.

On the surface we have also arcs, represented in blue, arising from the identification of C_i^+ with C_i^-, $i = 0, 1$. Clearly, those arcs are contained in the two handles bounded by C_{Tl} and C_{Bl} on the left and C_{Tr} and C_{Br} on the right, and connect the couple of vertices with the same label in the corresponding top and bottom circles, eventually winding around the handle (see an example in Fig. 3.8b).

To avoid ambiguity we describe precisely how the connections are realized. Following their orientation, denote by X (resp. Y) the first (resp. last) vertex in the front part of both C_{Bl} and C_{Tr}, as well as the corresponding vertices in C_{Tl} and C_{Br}. Now denote by L:

- the first (resp. last) vertex of C_{Tl} connected a bottom circle;
- the last (resp. first) vertex of C_{Br} connected to a left circle in the first three cases (resp. in case 4) of Proposition 3.0.1, as well as the corresponding vertices in C_{Bl} and C_{Tr};

Moreover, given two vertices A, B on one circle, we denote with $\widehat{AB}$ the oriented arc from A to B (end-points included). Now we focus on the first three cases of Proposition 3.0.1. If $L \in \widehat{XY}$, connect:

- each vertex in $\widehat{LX} \subset C_{Ti}$, with the exception of X, with the corresponding vertex in C_{Bi} winding once along the handle in the direction of b_i, with $i = l, r$;

- all the other vertices without winding.

Otherwise, that is if $L \notin \widehat{XY}$, connect:

- all vertices in $\widehat{XY}$ without winding;

- the vertices in the internal part of $\widehat{YL} \subset C_{Ti}$ winding once along the handle in the direction opposite to b_i;

- the remaining vertices of C_{Ti} winding once in the direction of b_i, with $i = l, r$.

In case 4, we do the following changes with respect to the previous construction: if $L \in \widehat{XY}$, the vertices labelled L in both circles are connected without winding and, in both cases, all the connections are done winding in the opposite directions.

In this way we obtain three closed curves on the surface each corresponding to one of the three colors of R_f. Note that along each curve the blue and red arcs alternate. We denote this curves with x_f^0, x_f^1, x_f^2. See the Fig. 3.9 for the three curves corresponding to $R_f = (4, 6, 10, 1, 1, 1)$.

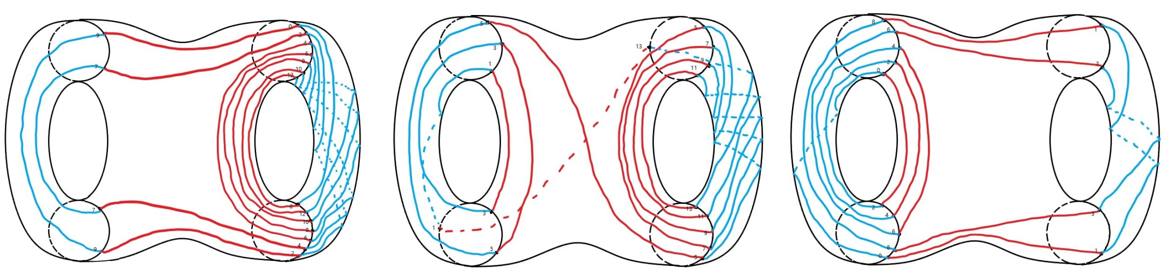

Figure 3.9: The curves x_f^0, x_f^1 and x_f^2 of $(4, 6, 10, 1, 1, 1)$.

As we have seen, any choice of a couple of curves among x_f^0, x_f^1, x_f^2 is a meridian system for a Heegaard splitting of M_f (being the other the standard one); so, in order to determine the *psl*-moves associated to such a splitting it is enough to find words $\chi_f^i \in \mathcal{B}_{2,2}$, such that $\widehat{\chi_f^i} = x_f^i$, for $i = 0, 1, 2$, and the move takes the form:

$$psl_i : \beta \to \chi_f^i \# \beta = \chi_f^i \beta$$

Theorem 3.1.1. *Let f be an admissible 6-tuple. There exists an algorithm depending only on f that computes the psl-slide moves corresponding to the Heegaard splitting associated to the rich Heegaard diagram R_f.*

Proof. It is clear, using the previous construction, that we can determine, starting from f and in an algorithmic way, the curves x_f^0, x_f^1 and x_f^2. To prove the statement we have only to describe, starting from x_f^i, how to compute the words $\chi_f^i \in \mathcal{B}_{2,2}$, $i = 0, 1, 2$. Clearly, the procedure is the same for each curve.
First of all, we orient x_f^i as follows. In case 1, 2, 3 (resp. 4) (see Fig. 3.1) we orient the curve so that a red arc exits from the last (resp. first) vertex on C_{Br}. If the curve has no intersection with C_{Br} then we orient the curve so that a red arc exits from the last (resp. first) vertex on C_{Bl}. In fact, at least two of three curves must intersect each C_i otherwise it would not be a proper Heegaard diagram [27]. In Fig. 3.10a and Fig. 3.11 we depict all the unwound different cases emerging from considering, along x_f^i, a couple of consecutive red and blue arcs: clearly in each case a possible winding of the blue arc in both the directions may appear (see Fig. 3.10b and Fig. 3.10c). We associate to each of the previous cases a closed loop by connecting the arc to a based point in a standard way through the violet or green arc (see Fig. 3.10d, 3.10e, 3.10f and Fig. 3.12). Now we interpret each loop as an element of $\mathcal{B}_{2,2}$ and call them "elementary words". All possible cases are depicted in Fig. 3.11.

We start with the first case, see Fig. 3.10a and Fig. 3.10d: clearly the word associated is a_l. The cases in Fig. 3.10b (resp. 3.10c) differ from the previous one for an outer (resp. inner) winding: we obtain $a_l b_l$ (resp. $a_l b_l^{-1}$) with the isotopy realized along the dashed disk as in Fig. 3.10e (resp. Fig. 3.10f). Note that the winding part affects the latter part of the word.

In general the same happens in the other cases, except for the last four where the situation needs to be studied carefully. The words that we obtain, without winding, are the following (see Fig. 3.12 for the related cases):

(a) a_r;

(b) a_r^{-1};

(c) a_l^{-1};

(d) the green one is a_r^{-1}, the violet one a_l;

(e) the green one is a_r, the violet one a_l^{-1};

(f) the green one is a_l, the violet one a_r^{-1};

(g) the green one is a_l^{-1}, the violet one a_r.

Now we discuss the last four cases that are affected differently by the winding:

(h) In this case (see Fig. 3.13) the word depends on the blue arc of the previous couple, so different cases arise due to this feature. More precisely, we have $b_l b_r^{-1} a_r^{-1} b_r$ if the blue arc is of type b_r^{-1} and previous blue arc is of type b_l^{-1}; otherwise we delete the first b_l or the last b_r;

(i) analogously to the previous case, we have $b_r^{-1} b_r a_l^{-1} b_l^{-1}$ if the blue arc is of type b_l and the previous blue arc is of type b_r; otherwise we delete the first b_r^{-1} or the last b_l^{-1};

(j) $b_r a_l^{-1} b_l^1$ if the blue arc is of type b_l; otherwise we delete the last b_l^{-1};

(k) $b_l b_r^{-1} a_l$ if the previous blue arc is of type b_l^{-1}; otherwise we delete the first b_l.

Traveling along x_f^i and chaining the elementary words we obtaing the word representing $\chi_f^i \in \mathcal{B}_{2,2}$, $i = 0, 1, 2$. □

3.2 Program and examples

In this last section, we describe the algorithm implemented in `C++` which realizes the procedure described in the previous sections. The source code can be found on GitHub [2]. Moreover, we report the results of the computation for a family of examples taken from [7].

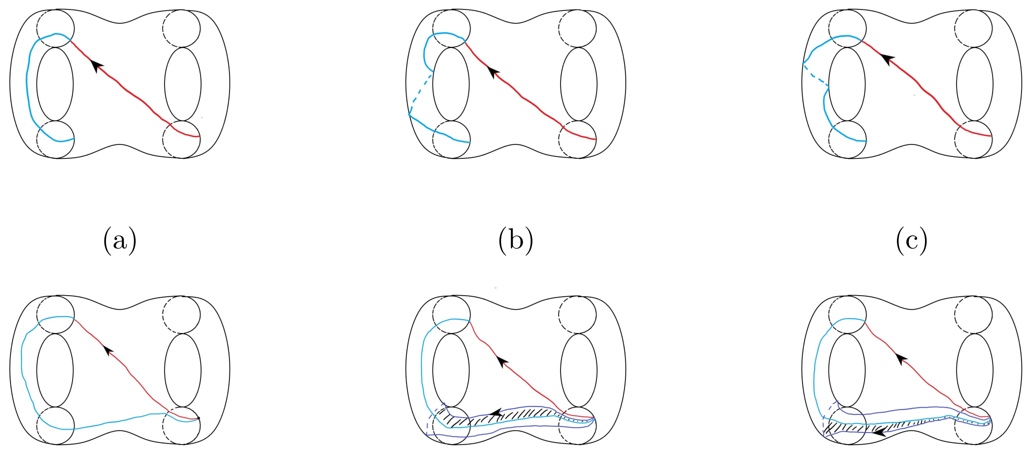

(a) (b) (c) (d) (e) (f)

Figure 3.10: The first case with all the possible windings.

The implementation is straightforward. After identifying among the different cases the one our 6-tuple belongs to, all the variables are initialized by using Proposition 3.0.1. Then, after computing all the connections and identifications, the software firstly keeps track of the words related to the single arcs then finds the three x^i_f. The words χ^i_f are then computed following each x^i_f. If during the construction phase exactly three x^i_f's are not found, it means that $f \notin \mathcal{F}$ and the program exits with an error.

We used the program to compute the plat-slide moves associated to the 6-tuples described in [7] together with the associated orientable manifold. In this article it is shown that there exist exactly 78 non-homeomorphic, closed, orientable, prime 3-manifolds with Heegaard genus two, admitting a coloured triangulation with at most 42 tetrahedra, each manifold being identified by a 6-tuple. In [7] the census is also extended (by means of a computer program) also to the non-orientable case.

Our goal is to find, for each one of the different 6-tuples in the orientable case, the three words associated to the curves of the Heegaard diagrams encoded by the 6-tuples.
The results are collected in the following tables, where we used the following notation:

- S^3/G is the quotient space of S^3 by the action of the group G; the involved groups are:
    - $Q_{4n} = < x, y \mid x^2 = (xy)^2 = y^n >$

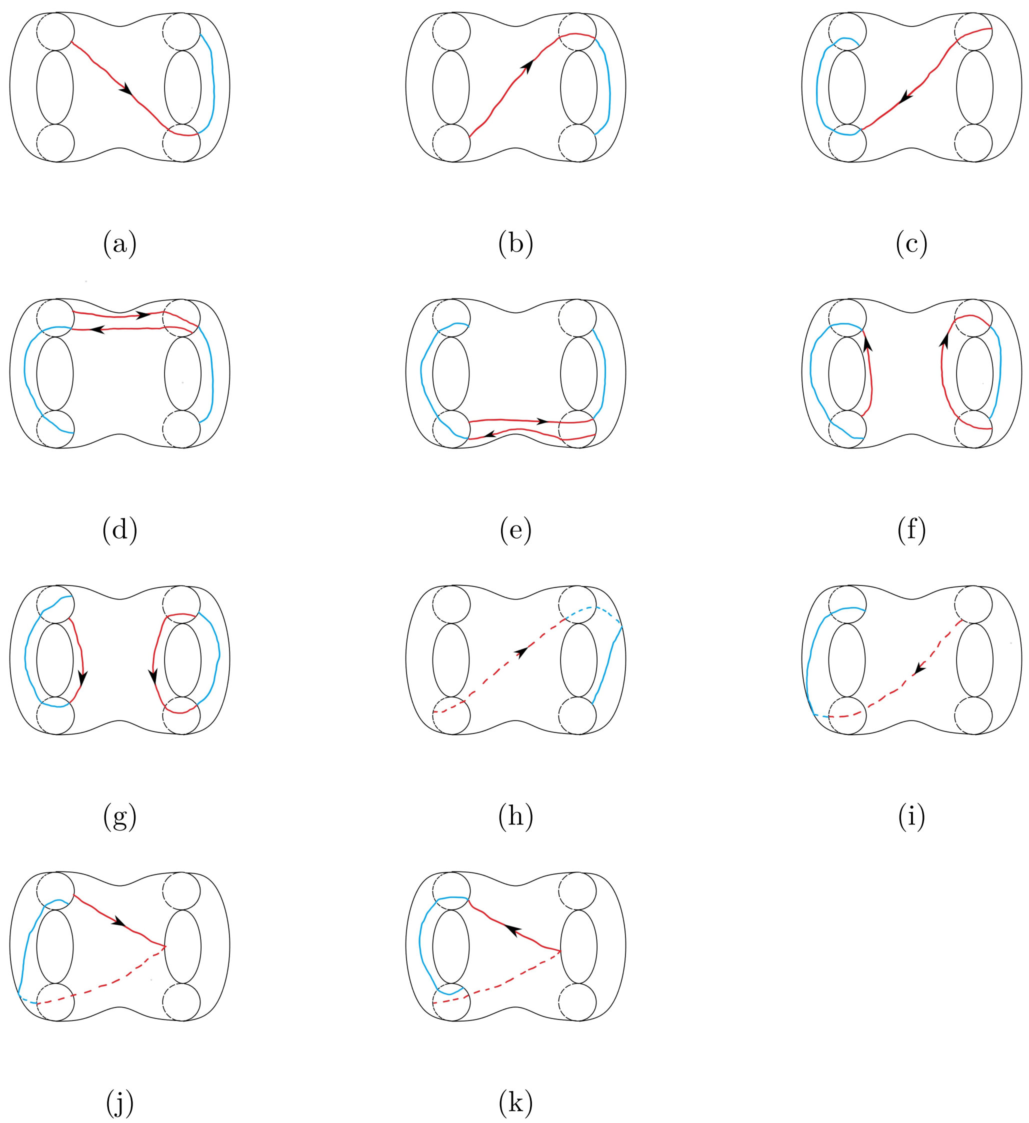

Figure 3.11: The remaining cases without winding.

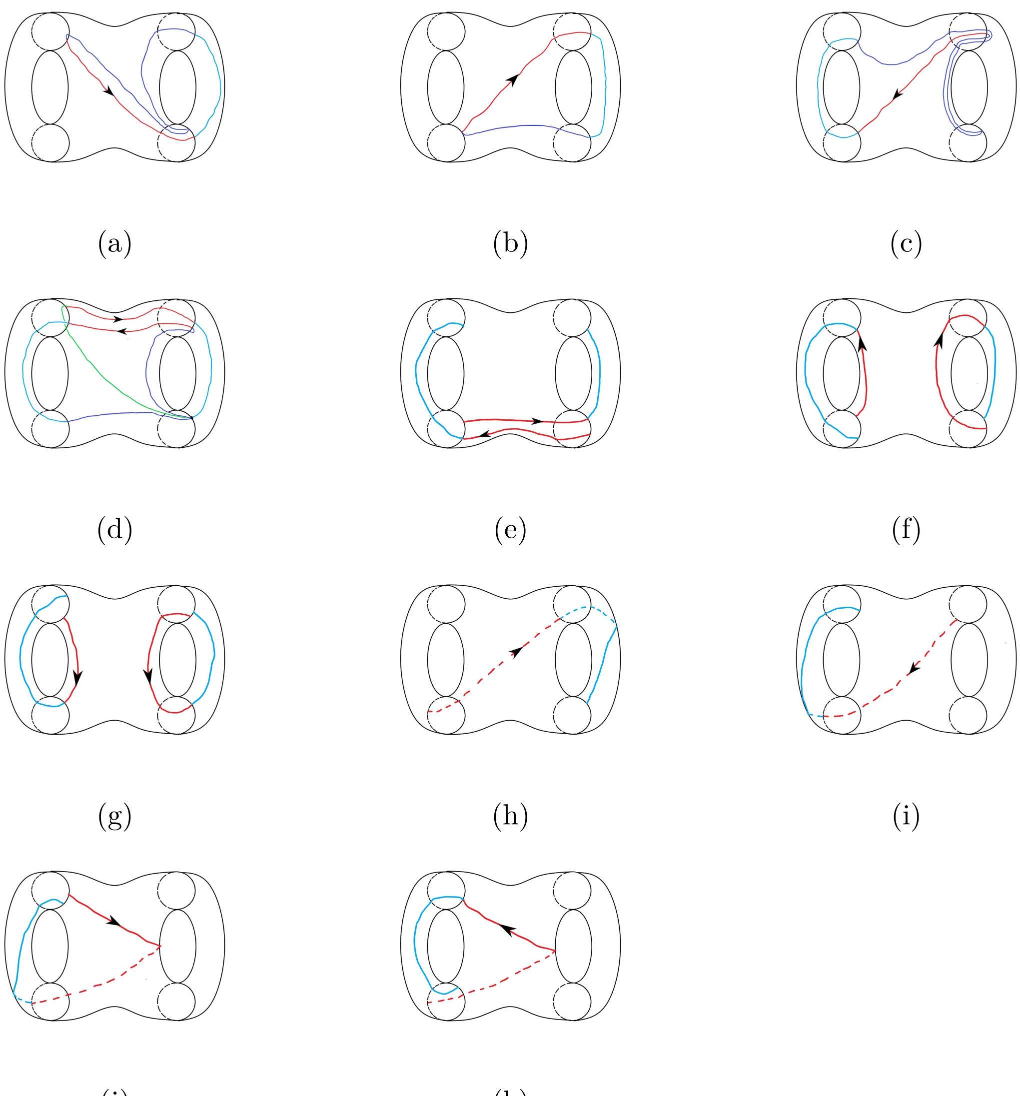

Figure 3.12: All the possible closings of the previous cases.

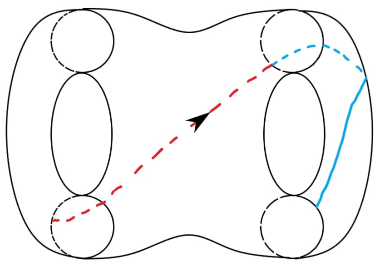

(a) With a b_l.

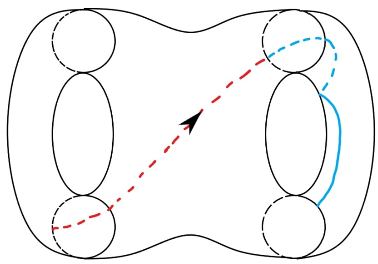

(b) With a b_l^{-1}.

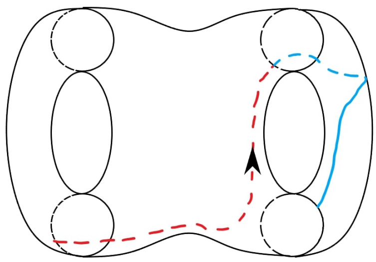

(c)

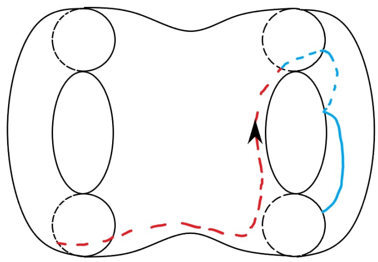

(d)

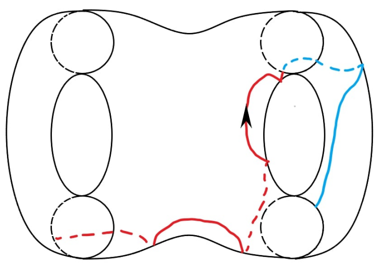

(e)

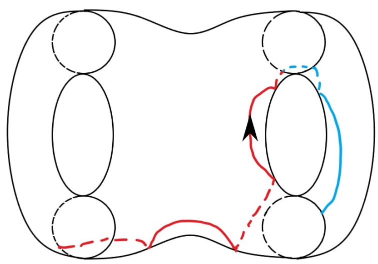

(f)

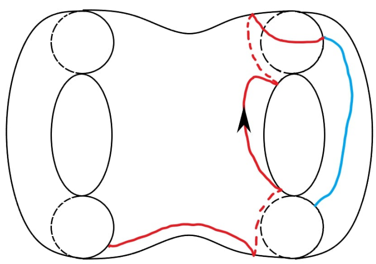

(g) Ending situation: there is still the b_l.

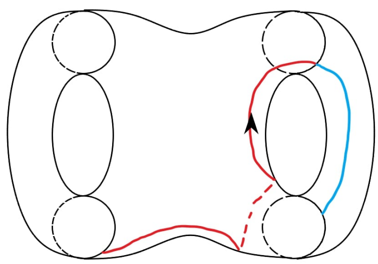

(h) Ending situation: there is no b_l^{-1}.

Figure 3.13: The case (h).

– $D_{2^k(2n+1)} = < x, y \mid x^{2^k} = 1,\ y^{2n+1} = 1,\ xyx^{-1} = y^{-1} >$, with $k \geq 3, n \geq 1$

– $P_{24} = < x, y \mid x^2 = (xy)^3 = y^3,\ x^4 = 1 >$

– $P_{48} = < x, y \mid x^2 = (xy)^3 = y^4,\ x^4 = 1 >$

– $P_{120} = < x, y \mid x^2 = (xy)^3 = y^5,\ x^4 = 1 >$

– $P'_{3^k8} = < x, y, z \mid x^2 = (xy)^2 = y^2,\ zxz^{-1} = y,\ zyz^{-1} = xy,\ z^{3^k} = 1 >$, with $k \geq 2$

– $\mathbb{Z}_n$, the cyclic group over n elements,

or direct products of these groups.

- E^3/G is the quotient space of E^3 by the action of the group G, which is described by using the International Tables for Crystallography [33].

- $(S, (\alpha_1, \beta_1), \ldots, (\alpha_n, \beta_n))$ is the Seifert fibered space whose orbit space is the surface S and having n exceptional fibers (with non-normalized parameters α_i, β_i).

- $TB(A)$, with $A \in GL(2;\mathbb{Z})$, is the torus bundle over S^1 with monodromy induced by A.

- $H_1 \cup_A H_2$ is the graph manifold obtained by gluing two Seifert manifolds H_1, H_2, with $\partial H_i = T,\ i = 1, 2$, along their boundary tori by means of the attaching map associated to matrix A.

- $Q_i(p, q)$ denotes the closed manifold obtained as the (p, q) Dehn filling of the compact manifold Q_i, whose interior is one of the 11 hyperbolic manifolds of finite volume with a single cusp and complexity at most 3 (see [46]).

The source files of the program can be found in the GitHub repository at [2].

6-tuple	**3-manifold**	**Words**
(3, 3, 3, 2, 2, 2)	S^3/Q_8	$a_r^{-1}b_ra_l^{-1}b_l^{-1}a_l^{-1}a_r^{-1}$; $a_lb_lb_r^{-1}a_r^{-1}b_ra_l^{-1}a_r^{-1}$; $a_lb_la_rb_r^{-1}a_lb_lb_r^{-1}a_r^{-1}b_r$;

Table 3.1 continued from previous page

6-tuple	3-manifold	Words
(3, 3, 5, 2, 2, 4)	S^3/Q_{12}	$a_l a_r a_l b_l^{-1} b_r^{-1} a_r^{-1} b_r^{-1}$; $a_l a_l b_l b_r^{-1} a_r^{-1} b_r a_l^{-1} a_r^{-1}$; $a_l b_l b_r^{-1} a_r^{-1} b_r a_l^{-1} b_r a_l^{-1} b_l a_r^{-1}$;
(4, 4, 4, 1, 1, 1)	S^3/Q_8	$a_r^{-1} b_r a_r^{-1} b_r a_l^{-1} a_r^{-1} b_r a_l^{-1} a_r^{-1}$; $a_r^{-1} b_r a_l a_l b_l b_r^{-1} a_r^{-1} b_r$; $a_l^{-1} a_r^{-1} b_r a_l^{-1} b_l^{-1} a_l^{-1} a_l^{-1} a_r^{-1} b_r$;
(4, 4, 4, 1, 1, 5)	S^3/D_{24}	$a_l^{-1} a_r^{-1} a_l^{-1} a_r^{-1} a_l b_l b_r^{-1} a_r^{-1} b_r$; $a_l^{-1} a_r^{-1} a_l^{-1} a_r b_r b_r a_l^{-1} b_l a_r^{-1}$; $a_l a_l b_l b_r^{-1} a_r^{-1} b_r^{-1} a_r^{-1}$;
(4, 4, 4, 3, 3, 3)	S^3/P_{24}	$a_r^{-1} b_r a_l^{-1} b_l^{-1} a_r b_r^{-1} b_r a_l^{-1} b_l^{-1} a_r^{-1}$; $a_l b_l b_r^{-1} a_r^{-1} b_r a_l^{-1} b_l^{-1} a_l^{-1} a_r^{-1}$; $a_l b_l a_r b_r^{-1} a_l b_l b_r^{-1} a_r^{-1} b_r a_l^{-1} a_r^{-1}$;
(3, 3, 7, 2, 2, 6)	S^3/Q_{16}	$a_l b_l b_r^{-1} a_r^{-1} b_r a_l^{-1} b_r a_l^{-1} b_l^{-1} a_l^{-1} b_r a_l^{-1}$ $b_l a_r^{-1} a_l b_l b_r^{-1} a_r^{-1} b_r^{-1}$; $a_l b_l b_r^{-1} a_r^{-1} b_r a_l^{-1} a_r^{-1}$; $a_l^{-1} b_r a_l^{-1} b_l a_r^{-1}$;
(4, 4, 6, 1, 1, 1)	S^3/D_{48}	$a_r^{-1} b_r a_r^{-1} b_r a_r^{-1} b_r a_l^{-1} a_r^{-1} b_r a_l^{-1} a_r^{-1}$; $a_r^{-1} b_r a_r^{-1} b_r a_l a_l b_l b_r^{-1} a_r^{-1} b_r$; $a_l^{-1} a_r^{-1} b_r a_l^{-1} b_l^{-1} a_l^{-1} a_l^{-1} a_r^{-1} b_r$;
(4, 4, 6, 1, 1, 7)	S^3/P'_{72}	$a_l^{-1} a_r^{-1} a_l^{-1} a_r^{-1} a_l b_l b_r^{-1} a_r^{-1} b_r$; $a_l^{-1} a_r^{-1} a_l^{-1} a_r a_r b_r b_r a_l^{-1} b_l a_r^{-1}$; $a_l a_l b_l b_r^{-1} a_r^{-1} b_r^{-1} a_r^{-1} a_r^{-1}$;
(4, 4, 6, 1, 5, 1)	S^3/Q_{16}	$a_r^{-1} b_r a_r^{-1} b_r a_r^{-1} b_r a_l^{-1} b_l^{-1} a_l^{-1} a_r^{-1}$; $a_r^{-1} b_r a_r^{-1} b_r a_l b_l a_r b_r^{-1} a_l b_l b_r^{-1} a_r^{-1} b_r$; $a_l^{-1} b_l^{-1} a_l^{-1} b_l^{-1} a_l^{-1} a_r^{-1} b_r a_l^{-1} b_l^{-1} a_r^{-1} b_r$;

Table 3.1 continued from previous page

6-tuple	3-manifold	Words
(4, 4, 6, 3, 3, 5)	S^3/P_{48}	$a_l a_r b_r^{-1} b_r a_l^{-1} b_l^{-1} a_r a_l b_l^{-1} b_r^{-1} a_r^{-1} b_r^{-1}$; $a_l a_r a_l b_l^{-1} b_r^{-1} a_r^{-1} b_r a_l^{-1} a_r^{-1}$; $a_l a_l b_l b_r^{-1} a_r^{-1} b_r a_l^{-1} b_r a_l^{-1} b_l a_r^{-1}$;
(3, 3, 9, 2, 2, 8)	S^3/Q_{20}	$a_l b_l b_r^{-1} a_r^{-1} b_r^{-1}$; $a_l b_l b_r^{-1} a_l a_r b_r^{-1} b_r a_l^{-1} b_l^{-1} b_r a_l^{-1} b_l a_r^{-1} a_l^{-1} b_r a_l^{-1}$ $b_l^{-1} a_r a_l b_l^{-1} b_r^{-1} a_l b_l b_r^{-1} a_r^{-1} b_r a_l^{-1} a_r^{-1}$; $b_r^{-1} a_l a_l b_l$;
(5, 5, 5, 2, 2, 2)	$E^3/P2_12_12_1$	$a_r^{-1} b_r a_l b_l b_r^{-1} a_r^{-1} b_r a_r^{-1} b_r a_l^{-1} a_r^{-1}$; $a_r^{-1} b_r a_l^{-1} a_r^{-1} b_r a_l^{-1} b_l^{-1} a_l^{-1} a_r^{-1} b_r a_l^{-1} a_r^{-1}$; $a_l a_l b_l a_r b_r^{-1} a_l a_l b_l b_r^{-1} a_r^{-1} b_r$;
(5, 5, 5, 4, 4, 4)	S^3/P_{120}	$a_r^{-1} b_r a_l^{-1} b_l^{-1} a_r a_l a_r b_r^{-1} b_r a_l^{-1} b_l^{-1} a_r^{-1}$; $a_l b_l b_r^{-1} a_r^{-1} b_r a_l^{-1} b_l^{-1} a_r b_r^{-1} b_r a_l^{-1} b_l^{-1} a_r^{-1}$; $a_l b_l a_r b_r^{-1} a_l b_l b_r^{-1} a_r^{-1} b_r a_l^{-1} b_l^{-1} a_l^{-1} a_r^{-1}$;
(4, 4, 8, 1, 1, 1)	S^3/Q_{16}	$a_r^{-1} b_r a_r^{-1} b_r a_r^{-1} b_r a_r^{-1} b_r a_l^{-1} a_r^{-1} b_r a_l^{-1} a_r^{-1}$; $a_r^{-1} b_r a_r^{-1} b_r a_r^{-1} b_r a_l a_l b_l b_r^{-1} a_r^{-1} b_r$; $a_l^{-1} a_r^{-1} b_r a_l^{-1} b_l^{-1} a_l^{-1} a_l^{-1} a_r^{-1} b_r$;
(4, 4, 8, 1, 1, 9)	$S^3/P_{48} \times \mathbb{Z}_5$	$a_l^{-1} a_r^{-1} a_l^{-1} a_r^{-1} a_l b_l b_r^{-1} a_r^{-1} b_r$; $a_l^{-1} a_r^{-1} a_l^{-1} a_r a_r a_r b_r b_r a_l^{-1} b_l a_r^{-1}$; $a_l a_l b_l b_r^{-1} a_r^{-1} b_r^{-1} a_r^{-1} a_r^{-1} a_r^{-1}$;
(4, 4, 8, 1, 5, 1)	S^3/D_{80}	$a_l^{-1} a_r^{-1} a_l^{-1} a_r^{-1} a_l b_l b_r^{-1} a_r^{-1} b_r$; $a_l^{-1} a_r^{-1} a_l^{-1} a_r a_r a_r b_r b_r a_l^{-1} b_l a_r^{-1}$; $a_l a_l b_l b_r^{-1} a_r^{-1} b_r^{-1} a_r^{-1} a_r^{-1} a_r^{-1}$;
(4, 6, 6, 1, 1, 1)	$S^3/P_{24} \times \mathbb{Z}_7$	$a_r^{-1} b_r a_r^{-1} b_r a_r^{-1} b_r a_l^{-1} a_r^{-1} b_r a_l^{-1} a_r^{-1}$; $a_r^{-1} b_r a_r^{-1} b_r a_l a_l a_l b_l b_r^{-1} a_r^{-1} b_r$; $a_l^{-1} a_r^{-1} b_r a_l^{-1} b_l^{-1} a_l^{-1} a_l^{-1} a_l^{-1} a_r^{-1} b_r$;

Table 3.1 continued from previous page

6-tuple	3-manifold	Words
(4, 6, 6, 1, 1, 9)	$TB\begin{pmatrix}-1 & 1\\ -1 & 0\end{pmatrix}$	$a_l^{-1}a_r^{-1}a_l^{-1}a_r^{-1}a_la_lb_lb_r^{-1}a_r^{-1}b_r$; $a_l^{-1}a_r^{-1}a_l^{-1}a_ra_rb_rb_ra_l^{-1}b_la_r^{-1}$; $a_la_la_lb_lb_r^{-1}a_r^{-1}b_r^{-1}a_r^{-1}a_r^{-1}$;
(4, 6, 6, 1, 7, 1)	$S^3/P_{48}\times\mathbb{Z}_7$	$a_r^{-1}b_ra_r^{-1}b_ra_r^{-1}b_ra_l^{-1}b_l^{-1}a_l^{-1}b_l^{-1}a_l^{-1}a_r^{-1}$; $a_r^{-1}b_ra_r^{-1}b_ra_lb_la_rb_r^{-1}a_lb_lb_r^{-1}a_r^{-1}b_r$; $a_l^{-1}b_l^{-1}a_l^{-1}b_l^{-1}a_l^{-1}b_l^{-1}a_l^{-1}a_r^{-1}b_ra_l^{-1}b_l^{-1}a_r^{-1}b_r$;
(4, 6, 6, 5, 5, 3)	$E^3/P4_1$	$a_r^{-1}b_ra_l^{-1}b_l^{-1}a_rb_r^{-1}b_ra_l^{-1}b_l^{-1}a_r^{-1}a_r^{-1}$; $a_r^{-1}b_ra_l^{-1}b_l^{-1}a_ra_la_lb_la_rb_r^{-1}b_ra_l^{-1}b_l^{-1}a_r^{-1}$; $a_lb_lb_r^{-1}a_r^{-1}b_ra_l^{-1}b_l^{-1}a_l^{-1}b_l^{-1}a_l^{-1}a_r^{-1}$;
(3, 3, 11, 2, 2, 4)	S^3/D_{40}	$a_la_ra_lb_l^{-1}b_r^{-1}a_r^{-1}b_r^{-1}$; $a_la_la_la_la_lb_lb_r^{-1}a_r^{-1}b_ra_l^{-1}a_r^{-1}$; $a_la_la_la_lb_lb_r^{-1}a_r^{-1}b_ra_l^{-1}b_ra_l^{-1}b_la_r^{-1}$;
(3, 3, 11, 2, 2, 10)	S^3/Q_{24}	$a_lb_lb_r^{-1}a_la_ra_lb_l^{-1}b_r^{-1}a_lb_lb_r^{-1}a_r^{-1}b_r^{-1}$; $a_lb_lb_r^{-1}a_la_lb_lb_r^{-1}a_lb_lb_r^{-1}a_r^{-1}b_ra_l^{-1}a_r^{-1}$; $a_lb_lb_r^{-1}a_lb_lb_r^{-1}a_r^{-1}b_ra_l^{-1}b_ra_l^{-1}b_l^{-1}b_ra_l^{-1}b_la_r^{-1}$;
(3, 7, 7, 2, 2, 2)	$S^3/P_{24}\times\mathbb{Z}_5$	$a_r^{-1}b_ra_r^{-1}b_ra_l^{-1}b_l^{-1}a_l^{-1}a_l^{-1}a_r^{-1}$; $a_r^{-1}b_ra_la_lb_lb_r^{-1}a_r^{-1}b_ra_r^{-1}b_ra_l^{-1}a_r^{-1}$; $a_r^{-1}b_ra_la_lb_la_rb_r^{-1}a_la_lb_lb_r^{-1}a_r^{-1}b_r$;
(5, 5, 7, 2, 4, 2)	$(\mathbb{RP}^2,(2,1),(2,1))$	$a_r^{-1}b_ra_r^{-1}b_ra_l^{-1}b_l^{-1}a_l^{-1}a_r^{-1}b_ra_l^{-1}b_l^{-1}a_l^{-1}a_r^{-1}$; $a_r^{-1}b_ra_lb_lb_r^{-1}a_r^{-1}b_ra_r^{-1}b_ra_l^{-1}a_r^{-1}$; $a_r^{-1}b_ra_lb_la_rb_r^{-1}a_la_lb_la_rb_r^{-1}a_lb_lb_r^{-1}a_r^{-1}b_r$;
(5, 5, 7, 2, 6, 6)	$E^3/P3_1$	$a_la_rb_r^{-1}b_ra_l^{-1}b_l^{-1}a_ra_lb_l^{-1}b_r^{-1}a_r^{-1}b_ra_l^{-1}a_r^{-1}$; $a_la_lb_lb_r^{-1}a_r^{-1}b_ra_l^{-1}a_r^{-1}a_l^{-1}a_r^{-1}$; $a_lb_lb_r^{-1}a_r^{-1}b_ra_lb_lb_r^{-1}a_r^{-1}b_ra_l^{-1}b_ra_l^{-1}b_la_r^{-1}$;
(5, 5, 7, 4, 4, 6)	$E^3/P6_1$	$a_la_rb_r^{-1}b_ra_l^{-1}b_l^{-1}a_l^{-1}a_ra_lb_l^{-1}b_r^{-1}a_r^{-1}b_r^{-1}$; $a_la_rb_r^{-1}b_ra_l^{-1}b_l^{-1}a_ra_lb_l^{-1}b_r^{-1}a_r^{-1}b_ra_l^{-1}a_r^{-1}$; $a_la_ra_lb_l^{-1}b_r^{-1}a_r^{-1}b_ra_l^{-1}b_ra_l^{-1}b_la_r^{-1}$;

Table 3.1 continued from previous page

6-tuple	3-manifold	Words
(4, 4, 10, 1, 1, 1)	$S^3/D_{40} \times \mathbb{Z}_3$	$a_r^{-1}b_ra_r^{-1}b_ra_r^{-1}b_ra_r^{-1}b_ra_r^{-1}b_ra_l^{-1}a_r^{-1}b_ra_l^{-1}a_r^{-1}$; $a_r^{-1}b_ra_r^{-1}b_ra_r^{-1}b_ra_r^{-1}b_ra_la_lb_lb_r^{-1}a_r^{-1}b_r$; $a_l^{-1}a_r^{-1}b_ra_l^{-1}b_l^{-1}a_l^{-1}a_l^{-1}a_r^{-1}b_r$;
(4, 4, 10, 1, 1, 7)	$S^3/Q_{12} \times \mathbb{Z}_5$	$a_la_lb_lb_r^{-1}a_la_lb_lb_r^{-1}a_r^{-1}b_r^{-1}a_lb_lb_r^{-1}a_r^{-1}b_r^{-1}$; $a_lb_lb_r^{-1}a_r^{-1}b_ra_l^{-1}a_r^{-1}a_l^{-1}a_r^{-1}a_lb_lb_r^{-1}a_r^{-1}b_r^{-1}$; $a_l^{-1}b_ra_l^{-1}b_l^{-1}a_l^{-1}b_ra_l^{-1}b_la_r^{-1}a_l^{-1}a_r^{-1}$;
(4, 4, 10, 1, 1, 11)	$S^3/P_{120} \times \mathbb{Z}_{11}$	$a_l^{-1}a_r^{-1}a_l^{-1}a_r^{-1}a_lb_lb_r^{-1}a_r^{-1}b_r$; $a_l^{-1}a_r^{-1}a_l^{-1}a_ra_ra_ra_rb_rb_ra_l^{-1}b_la_r^{-1}$; $a_la_lb_lb_r^{-1}a_r^{-1}b_r^{-1}a_r^{-1}a_r^{-1}a_r^{-1}a_r^{-1}$;
(4, 4, 10, 1, 5, 1)	$S^3/Q_{24} \times \mathbb{Z}_5$	$a_r^{-1}b_ra_r^{-1}b_ra_r^{-1}b_ra_r^{-1}b_ra_r^{-1}b_ra_l^{-1}b_l^{-1}a_l^{-1}a_r^{-1}$; $a_r^{-1}b_ra_r^{-1}b_ra_r^{-1}b_ra_r^{-1}b_ra_lb_la_rb_r^{-1}a_lb_lb_r^{-1}a_r^{-1}b_r$; $a_l^{-1}b_l^{-1}a_l^{-1}b_l^{-1}a_l^{-1}a_r^{-1}b_ra_l^{-1}b_l^{-1}a_r^{-1}b_r$;
(4, 4, 10, 1, 5, 7)	$S^3/Q_{20} \times \mathbb{Z}_3$	$a_la_lb_lb_r^{-1}a_la_lb_lb_r^{-1}a_r^{-1}b_ra_l^{-1}a_r^{-1}$; $a_lb_lb_r^{-1}a_r^{-1}b_ra_lb_lb_r^{-1}a_r^{-1}b_ra_l^{-1}a_r^{-1}a_l^{-1}a_r^{-1}$; $a_lb_lb_r^{-1}a_r^{-1}b_ra_l^{-1}b_ra_l^{-1}b_l^{-1}a_l^{-1}b_ra_l^{-1}b_la_r^{-1}$;
(4, 4, 10, 3, 3, 3)	$S^3/P_{120} \times \mathbb{Z}_7$	$a_r^{-1}b_ra_r^{-1}b_ra_l^{-1}b_l^{-1}a_rb_r^{-1}a_rb_r^{-1}b_ra_l^{-1}b_l^{-1}a_r^{-1}$; $a_r^{-1}b_ra_lb_lb_r^{-1}a_r^{-1}b_ra_r^{-1}b_ra_l^{-1}b_l^{-1}a_l^{-1}a_r^{-1}$; $a_r^{-1}b_ra_lb_la_rb_r^{-1}a_lb_lb_r^{-1}a_r^{-1}b_ra_r^{-1}b_ra_l^{-1}a_r^{-1}$;
(4, 6, 8, 1, 1, 1)	$S^3/P_{48} \times \mathbb{Z}_{13}$	$a_r^{-1}b_ra_r^{-1}b_ra_r^{-1}b_ra_r^{-1}b_ra_l^{-1}a_r^{-1}b_ra_l^{-1}a_r^{-1}$; $a_r^{-1}b_ra_r^{-1}b_ra_r^{-1}b_ra_la_la_lb_lb_r^{-1}a_r^{-1}b_r$; $a_l^{-1}a_r^{-1}b_ra_l^{-1}b_l^{-1}a_l^{-1}a_l^{-1}a_l^{-1}a_r^{-1}b_r$;
(4, 6, 8, 1, 1, 11)	$(S^2,(3,1),(3,2),(4,-3))$	$a_l^{-1}a_r^{-1}a_l^{-1}a_r^{-1}a_la_lb_lb_r^{-1}a_r^{-1}b_r$; $a_l^{-1}a_r^{-1}a_l^{-1}a_ra_ra_rb_rb_ra_l^{-1}b_la_r^{-1}$; $a_la_la_lb_lb_r^{-1}a_r^{-1}b_r^{-1}a_r^{-1}a_r^{-1}a_r^{-1}$;
(4, 6, 8, 1, 7, 1)	$S^3/P_{120} \times \mathbb{Z}_{19}$	$a_r^{-1}b_ra_r^{-1}b_ra_r^{-1}b_ra_r^{-1}b_ra_l^{-1}b_l^{-1}a_l^{-1}b_l^{-1}a_l^{-1}a_r^{-1}$; $a_r^{-1}b_ra_r^{-1}b_ra_r^{-1}b_ra_lb_la_rb_r^{-1}a_lb_lb_r^{-1}a_r^{-1}b_r$; $a_l^{-1}b_l^{-1}a_l^{-1}b_l^{-1}a_l^{-1}b_l^{-1}a_l^{-1}a_r^{-1}b_ra_l^{-1}b_l^{-1}a_r^{-1}b_r$;

Table 3.1 continued from previous page

6-tuple	**3-manifold**	**Words**
(4, 6, 8, 3, 9, 13)	$(S^2,(2,1),(4,1),(4,-1))$	$a_l^{-1}a_l^{-1}a_l^{-1}a_l^{-1}a_r^{-1}a_r^{-1}a_r^{-1}a_r^{-1}b_r$; $a_l^{-1}a_r^{-1}a_l^{-1}a_r^{-1}a_r^{-1}a_r^{-1}a_r^{-1}a_r^{-1}b_r$; $a_l^{-1}a_r^{-1}a_la_la_lb_lb_r^{-1}a_r^{-1}b_r$;
(4, 6, 8, 5, 5, 11)	$(S^2,(2,1),(4,1),(5,-4))$	$a_l^{-1}b_l^{-1}a_ra_la_lb_la_rb_r^{-1}b_ra_l^{-1}b_l^{-1}a_r^{-1}a_r^{-1}a_r^{-1}b_r$; $a_l^{-1}b_l^{-1}a_rb_r^{-1}b_ra_l^{-1}b_l^{-1}a_r^{-1}a_r^{-1}a_r^{-1}a_r^{-1}b_r$; $a_l^{-1}b_l^{-1}a_l^{-1}b_l^{-1}a_l^{-1}a_r^{-1}a_lb_lb_r^{-1}a_r^{-1}b_r$;
(6, 6, 6, 1, 1, 1)	$(S^2,(3,1),(3,1),(3,1))$	$a_r^{-1}b_ra_r^{-1}b_ra_r^{-1}b_ra_l^{-1}a_r^{-1}b_ra_l^{-1}a_r^{-1}b_ra_l^{-1}a_r^{-1}$; $a_r^{-1}b_ra_r^{-1}b_ra_la_la_lb_lb_r^{-1}a_r^{-1}b_r$; $a_l^{-1}a_r^{-1}b_ra_l^{-1}a_r^{-1}b_ra_l^{-1}b_l^{-1}a_l^{-1}a_l^{-1}a_l^{-1}a_r^{-1}b_r$;
(6, 6, 6, 1, 1, 9)	$(S^2,(3,1),(3,1),(4,-1))$	$a_l^{-1}a_r^{-1}a_l^{-1}a_r^{-1}a_l^{-1}a_r^{-1}a_la_lb_lb_r^{-1}a_r^{-1}b_r$; $a_l^{-1}a_r^{-1}a_l^{-1}a_r^{-1}a_l^{-1}a_ra_rb_rb_ra_l^{-1}b_la_r^{-1}$; $a_la_la_lb_lb_r^{-1}a_r^{-1}b_r^{-1}a_r^{-1}a_r^{-1}$;
(6, 6, 6, 1, 7, 7)	$TB\begin{pmatrix}-1 & 0\\ -1 & -1\end{pmatrix}$	$a_l^{-1}b_l^{-1}a_rb_rb_ra_l^{-1}b_l^{-1}a_r^{-1}a_lb_la_ra_lb_lb_r^{-1}a_r^{-1}b_r$; $a_l^{-1}b_l^{-1}a_rb_rb_ra_l^{-1}b_l^{-1}a_rb_rb_ra_l^{-1}b_l^{-1}a_r^{-1}a_l^{-1}a_r^{-1}$; $a_l^{-1}b_l^{-1}a_ra_rb_rb_ra_l^{-1}b_l^{-1}a_r^{-1}a_l^{-1}b_l^{-1}a_l^{-1}a_r^{-1}$;
(6, 6, 6, 5, 5, 5)	$TB\begin{pmatrix}1 & 0\\ 1 & 1\end{pmatrix}$	$a_r^{-1}b_ra_l^{-1}b_l^{-1}a_ra_la_lb_la_rb_r^{-1}b_ra_l^{-1}b_l^{-1}a_r^{-1}$; $a_lb_lb_r^{-1}a_r^{-1}b_ra_l^{-1}b_l^{-1}a_ra_la_rb_r^{-1}b_ra_l^{-1}b_l^{-1}a_r^{-1}$; $a_lb_la_rb_r^{-1}a_lb_lb_r^{-1}a_r^{-1}b_ra_l^{-1}b_l^{-1}a_rb_r^{-1}b_ra_l^{-1}b_l^{-1}a_r^{-1}$;
(3, 3, 13, 2, 2, 12)	S^3/Q_{28}	$a_lb_lb_r^{-1}a_lb_lb_r^{-1}a_r^{-1}b_ra_l^{-1}b_ra_l^{-1}b_l^{-1}b_ra_l^{-1}b_l^{-1}a_l^{-1}$ $b_ra_l^{-1}b_l^{-1}b_ra_l^{-1}b_la_r^{-1}a_lb_lb_r^{-1}a_lb_lb_r^{-1}a_r^{-1}b_r^{-1}$; $a_lb_lb_r^{-1}a_lb_lb_r^{-1}a_r^{-1}b_ra_l^{-1}a_r^{-1}$; $a_l^{-1}b_ra_l^{-1}b_l^{-1}b_ra_l^{-1}b_la_r^{-1}$;
(5, 5, 9, 2, 2, 2)	$(\mathbb{RP}^2,(2,1),(3,-1))$	$a_r^{-1}b_ra_r^{-1}b_ra_lb_lb_r^{-1}a_r^{-1}b_ra_r^{-1}b_ra_r^{-1}b_ra_l^{-1}a_r^{-1}$; $a_r^{-1}b_ra_r^{-1}b_ra_l^{-1}a_r^{-1}b_ra_l^{-1}b_l^{-1}a_l^{-1}a_r^{-1}b_ra_l^{-1}a_r^{-1}$; $a_r^{-1}b_ra_la_lb_la_rb_r^{-1}a_la_lb_lb_r^{-1}a_r^{-1}b_r$;

Table 3.1 continued from previous page

6-tuple	3-manifold	Words
(5, 5, 9, 4, 4, 8)	$(S^2,(2,1),(3,1),(7,-6))$	$a_la_rb_r^{-1}b_ra_l^{-1}b_l^{-1}a_l^{-1}b_l^{-1}a_l^{-1}a_ra_lb_l^{-1}b_r^{-1}a_r^{-1}b_r^{-1}$; $a_la_rb_r^{-1}b_ra_l^{-1}b_l^{-1}a_l^{-1}b_l^{-1}a_ra_lb_l^{-1}b_r^{-1}a_r^{-1}b_ra_l^{-1}a_r^{-1}$; $a_la_ra_lb_l^{-1}b_r^{-1}a_r^{-1}b_ra_l^{-1}b_ra_l^{-1}b_la_r^{-1}$;
(5, 7, 7, 4, 6, 12)	$(S^2,(3,1),(3,1),(4,-3))$	$a_l^{-1}b_l^{-1}a_ra_la_lb_la_rb_r^{-1}b_ra_l^{-1}b_l^{-1}a_r^{-1}a_r^{-1}a_r^{-1}b_r$; $a_l^{-1}b_l^{-1}a_l^{-1}b_l^{-1}a_l^{-1}a_r^{-1}a_r^{-1}a_r^{-1}a_r^{-1}b_r$; $a_l^{-1}b_l^{-1}a_l^{-1}a_r^{-1}a_l^{-1}b_l^{-1}a_l^{-1}a_r^{-1}a_lb_lb_r^{-1}a_r^{-1}b_r$;
(4, 4, 12, 1, 1, 1)	$S^3/Q_{24}\times\mathbb{Z}_7$	$a_r^{-1}b_ra_r^{-1}b_ra_r^{-1}b_ra_r^{-1}b_ra_r^{-1}b_ra_r^{-1}b_ra_l^{-1}a_r^{-1}b_r$ $a_l^{-1}a_r^{-1}$; $a_r^{-1}b_ra_r^{-1}b_ra_r^{-1}b_ra_r^{-1}b_ra_r^{-1}b_ra_la_lb_lb_r^{-1}a_r^{-1}b_r$; $a_l^{-1}a_r^{-1}b_ra_l^{-1}b_l^{-1}a_l^{-1}a_l^{-1}a_r^{-1}b_r$;
(4, 4, 12, 1, 1, 5)	$S^3/Q_8\times\mathbb{Z}_5$	$a_lb_r^{-1}a_la_lb_lb_r^{-1}a_lb_r^{-1}a_r^{-1}b_r^{-1}a_lb_lb_r^{-1}a_lb_r^{-1}a_r^{-1}b_r^{-1}$; $a_lb_lb_r^{-1}a_lb_r^{-1}a_r^{-1}b_ra_l^{-1}a_r^{-1}a_l^{-1}a_r^{-1}a_lb_lb_r^{-1}a_l$ $b_r^{-1}a_r^{-1}b_r^{-1}$; $a_l^{-1}b_ra_l^{-1}b_ra_l^{-1}b_la_r^{-1}a_l^{-1}a_r^{-1}$;
(4, 4, 12, 1, 1, 13)	$(S^2,(2,1),(3,2),(6,-5))$	$a_l^{-1}a_r^{-1}a_l^{-1}a_r^{-1}a_lb_lb_r^{-1}a_r^{-1}b_r$; $a_l^{-1}a_r^{-1}a_l^{-1}a_ra_ra_ra_ra_rb_rb_ra_l^{-1}b_la_r^{-1}$; $a_la_lb_lb_r^{-1}a_r^{-1}b_r^{-1}a_r^{-1}a_r^{-1}a_r^{-1}a_r^{-1}a_r^{-1}$;
(4, 4, 12, 1, 5, 1)	$S^3/D_{56}\times\mathbb{Z}_3$	$a_r^{-1}b_ra_r^{-1}b_ra_r^{-1}b_ra_r^{-1}b_ra_r^{-1}b_ra_r^{-1}b_ra_l^{-1}b_l^{-1}$ $a_l^{-1}a_r^{-1}$; $a_r^{-1}b_ra_r^{-1}b_ra_r^{-1}b_ra_r^{-1}b_ra_r^{-1}b_ra_lb_la_rb_r^{-1}a_lb_lb_r^{-1}$ $a_r^{-1}b_r$; $a_l^{-1}b_l^{-1}a_l^{-1}b_l^{-1}a_l^{-1}a_r^{-1}b_ra_l^{-1}b_l^{-1}a_r^{-1}b_r$;
(4, 6, 10, 1, 1, 1)	$S^3/P_{120}\times\mathbb{Z}_{31}$	$a_r^{-1}b_ra_r^{-1}b_ra_r^{-1}b_ra_r^{-1}b_ra_r^{-1}b_ra_l^{-1}a_r^{-1}b_ra_l^{-1}a_r^{-1}$; $a_r^{-1}b_ra_r^{-1}b_ra_r^{-1}b_ra_r^{-1}b_ra_la_la_lb_lb_r^{-1}a_r^{-1}b_r$; $a_l^{-1}a_r^{-1}b_ra_l^{-1}b_l^{-1}a_l^{-1}a_l^{-1}a_l^{-1}a_r^{-1}b_r$;

Table 3.1 continued from previous page

6-tuple	3-manifold	Words
(4, 6, 10, 1, 1, 13)	$(S^2,(3,1),(3,2),(5,-4))$	$a_l^{-1}a_r^{-1}a_l^{-1}a_r^{-1}a_la_lb_lb_r^{-1}a_r^{-1}b_r$; $a_l^{-1}a_r^{-1}a_l^{-1}a_ra_ra_ra_rb_rb_ra_l^{-1}b_la_r^{-1}$; $a_la_la_lb_lb_r^{-1}a_r^{-1}b_r^{-1}a_r^{-1}a_r^{-1}a_r^{-1}a_r^{-1}$;
(4, 6, 10, 1, 7, 1)	$(S^2,(2,1),(3,1),(6,-1))$	$a_r^{-1}b_ra_r^{-1}b_ra_r^{-1}b_ra_r^{-1}b_ra_r^{-1}b_ra_l^{-1}b_l^{-1}a_l^{-1}b_l^{-1}$ $a_l^{-1}a_r^{-1}$; $a_r^{-1}b_ra_r^{-1}b_ra_r^{-1}b_ra_r^{-1}b_ra_lb_la_rb_r^{-1}a_lb_lb_r^{-1}a_r^{-1}b_r$; $a_l^{-1}b_l^{-1}a_l^{-1}b_l^{-1}a_l^{-1}b_l^{-1}a_l^{-1}a_r^{-1}b_ra_l^{-1}b_l^{-1}a_r^{-1}b_r$;
(4, 6, 10, 3, 5, 3)	$(S^2,(2,1),(4,1),(5,-3))$	$a_r^{-1}b_ra_r^{-1}b_ra_l^{-1}b_l^{-1}a_rb_r^{-1}a_rb_r^{-1}b_ra_l^{-1}b_l^{-1}a_r^{-1}$; $a_r^{-1}b_ra_lb_lb_r^{-1}a_r^{-1}b_ra_r^{-1}b_ra_l^{-1}b_l^{-1}a_l^{-1}b_l^{-1}a_l^{-1}a_r^{-1}$; $a_r^{-1}b_ra_lb_la_rb_r^{-1}a_lb_lb_r^{-1}a_r^{-1}b_ra_r^{-1}b_ra_l^{-1}b_l^{-1}a_l^{-1}a_r^{-1}$;
(4, 6, 10, 3, 9, 15)	$(S^2,(2,1),(4,3),(5,-4))$	$a_l^{-1}a_l^{-1}a_l^{-1}a_l^{-1}a_r^{-1}a_r^{-1}a_r^{-1}a_r^{-1}a_r^{-1}b_r$; $a_l^{-1}a_r^{-1}a_l^{-1}a_r^{-1}a_r^{-1}a_r^{-1}a_r^{-1}a_r^{-1}a_r^{-1}b_r$; $a_l^{-1}a_r^{-1}a_la_la_lb_lb_r^{-1}a_r^{-1}b_r$;
(4, 6, 10, 5, 1, 1)	$S^3/P_{48}\times\mathbb{Z}_{11}$	$a_r^{-1}b_ra_r^{-1}b_ra_l^{-1}a_r^{-1}a_r^{-1}b_ra_l^{-1}a_r^{-1}a_r^{-1}b_ra_r^{-1}$; $a_r^{-1}b_ra_r^{-1}b_ra_l^{-1}b_l^{-1}a_l^{-1}a_l^{-1}a_l^{-1}a_r^{-1}$; $a_r^{-1}b_ra_la_la_lb_lb_r^{-1}a_r^{-1}b_ra_r^{-1}b_ra_l^{-1}a_r^{-1}$;
(4, 6, 10, 5, 5, 13)	$(S^2,(2,1),(4,1),(6,-5))$	$a_l^{-1}b_l^{-1}a_ra_la_lb_la_rb_r^{-1}b_ra_l^{-1}b_l^{-1}a_r^{-1}a_r^{-1}a_r^{-1}a_r^{-1}b_r$; $a_l^{-1}b_l^{-1}a_rb_r^{-1}b_ra_l^{-1}b_l^{-1}a_r^{-1}a_r^{-1}a_r^{-1}a_r^{-1}a_r^{-1}b_r$; $a_l^{-1}b_l^{-1}a_l^{-1}b_l^{-1}a_l^{-1}a_r^{-1}a_lb_lb_r^{-1}a_r^{-1}b_r$;
(4, 6, 10, 5, 9, 3)	$(S^2,(3,1),(3,2),(3,-1))$	$a_r^{-1}b_ra_la_la_lb_lb_r^{-1}a_r^{-1}b_ra_r^{-1}$; $a_r^{-1}b_ra_la_lb_lb_r^{-1}a_r^{-1}b_ra_r^{-1}b_ra_l^{-1}a_r^{-1}a_r^{-1}b_ra_l^{-1}a_r^{-1}$; $a_r^{-1}b_ra_l^{-1}a_rb_r^{-1}b_ra_l^{-1}b_la_r^{-1}a_r^{-1}b_ra_l^{-1}a_r^{-1}$;
(4, 6, 10, 7, 1, 1)	S^3/P'_{216}	$a_r^{-1}b_ra_r^{-1}a_r^{-1}b_ra_l^{-1}a_r^{-1}a_r^{-1}b_ra_l^{-1}a_r^{-1}a_r^{-1}$; $a_r^{-1}b_ra_la_la_lb_lb_r^{-1}a_r^{-1}b_ra_r^{-1}$; $a_r^{-1}b_ra_l^{-1}a_r^{-1}a_r^{-1}b_ra_l^{-1}b_l^{-1}a_l^{-1}a_l^{-1}a_l^{-1}a_r^{-1}$;

Table 3.1 continued from previous page

6-tuple	3-manifold	Words
(4, 6, 10, 7, 3, 15)	$S^3/P_{120} \times \mathbb{Z}_{13}$	$a_l^{-1}b_l^{-1}a_r^{-1}a_r^{-1}b_ra_l^{-1}b_l^{-1}a_l^{-1}b_l^{-1}a_l^{-1}b_l^{-1}a_l^{-1}$ $a_r^{-1}a_r^{-1}b_r$; $a_l^{-1}b_l^{-1}a_rb_r^{-1}a_ra_rb_r^{-1}b_ra_l^{-1}b_l^{-1}a_r^{-1}a_r^{-1}b_r$; $a_l^{-1}b_l^{-1}a_l^{-1}b_l^{-1}a_l^{-1}a_r^{-1}a_r^{-1}a_r^{-1}b_ra_r^{-1}a_r^{-1}b_r$;
(4, 8, 8, 1, 1, 1)	$(S^2,(2,1),(4,1),(4,1))$	$a_r^{-1}b_ra_r^{-1}b_ra_r^{-1}b_ra_r^{-1}b_ra_l^{-1}a_r^{-1}b_ra_l^{-1}a_r^{-1}$; $a_r^{-1}b_ra_r^{-1}b_ra_r^{-1}b_ra_la_la_la_lb_lb_r^{-1}a_r^{-1}b_r$; $a_l^{-1}a_r^{-1}b_ra_l^{-1}b_l^{-1}a_l^{-1}a_l^{-1}a_l^{-1}a_l^{-1}a_r^{-1}b_r$;
(4, 8, 8, 1, 1, 13)	$(S^2,(3,2),(4,1),(4,-3))$	$a_l^{-1}a_r^{-1}a_l^{-1}a_r^{-1}a_la_la_lb_lb_r^{-1}a_r^{-1}b_r$; $a_l^{-1}a_r^{-1}a_l^{-1}a_ra_ra_rb_rb_ra_l^{-1}b_la_r^{-1}$; $a_la_la_la_lb_lb_r^{-1}a_r^{-1}b_r^{-1}a_r^{-1}a_r^{-1}a_r^{-1}$;
(4, 8, 8, 1, 9, 1)	$(S^2,(2,1),(4,1),(5,-1))$	$a_r^{-1}b_ra_r^{-1}b_ra_r^{-1}b_ra_r^{-1}b_ra_l^{-1}b_l^{-1}a_l^{-1}b_l^{-1}a_l^{-1}$ $b_l^{-1}a_l^{-1}a_r^{-1}$; $a_r^{-1}b_ra_r^{-1}b_ra_r^{-1}b_ra_lb_la_rb_r^{-1}a_lb_lb_r^{-1}a_r^{-1}b_r$; $a_l^{-1}b_l^{-1}a_l^{-1}b_l^{-1}a_l^{-1}b_l^{-1}a_l^{-1}b_l^{-1}a_l^{-1}a_r^{-1}b_ra_l^{-1}$ $b_l^{-1}a_r^{-1}b_r$;
(4, 8, 8, 5, 5, 13)	$(S^2,(2,1),(5,1),(5,-4))$	$a_l^{-1}b_l^{-1}a_ra_la_lb_la_lb_la_rb_r^{-1}b_ra_l^{-1}b_l^{-1}a_r^{-1}a_r^{-1}a_r^{-1}b_r$; $a_l^{-1}b_l^{-1}a_rb_r^{-1}b_ra_l^{-1}b_l^{-1}a_r^{-1}a_r^{-1}a_r^{-1}a_r^{-1}b_r$; $a_l^{-1}b_l^{-1}a_l^{-1}b_l^{-1}a_l^{-1}b_l^{-1}a_l^{-1}a_r^{-1}a_lb_lb_r^{-1}a_r^{-1}b_r$;
(6, 6, 8, 1, 1, 1)	$(S^2,(3,1),(3,1),(4,1))$	$a_r^{-1}b_ra_r^{-1}b_ra_r^{-1}b_ra_r^{-1}b_ra_l^{-1}a_r^{-1}b_ra_l^{-1}a_r^{-1}b_ra_l^{-1}a_r^{-1}$; $a_r^{-1}b_ra_r^{-1}b_ra_r^{-1}b_ra_la_la_lb_lb_r^{-1}a_r^{-1}b_r$; $a_l^{-1}a_r^{-1}b_ra_l^{-1}a_r^{-1}b_ra_l^{-1}b_l^{-1}a_l^{-1}a_l^{-1}a_l^{-1}a_r^{-1}b_r$;
(6, 6, 8, 1, 1, 11)	$(S^2,(3,1),(4,1),(4,-1))$	$a_l^{-1}a_r^{-1}a_l^{-1}a_r^{-1}a_l^{-1}a_r^{-1}a_la_lb_lb_r^{-1}a_r^{-1}b_r$; $a_l^{-1}a_r^{-1}a_l^{-1}a_r^{-1}a_l^{-1}a_ra_ra_rb_rb_ra_l^{-1}b_la_r^{-1}$; $a_la_la_lb_lb_r^{-1}a_r^{-1}b_r^{-1}a_r^{-1}a_r^{-1}a_r^{-1}$;

Table 3.1 continued from previous page

6-tuple	3-manifold	Words
(6, 6, 8, 1, 9, 1)	$(S^2),(3,1),(3,1),(5,-1))$	$a_r^{-1}b_ra_r^{-1}b_ra_r^{-1}b_ra_r^{-1}b_ra_l^{-1}b_l^{-1}a_l^{-1}b_l^{-1}a_l^{-1}a_r^{-1}$; $a_r^{-1}b_ra_r^{-1}b_ra_r^{-1}b_ra_lb_la_rb_r^{-1}a_lb_la_rb_r^{-1}a_lb_lb_r^{-1}a_r^{-1}b_r$; $a_l^{-1}b_l^{-1}a_l^{-1}b_l^{-1}a_l^{-1}b_l^{-1}a_l^{-1}a_r^{-1}b_ra_l^{-1}b_l^{-1}a_r^{-1}b_r$ $a_l^{-1}b_l^{-1}a_r^{-1}b_r$;
(6, 6, 8, 5, 5, 7)	$TB\begin{pmatrix}0 & 1\\ -1 & 3\end{pmatrix}$	$a_la_rb_r^{-1}b_ra_l^{-1}b_la_r^{-1}a_l^{-1}a_ra_lb_l^{-1}b_r^{-1}a_r^{-1}b_r^{-1}$; $a_la_rb_r^{-1}b_ra_l^{-1}b_l^{-1}a_l^{-1}a_ra_lb_l^{-1}b_r^{-1}a_r^{-1}b_ra_l^{-1}a_r^{-1}$; $a_la_rb_r^{-1}b_ra_l^{-1}b_l^{-1}a_ra_lb_l^{-1}b_r^{-1}a_r^{-1}b_ra_l^{-1}b_ra_l^{-1}b_la_r^{-1}$;
(6, 6, 8, 5, 11, 7)	$TB\begin{pmatrix}0 & 1\\ -1 & -3\end{pmatrix}$	$a_la_rb_r^{-1}a_lb_l^{-1}b_r^{-1}a_r^{-1}b_ra_l^{-1}a_rb_r^{-1}b_ra_l^{-1}b_la_r^{-1}$; $a_la_rb_r^{-1}a_lb_l^{-1}b_r^{-1}a_la_rb_r^{-1}a_lb_l^{-1}b_r^{-1}a_r^{-1}b_ra_lb_l$ $b_r^{-1}a_r^{-1}b_r$; $a_la_rb_r^{-1}a_la_rb_r^{-1}a_lb_l^{-1}b_r^{-1}a_r^{-1}b_ra_la_lb_lb_r^{-1}a_r^{-1}b_r$;
(3, 3, 15, 2, 2, 6)	S^3/D_{56}	$a_lb_r^{-1}a_la_ra_lb_l^{-1}b_r^{-1}a_lb_r^{-1}a_r^{-1}b_r^{-1}$; $a_lb_r^{-1}a_la_lb_lb_r^{-1}a_la_lb_lb_r^{-1}a_lb_r^{-1}a_r^{-1}b_ra_l^{-1}a_r^{-1}$; $a_lb_lb_r^{-1}a_la_lb_lb_r^{-1}a_lb_r^{-1}a_r^{-1}b_ra_l^{-1}b_ra_l^{-1}b_ra_l^{-1}b_la_r^{-1}$;
(3, 3, 15, 2, 2, 14)	S^3/Q_{32}	$a_la_ra_lb_l^{-1}b_r^{-1}a_r^{-1}b_r^{-1}$; $a_la_lb_la_lb_la_lb_la_lb_la_lb_la_lb_lb_r^{-1}a_r^{-1}b_ra_l^{-1}a_r^{-1}$; $a_lb_la_lb_la_lb_la_lb_la_lb_la_lb_lb_r^{-1}a_r^{-1}b_ra_l^{-1}b_ra_l^{-1}b_la_r^{-1}$;
(3, 7, 11, 4, 2, 2)	$S^3/P_{120}\times\mathbb{Z}_{17}$	$a_r^{-1}b_ra_r^{-1}b_ra_l^{-1}b_l^{-1}a_l^{-1}a_l^{-1}a_r^{-1}a_r^{-1}b_ra_r^{-1}$; $a_r^{-1}b_ra_r^{-1}b_ra_l^{-1}b_l^{-1}a_l^{-1}a_rb_r^{-1}a_rb_r^{-1}b_ra_l^{-1}$ $b_l^{-1}a_l^{-1}a_r^{-1}$; $a_r^{-1}b_ra_la_lb_lb_r^{-1}a_r^{-1}b_ra_r^{-1}b_ra_l^{-1}a_r^{-1}$;
(5, 5, 11, 2, 4, 2)	$(\mathbb{RP}^2,(2,1),(3,1))$	$a_r^{-1}b_ra_r^{-1}b_ra_r^{-1}b_ra_l^{-1}b_l^{-1}a_l^{-1}a_r^{-1}b_ra_l^{-1}b_l^{-1}$ $a_l^{-1}a_r^{-1}$; $a_r^{-1}b_ra_r^{-1}b_ra_lb_lb_r^{-1}a_r^{-1}b_ra_r^{-1}b_r$ $a_r^{-1}b_ra_l^{-1}a_r^{-1}$; $a_r^{-1}b_ra_r^{-1}b_ra_lb_la_rb_r^{-1}a_la_lb_la_rb_r^{-1}a_lb_lb_r^{-1}a_r^{-1}b_r$;

Table 3.1 continued from previous page

6-tuple	3-manifold	Words
(5, 5, 11, 4, 4, 10)	$(S^2,(2,1),(3,1),(8,-7))$	$a_la_rb_r^{-1}b_ra_l^{-1}b_l^{-1}a_l^{-1}b_l^{-1}a_l^{-1}b_l^{-1}a_l^{-1}a_ra_lb_l^{-1}$ $b_r^{-1}a_r^{-1}b_r^{-1}$; $a_la_rb_r^{-1}b_ra_l^{-1}b_l^{-1}a_l^{-1}b_l^{-1}a_l^{-1}b_l^{-1}a_ra_lb_l^{-1}b_r^{-1}$ $a_r^{-1}b_ra_l^{-1}a_r^{-1}$; $a_la_ra_lb_l^{-1}b_r^{-1}a_r^{-1}b_ra_l^{-1}b_ra_l^{-1}b_la_r^{-1}$;
(5, 5, 11, 4, 8, 4)	$(S^2,(2,1),(3,1),(7,-5))$	$a_r^{-1}b_ra_la_rb_r^{-1}a_ra_lb_l^{-1}b_r^{-1}a_r^{-1}b_ra_r^{-1}b_ra_l^{-1}a_r^{-1}$; $a_r^{-1}b_ra_la_lb_lb_r^{-1}a_r^{-1}b_ra_r^{-1}b_ra_l^{-1}a_r^{-1}b_ra_l^{-1}a_r^{-1}$; $a_r^{-1}b_ra_lb_lb_r^{-1}a_r^{-1}b_ra_r^{-1}b_ra_l^{-1}a_rb_r^{-1}b_ra_l^{-1}b_la_r^{-1}$;
(5, 7, 9, 2, 4, 4)	$(\mathbb{D},(2,1),(2,-3))\cup_{\left(\begin{smallmatrix}0&1\\1&0\end{smallmatrix}\right)}$ $(\mathbb{D},(2,1),(3,-2))$	$a_r^{-1}b_ra_lb_lb_r^{-1}a_r^{-1}b_ra_r^{-1}b_ra_l^{-1}b_l^{-1}a_l^{-1}a_r^{-1}b_ra_l^{-1}$ $b_l^{-1}a_l^{-1}a_r^{-1}$; $a_r^{-1}b_ra_lb_lb_r^{-1}a_r^{-1}b_ra_lb_lb_r^{-1}a_r^{-1}b_ra_r^{-1}b_ra_l^{-1}a_r^{-1}$; $a_r^{-1}b_ra_lb_la_rb_r^{-1}a_la_lb_la_rb_r^{-1}a_lb_lb_r^{-1}a_r^{-1}b_r$;
(5, 7, 9, 4, 6, 14)	$(S^2,(3,1),(3,1),(5,-4))$	$a_l^{-1}b_l^{-1}a_ra_la_lb_la_rb_r^{-1}b_ra_l^{-1}b_l^{-1}a_r^{-1}a_r^{-1}a_r^{-1}a_r^{-1}b_r$; $a_l^{-1}b_l^{-1}a_l^{-1}b_l^{-1}a_l^{-1}a_r^{-1}a_r^{-1}a_r^{-1}a_r^{-1}a_r^{-1}b_r$; $a_l^{-1}b_l^{-1}a_l^{-1}a_r^{-1}a_l^{-1}b_l^{-1}a_l^{-1}a_r^{-1}a_lb_lb_r^{-1}a_r^{-1}b_r$;
(7, 7, 7, 2, 2, 2)	$Q_1(2,-3)$	$a_r^{-1}b_ra_r^{-1}b_ra_l^{-1}a_r^{-1}b_ra_l^{-1}b_l^{-1}a_l^{-1}a_l^{-1}a_r^{-1}b_ra_l^{-1}a_r^{-1}$; $a_r^{-1}b_ra_la_lb_lb_r^{-1}a_r^{-1}b_ra_r^{-1}b_ra_l^{-1}a_r^{-1}b_ra_l^{-1}a_r^{-1}$; $a_r^{-1}b_ra_la_lb_la_rb_r^{-1}a_la_rb_r^{-1}a_la_lb_lb_r^{-1}a_r^{-1}b_r$;
(7, 7, 7, 2, 6, 10)	$(\mathbb{D},(2,1),(2,1))\cup_{\left(\begin{smallmatrix}0&1\\1&0\end{smallmatrix}\right)}$ $(\mathbb{D},(2,1),(3,1))$	$a_l^{-1}b_l^{-1}a_r^{-1}a_lb_la_ra_la_lb_la_lb_la_ra_lb_lb_r^{-1}a_r^{-1}b_r$; $a_l^{-1}b_l^{-1}a_ra_rb_rb_ra_l^{-1}b_l^{-1}a_r^{-1}a_lb_la_ra_lb_lb_r^{-1}a_r^{-1}b_r$; $a_l^{-1}b_l^{-1}a_ra_ra_rb_rb_ra_l^{-1}b_l^{-1}a_r^{-1}a_l^{-1}b_l^{-1}a_l^{-1}a_r^{-1}$;

Table 3.1: Table containing all the words produced by the algorithm.

Chapter 4

Plat slide moves in Dunwoody and Takahashi manifolds

In this chapter we will solve the problem of finding plat slide moves also in the two settings of Dunwoody and Takahashi manifolds, since the idea behind the algorithm solving the problem for 3-manifolds of Heegaard genus 2 can be used for these two families of 3-manifolds of higher Heegaard genus.

4.1 Computing psl-moves

Following the construction in Chapter 3, we can use the presentation of Dunwoody and Takahashi manifolds by an open Heegaard diagram to compute plat slide moves for links in manifolds of these manifolds described as plat closure of a braid.

In this case, the attaching circles of the 2-handles of the handle decomposition of the manifold will be still represented by one of the two set of curves of the open Heegaard diagram. Moreover, as in Section 3.1, we can think these curves as composed by red and blue arcs: the red ones come from the arcs depicted in the open Heegaard diagram while the blue ones come from the circle attaching operations, as in Figure 4.1, where an example for the Dunwoody manifold

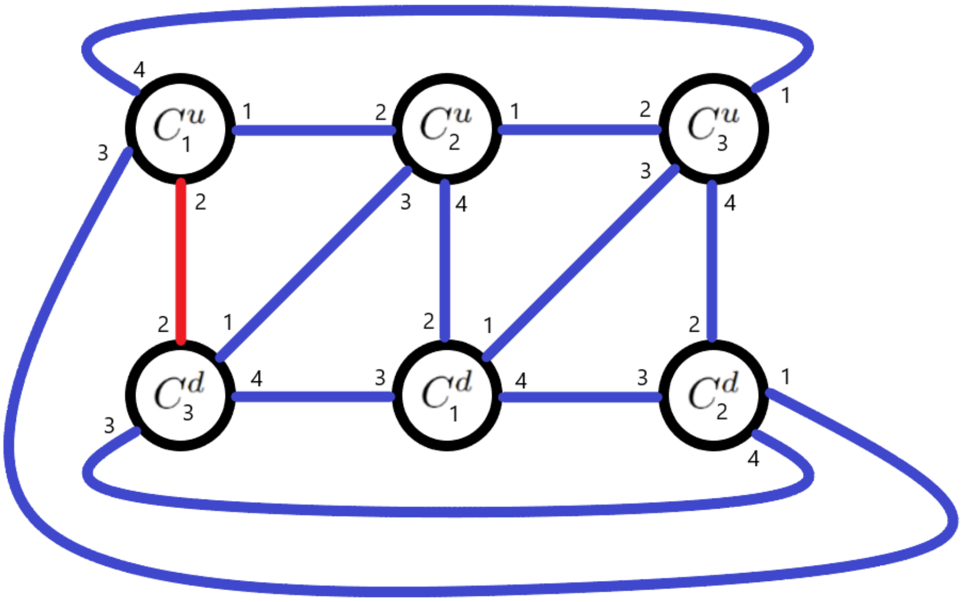

Figure 4.1: An example of the construction on $M(1,1,1,3,2,1)$.

$H(1,1,1,3,2,1)$ is depicted. This manifold represents $S^1 \times S^1 \times S^1$ [18].

According to the proof of Theorem 3.1.1, we need to define a base point on the Heegaard surface and give a standard orientation to the attaching curves, then divide them into couples of one red and one blue arc. Finally, we compute all possible words that can arise from such a subdivision, and collect them into a *dictionary*. This dictionary will depend only on the parameters of the manifold. Once the dictionary is ready, we can simply follow the path of the curves, as we did before in the proof of Theorem 3.1.1, substituting any blue-red couple of arcs with the associated word of the dictionary, thus obtaining the word representing the plat slide move one piece at a time.

The construction is analogous for both Dunwoody and Takahashi manifolds, the resulting dictionary being the only difference.

4.1.1 The case of Dunwoody manifolds

For the construction of the dictionary in the setting of Dunwoody manifolds, we refer to the Heegaard diagram of Figure 1.8. Let $M(a,b,c,n,s,r)$ be an admissible Dunwoody manifold.

With generators a_i, b_i depicted in Figure 4.2 and following Figures 4.3, 4.4, 4.5 down below, we can describe the words associated to the possible arcs as:

- arc a; we have four possible cases, depending on the orientation of the arc, left or right, and the position, connecting lower or upper C_i's:

$$\overrightarrow{a_U} = b_{i+1}^{-1} a_{i+1}$$
$$\overleftarrow{a_U} = b_{i+1} a_i$$
$$\overrightarrow{a_L} = a_{i+1}^{-1}$$
$$\overleftarrow{a_L} = a_i^{-1}.$$

- arc c; in this case it is important to note that, if we go past the base point of the Heegaard surface, we have to completely turn round the surface in order to represent the arc. When addressing this case, we define a quantity w as:

$$w = \prod_{j=1}^{i-s+1} b_j, \quad j \in \mathbb{Z}_n.$$

  In this way, following Figure 4.4, we obtain:

$$\downarrow c_i^s = w a_{i-s}^{-1}, \quad i = 1, \dots, n$$

$$\uparrow c_i^s = w^{-1} a_i, \quad i = 1, \dots, n.$$

- arc b; following the construction in Figure 4.5, it is quite straightforward to see that a b-move has the same representation as a c-move but with a different shifting:

$$\downarrow b_i^s = \downarrow c_i^{s+1}$$

$$\uparrow b_i^s = \uparrow c_i^{s+1}.$$

Once we got the dictionary, it is sufficient to follow the attaching curves whose associated plat

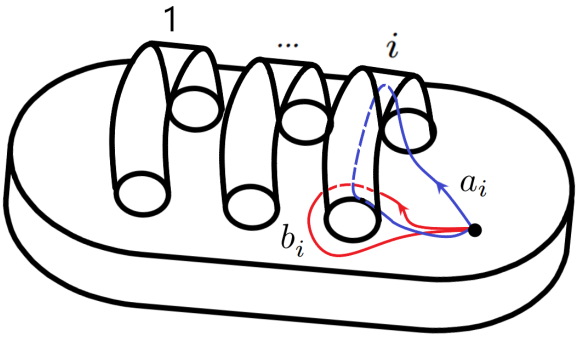

Figure 4.2: The two possible types of generators for the Dunwoody and Takahashi manifold.

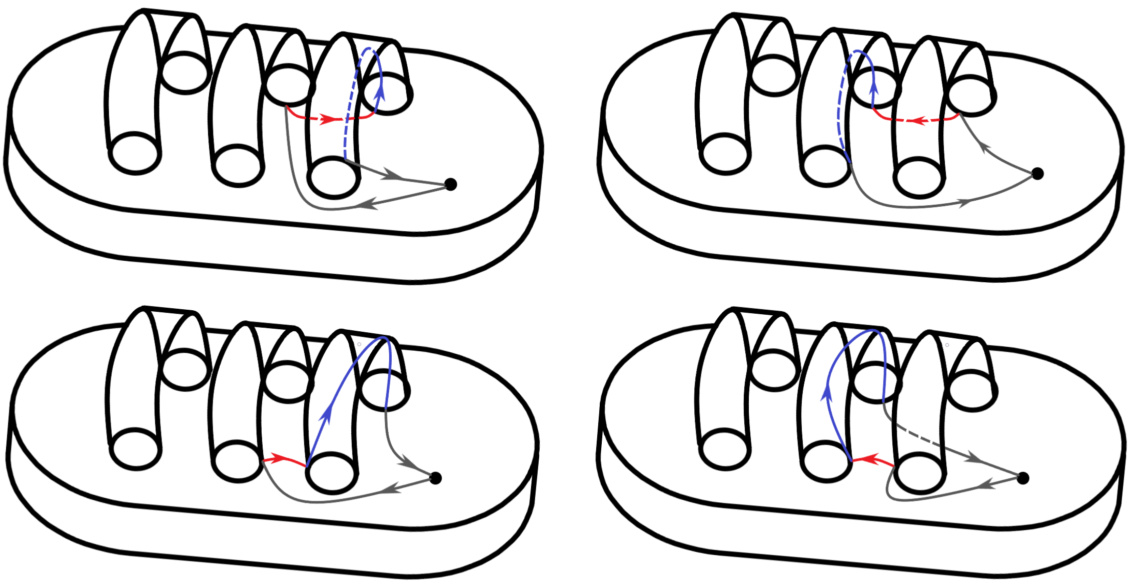

Figure 4.3: The four possible a-moves.

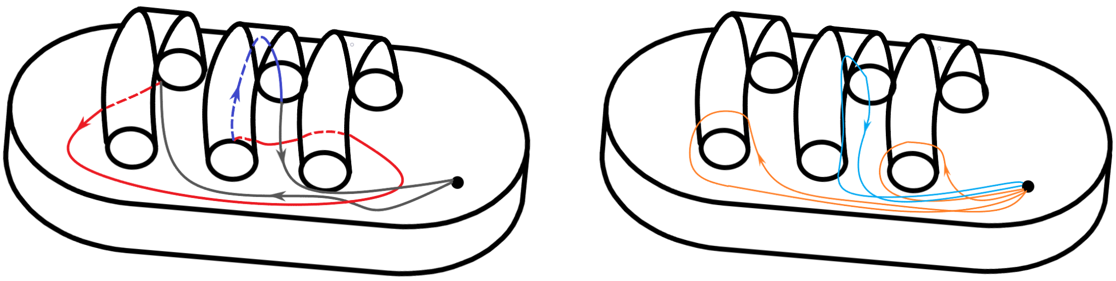

Figure 4.4: An example of $\downarrow c$-move - in this case $\downarrow c_1^3 = b_1 b_3 a_2^{-1}$.

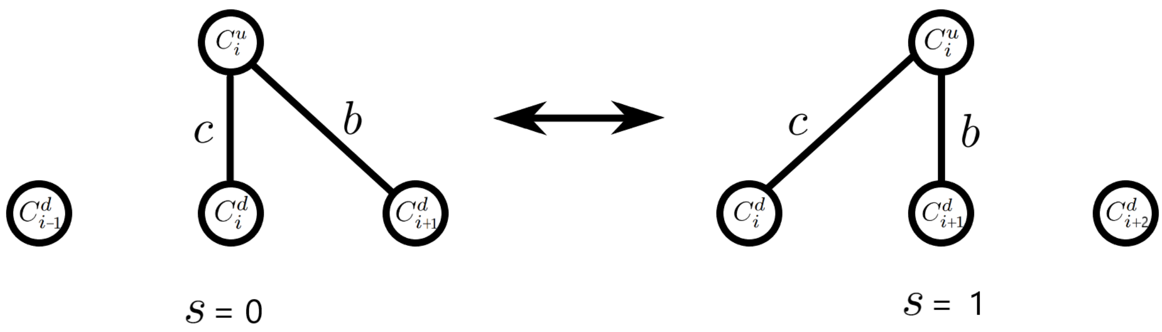

Figure 4.5: The equivalence between the c-move in the example with $s = 0$ and the b-move in the example with $s = 1$. On the left C_i^u is glued to C_i^d, while on the right it is glued to C_{i+1}^d.

slide moves we want to calculate to get the word associated to the plat braid representative of such curves. Substituting every couple of red and blue arc with the correspondent entry of the dictionary and paying attention to the twists of the blue arcs around the handles, we get the final word.

4.1.2 The case of Takahashi manifolds

For the construction of the dictionary in the setting of Takahashi manifolds, we refer to the Heegaard diagram of Figure 1.17, with the labels of Figure 4.6. Let $T_{n,m}(p_{k,j}/q_{k,j}; r_{k,j}/s_{k,j})$ be a Takahashi manifold. For the generators a_i's and b_i's, the graphic representation is the same as in Figure 4.2, since the construction of the Heegaard surface is really similar. Following Figure 4.7 down below, we can describe the words connected to the possible arcs as:

- arc a; since the a-arc of the Dunwoody case is exactly the same as the a-arc of the Takahashi case, the results are the same (see Fig. 4.3):

$$\overrightarrow{a_U} = b_{i+1}^{-1} a_{i+1}$$

$$\overleftarrow{a_U} = b_{i+1} a_i$$

$$\overrightarrow{a_L} = a_{i+1}^{-1}$$

$$\overleftarrow{a_L} = a_i^{-1}.$$

- arc b; since the c-arc of the Dunwoody case with $s = 0$ is exactly the same as the b-arc of the Takahashi case, the results are:

$$\downarrow b = a_i^{-1}$$
$$\uparrow b = a_i.$$

- arc c; after closing the red and blue arcs, we obtain the situation depicted in Figure 4.7. In order to achieve the correct word we need to decompose the original loop into three elements, see Figure 4.8. Following these three elementary pieces we obtain:

$$\vec{c} = [a_{i+1}, b_{i+1}]b_{i+2}^{-1}a_{i+2} = a_{i+1}^{-1}b_{i+1}^{-1}a_{i+1}b_{i+1}b_{i+2}^{-1}a_{i+2}$$
$$\overleftarrow{c} = b_{i+2}[b_{i+1}, a_{i+1}]a_i = b_{i+2}b_{i+1}^{-1}a_{i+1}^{-1}b_{i+1}a_{i+1}a_i$$

where $[a, b] = a^{-1}b^{-1}ab$.

- arc d, e, f and g; for all these kinds of arcs the procedure is quite similar, obtaining the following sequence of moves:

$$\vec{d} = b_{i+1}^{-1}b_{i+2}^{-1}a_{i+2}$$
$$\overleftarrow{d} = b_{i+2}b_{i+1}a_i$$
$$\vec{e} = b_{i+1}^{-1}a_{i+2}^{-1}$$
$$\overleftarrow{e} = b_{i+1}^{-1}a_i^{-1}$$
$$\vec{f} = a_{i+2}^{-1}$$
$$\overleftarrow{f} = a_i^{-1}$$
$$\vec{g} = a_{i+1}^{-1}$$
$$\overleftarrow{g} = a_i.$$

As in the case of Dunwoody manifolds, once we got the dictionary, it is sufficient to follow the attaching curves whose plat slide moves we want to calculate to get the word associated to the plat braid representative of each curve. Substituting every couple of red and blue arc with

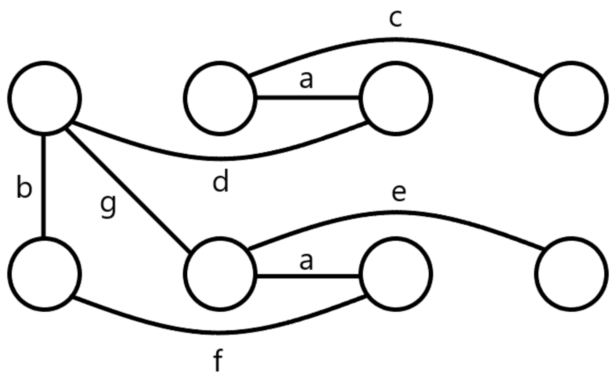

Figure 4.6: All the possible arcs in the Takahashi case.

the correspondent entry in the dictionary and paying attention to the twists of the blue arcs around the handles, we get the final word.

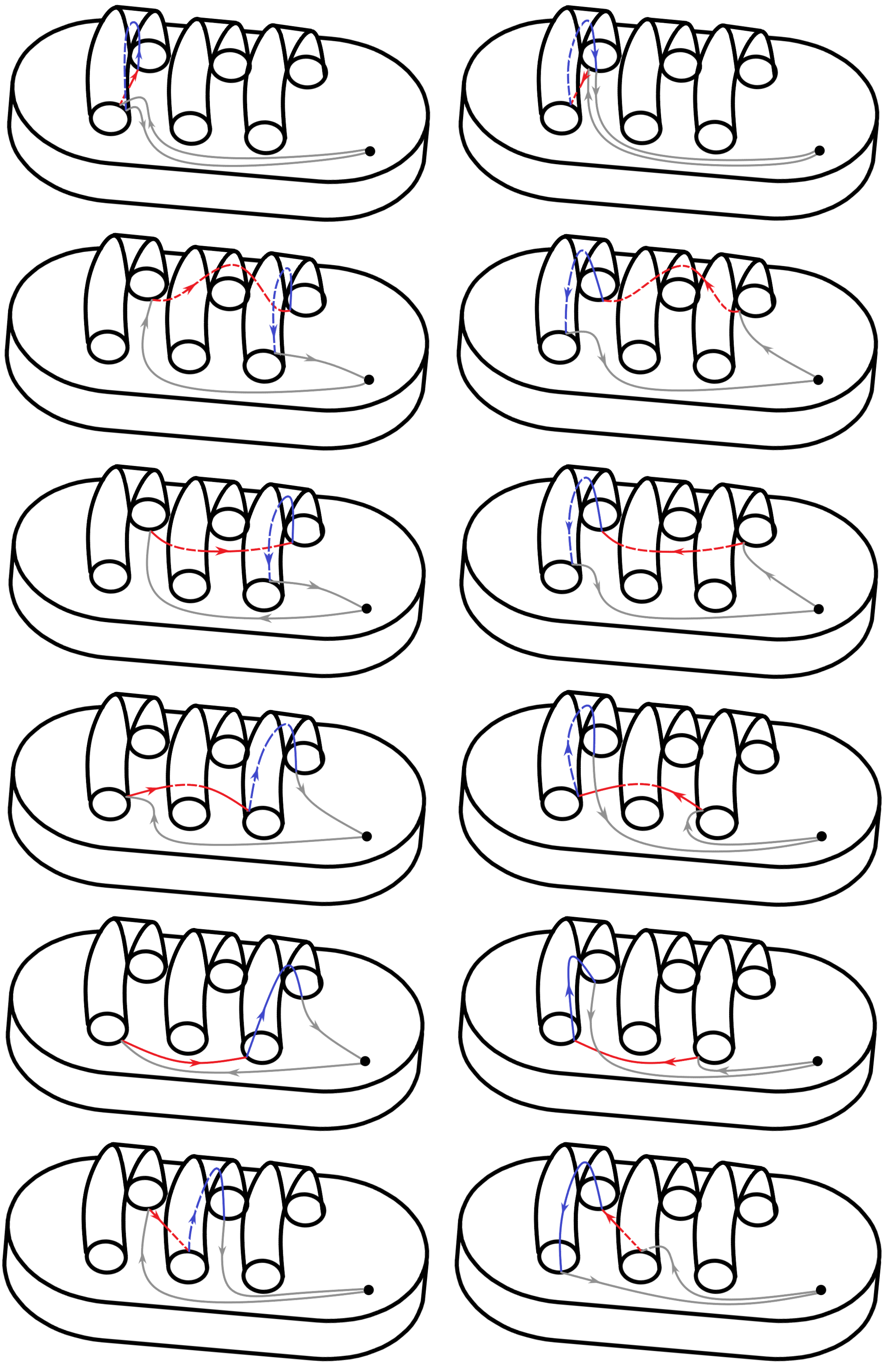

Figure 4.7: From top to bottom, the two possible b-moves, c-moves, d-moves, e-moves, f-moves and g-moves.

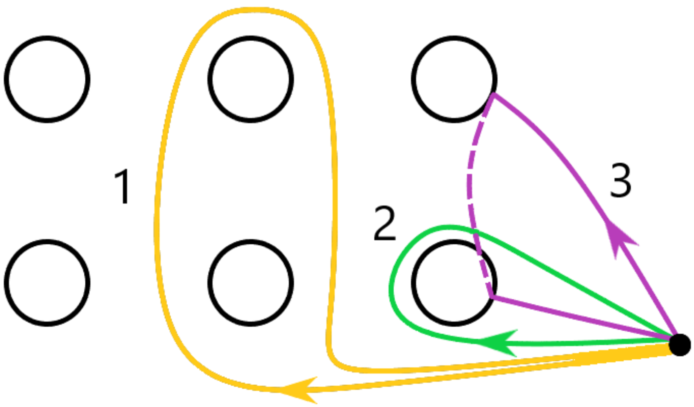

Figure 4.8: The partitioning of case $\vec{c}$.

Chapter 5

An algorithm for passing from plat to standard closure of braids and vice versa

In the preliminaries we saw how links could be represented using closures of braids, both with the standard procedure and the plat one. The goal of this chapter is to give an algorithmic way to pass from one representation to the other, in the three cases of $\mathbb{R}^3$, handlebodies and thickened surfaces. We will also produce a C++ program that reproduces the construction and has linear computational complexity on the number of crossings. In this chapter we will usually employ capital letters for braids in plat form and small greek letters for braids with standard closure.

Theorem 5.0.1. *Let X be $\mathbb{R}^3$ (or S^3), a handlebody H_g of genus g or a thickened closed, oriented and orientable (from now on c.c.o.) surface $N(\Sigma_g)$. Given a link L in X represented by a braid B with plat closure, it is algorithmically possible to generate a braid B' which represents an equivalent link in X but with standard closure. The algorithm has a computational complexity of $O(N')$ where N' is the sum of the number of crossings, a_i and b_i type generators present in the braid B.*

In what follows we will prove Theorem 5.0.1 separately for each kind of X.

It is straightforward to produce, for a given link represented by a braid with standard closure, a braid in plat form representing the same isotopy class of the link. It is more elaborate to find the opposite one, passing from plat to standard closure of a braid. In the subsections below we start from the easy way round, then, defining some useful constructions, we obtain the results for the three settings of $\mathbb{R}^3$, handlebodies and thickened surfaces in Sections 5.1.2, 5.2 and 5.3 respectively.

5.1 The $\mathbb{R}^3$ case

5.1.1 From standard closure to plat closure of braids

Let L be a link in $\mathbb{R}^3$ and $B' \in \mathcal{B}_m$ be a braid which represents L via standard closure. We want to produce a new braid $B \in \mathcal{B}_{2n}$ which represents the same link but via the plat closure. In fact, it is easy to produce B given B': in facts, it can be done taking the i-th closure strand and let it pass behind on the right of the i-th strand, becoming the $(2i-1)$-th and $2i$-th strands in the other representation. Fig. 5.1 is an example of the transformation. Note that, given the standard orientation of a classical braid, all the new strands that we have are oriented upward (the red arcs in Fig. 5.1).

In algebraic terms, it is possible to obtain the transformation replacing each σ_i^k by:

$$\sigma_i^k \to \sigma_{2i-1}^{-1}\sigma_{2i}^k\sigma_{2i-1}, \qquad k = \pm 1. \tag{5.1}$$

We shall now define a useful notion:

Definition 5.1.1. We will say that a braid B representing a link via plat closure is in *canonical plat form* if each corresponding pair of even numbered endpoints are joined by a simple arc running entirely underneath the rest of the plat diagram, like in Fig. 5.1.

We can now state the following:

Lemma 5.1.1. *Every link is isotopic to a closed braid in canonical plat form.*

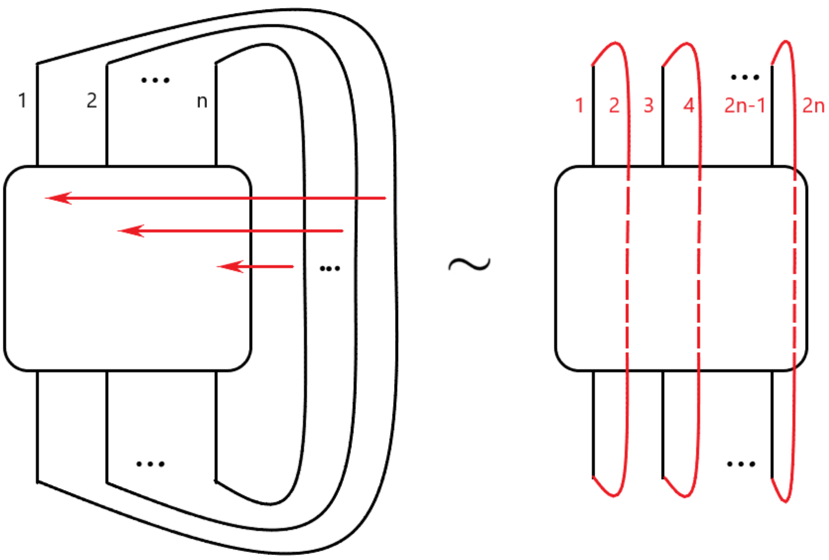

Figure 5.1: Passing from standard closure to the canonical plat form.

This is easily proven by assigning an orientation to each link component and using the Alexander theorem. Then we apply the isotopy illustrated in Fig. 5.1 and Definition 5.1.1. Note that, in this case we can orient the braid such that the strands connecting the even numbered endpoints are oriented upward. In fact, it follows from above that we can always orient a plat in canonical form in this way.

Furthermore, we have:

Lemma 5.1.2. *A braid B in canonical plat form is equivalent to a braid B' in plat form with some corresponding pairs of even numbered endpoints joined with simple arcs running entirely above (and not below) the rest of the braid.*

Since B is in canonical plat form, Lemma 5.1.2 is clear, as illustrated in Fig. 5.2.

5.1.2 From plat closure to standard closure of braids

Let L be a link and $B \in \mathcal{B}_{2n}$ a braid representing L via plat closure. Our aim is to prove the following:

Theorem 5.1.1. *Given a link L represented by a braid $B \in \mathcal{B}_{2n}$ with plat closure, it is possible algorithmically to generate a braid β which represents an equivalent link but with standard*

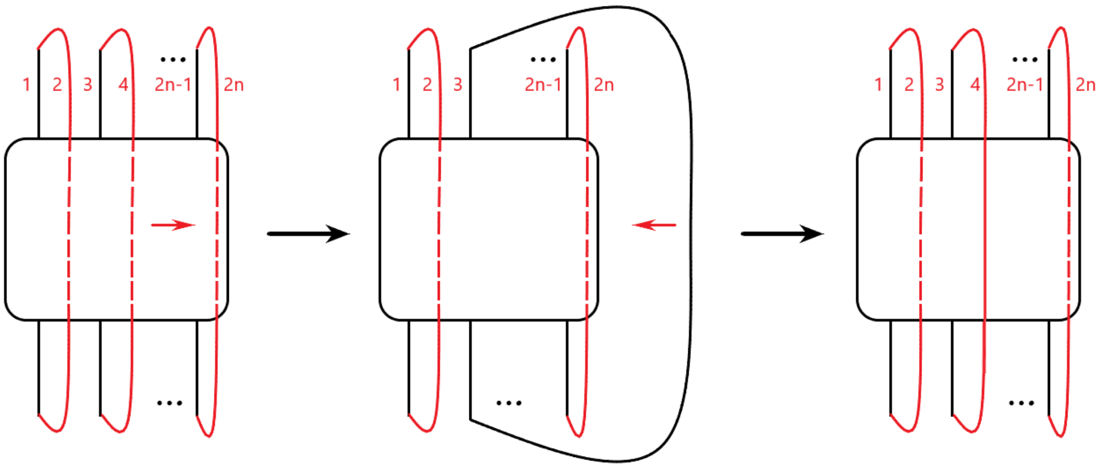

Figure 5.2: Passing one under arc into an over arc.

closure and vice versa. The algorithm has a computational complexity of $O(N^2)$ *where* N *is the number of crossings.*

Our strategy for proving Theorem 5.1.1 is to generate from B a plat B' in canonical plat form with isotopic plat closure. Before proving the theorem, we shall give some useful constructions.

First, we give an orientation to the braid. As a standard procedure, we give downward orientation to the leftmost strand of B. Then we orient subsequent strands by following this orientation also in the plat closures. If any strand of B lacks orientation (in the case of B representing a link with at least 2 components) then we take the first strand from the left with no orientation (it will be an odd strand) and give it a downward orientation.

Then we focus on the crossings. We divide them in four categories as illustrated in Fig. 5.3, where in the region of the red dot there is an over or an under crossing. We want to create a braid with all crossing of type a. For this reason, we shall to apply S-moves (see next section) to every crossing of type b, c, d.

The S**-move**

As we recall in Section 2.2, Birman introduced the *stabilization move* as a move between braids in plat form with isotopic plat closure, see Fig. 2.17. Here we use an “open-ended” version of

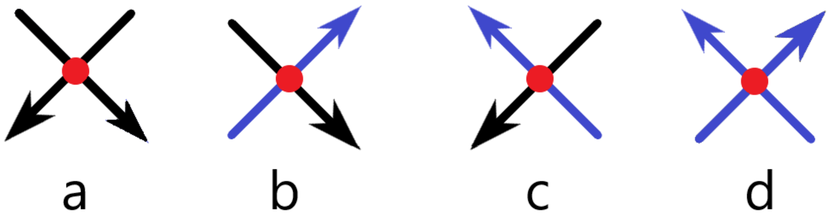

Figure 5.3: The four possible crossings.

a special case of the stabilization move; this shall be called *S-move*, more precisely:

Definition 5.1.2 (S-move)**.** The *S-move* is an adaptation of the stabilization move in the case of oriented plats, with the following features:

- it is applied on up-arcs;
- the two isotopy spikes take place both entirely underneath or entirely above the rest of the diagram according to whether it is an under or over up-arc;
- it eliminates the up-arc and produces two open-ended down-arcs which make a pair of corresponding braid strands.

Take, for example, a b, c or d type of crossing and consider a small piece of the up going strand (in case d we do the operation for both strands one after the other). Fig. 5.4 illustrates the case of a type b crossing where the up-arc is an "under" arc. The S-move starts with an isotopy which carries this arc across a small sliding triangle so that the arc is replaced by the horizontal and vertical sides of the triangle. Then a stabilization move is applied to the vertical side of the triangle, so the two isotopy spikes take place both entirely underneath or entirely above the rest of the diagram. In Fig. 5.4 this is depicted by the addition of two blue and one red arcs. The S-move is completed by omitting the red arc from the representation. In Fig. 5.5 are represented the three possible cases of crossings. In both figures, as well in subsequent figures, we have indicated with dust-grey lines the arcs that may appear in the plat closure. Notice that there could be instances where there are no closure arcs (when the left hand side strand is an even numbered one).

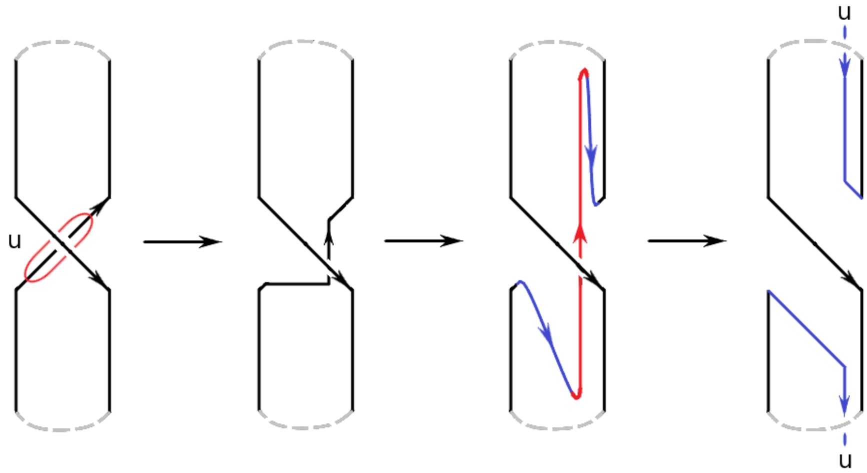

Figure 5.4: The S-move.

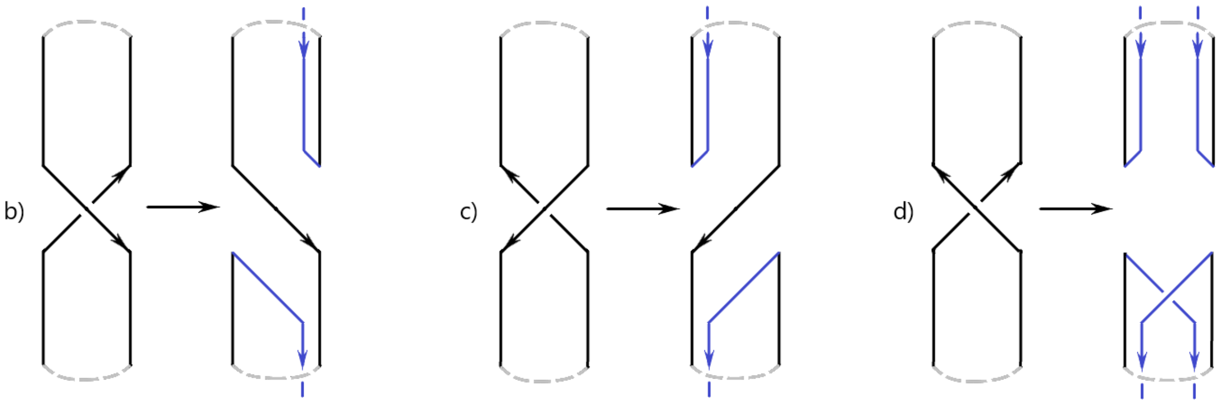

Figure 5.5: The three possible outcomes of a S-move.

Remark 3. The elimination of the up-arc in Definition 5.1.2 is really crucial so that the application of an S-move will not create other b, c or d-type crossings.

Managing crossings on the same column

If we have different S-moves applied on the same column, we do them in such a way that blue arcs coming from the same type of crossings never intersect each other. An example can be seen in Fig. 5.7: the red arcs coming from the c-type crossings are all on the left, one after the other, while the blue arcs coming from the b-type crossings are all on the right in a similar manner. d-type crossings generate one left and one right string. It is important to note that, once we have the sequence of all the crossing (with labelled type), we can reconstruct all the generated crossings.

Suppose now that we have, in the column i, a total number of H type c and d crossings and K type b and d crossings. After an a, b, c or d type crossing, say $\bar{\sigma}_i$, we will have a situation like in Fig. 5.8. Here, we can see how all different cases present different outcomes for the starting and ending strand. The resulting sequence of crossings can be described in these explicit formulas:

$$\begin{aligned}C_a(\bar{\sigma}_i) =&(\sigma_i^{\delta_i}\sigma_{i+1}^{\delta_{i+1}} \dots \sigma_{i+H-1}^{\delta_{i+H-1}})(\sigma_{i+H+K}^{\delta_{i+H+K}}\sigma_{i+H+K-1}^{\delta_{i+H+K-1}} \dots \sigma_{i+H+1}^{\delta_{i+H+1}})\bar{\sigma}_{i+H}\\ &(\sigma_{i+H-1}^{-\delta_{i+H-1}}\sigma_{i+H-2}^{-\delta_{i+H-2}} \dots \sigma_i^{-\delta_i})(\sigma_{i+H+1}^{-\delta_{i+H+1}}\sigma_{i+H+2}^{-\delta_{i+H+2}} \dots \sigma_{i+H+K}^{-\delta_{i+H+K}})\end{aligned} \tag{5.2}$$

$$C_b(\bar{\sigma}_i) =(\sigma_i^{\delta_i}\sigma_{i+1}^{\delta_{i+1}} \dots \sigma_{i+H-1}^{\delta_{i+H-1}})(\sigma_{i+H}^{\delta_{i+H}}\sigma_{i+H+1}^{\delta_{i+H+1}} \dots \sigma_{i+H+K-1}^{\delta_{i+H+K-1}})(\sigma_{i-1}^{\delta_{i-1}}\sigma_i^{\delta_i} \dots \sigma_{i+H-2}^{\delta_{i+H-2}}) \tag{5.3}$$

$$C_c(\bar{\sigma}_i) =(\sigma_{i+H+K}^{\delta_{i+H+K}}\sigma_{i+H+K-1}^{\delta_{i+H+K-1}} \dots \sigma_{i+H+1}^{\delta_{i+H+1}})(\sigma_{i+H}^{\delta_{i+H}}\sigma_{i+H-1}^{\delta_{i+H-1}} \dots \sigma_{i+1}^{\delta_{i+1}})(\sigma_{i+H+K+1}^{\delta_{i+H+K+1}}\sigma_{i+H+K}^{\delta_{i+H+K}} \dots \sigma_{i+H+2}^{\delta_{i+H+2}}) \tag{5.4}$$

$$C_d(\bar{\sigma}_i) =(\sigma_i^{\delta_i}\sigma_{i+1}^{\delta_{i+1}} \dots \sigma_{i+H-1}^{\delta_{i+H-1}})(\sigma_{i+H+K}^{\delta_{i+H+K}}\sigma_{i+H+K-1}^{\delta_{i+H+K-1}} \dots \sigma_{i+H+1}^{\delta_{i+H+1}})\bar{\sigma}_{i+H}^{-1} \tag{5.5}$$

With $\delta_{i-1}, \delta_i, \delta_{i+1}, \dots, \delta_{i+H+K} \in \{+1, -1\}$ depending on the S-moves: if the relative S-move is over or under then the signs will be positive or negative.

When dealing with this transformation is easy to check that we actually create some local minima or maxima along our braid. Checking all possibilities of subsequent a, b, c and d type crossings, according to the orientation of the strands, the situation can be brought to a standard braid with a local isotopy move or a Reidemeister I move. In Fig. 5.9 there are some interesting cases. Note that, in fact, these are the only cases where Reidemeister I will appear, indeed when we consider braids with multiple columns, the process will eliminate all up arcs in the boundary of the columns with the process we describe. If we have a Reidemeister I move it is important to note that we have to eliminate the related crossing, following this scheme:

- two d-type crossings one after the other on the same column: remove $\sigma_i^{\delta_i}$ and $\sigma_{i+H+K}^{\delta_{i+H+K}}$ from the first C_d;
- a b-type crossing followed by a c-type crossing on the same column: remove $\sigma_{i-1}^{\delta_{i-1}}$ from C_b;
- a c-type crossing followed by a b-type crossing on the same column: remove $\sigma_{i+H+2}^{\delta_{i+H+2}}$ from C_c;

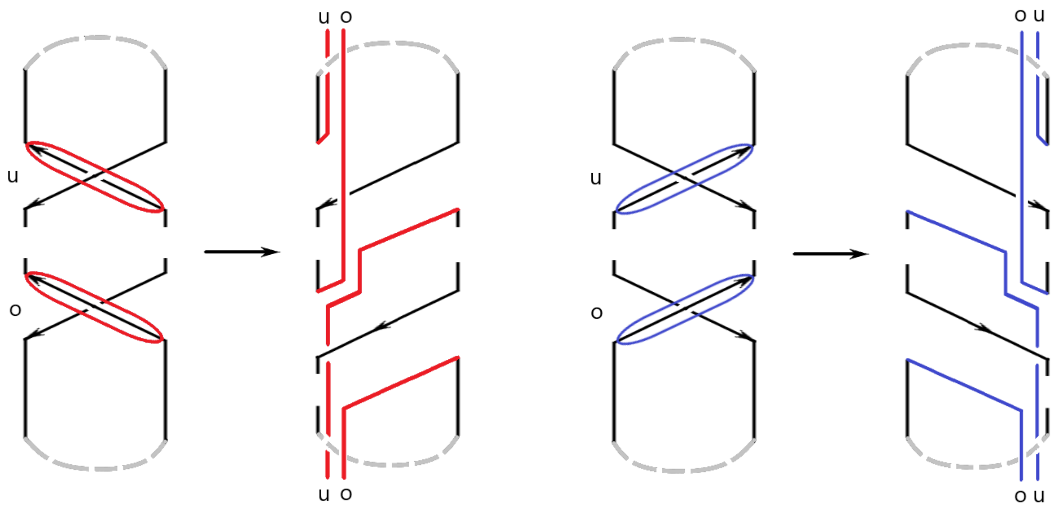

Figure 5.6: The S-move applied on different crossings on the same column, which creates only left or right new strands.

Top part and bottom part management

Now that we have dealt with all the possibilities in the braid, we have to address the problem of the intersections of the new strands with the plat closure arcs of the braid. In fact, the new

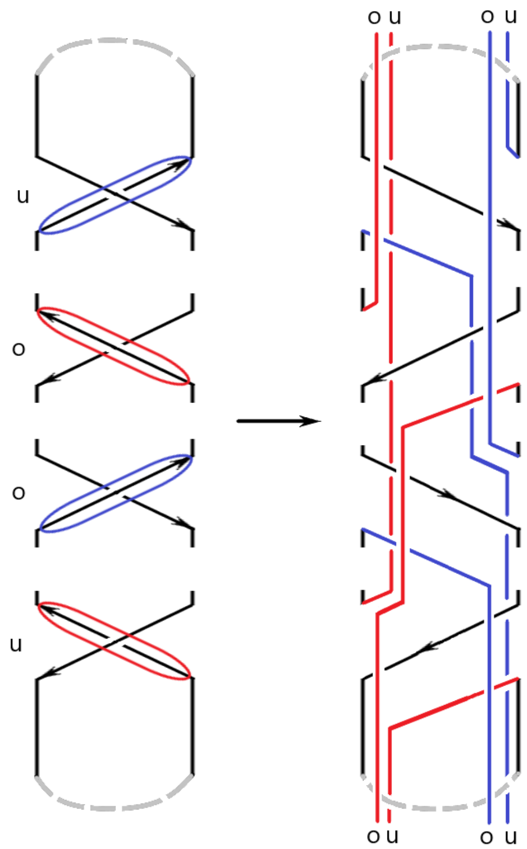

Figure 5.7: The S-move applied on different crossings on the same column.

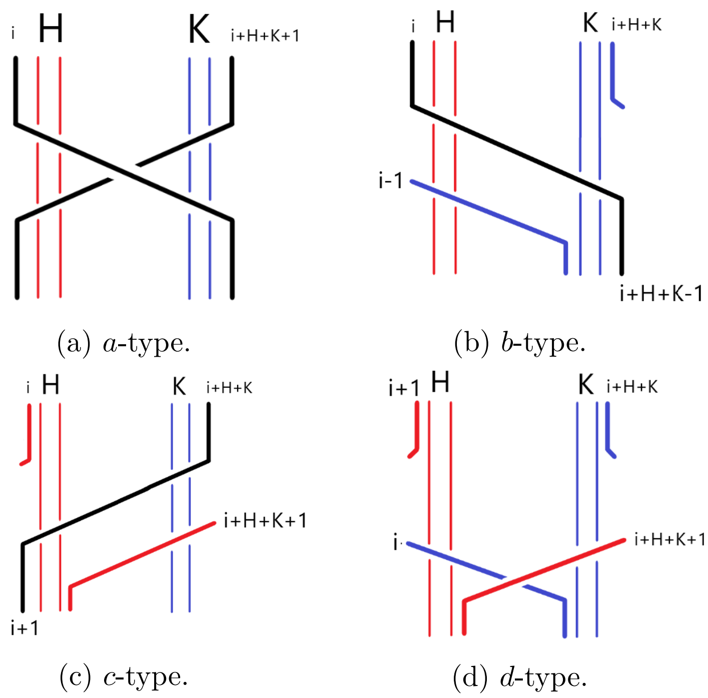

Figure 5.8: The four possible outcomes after all the S-moves in a column.

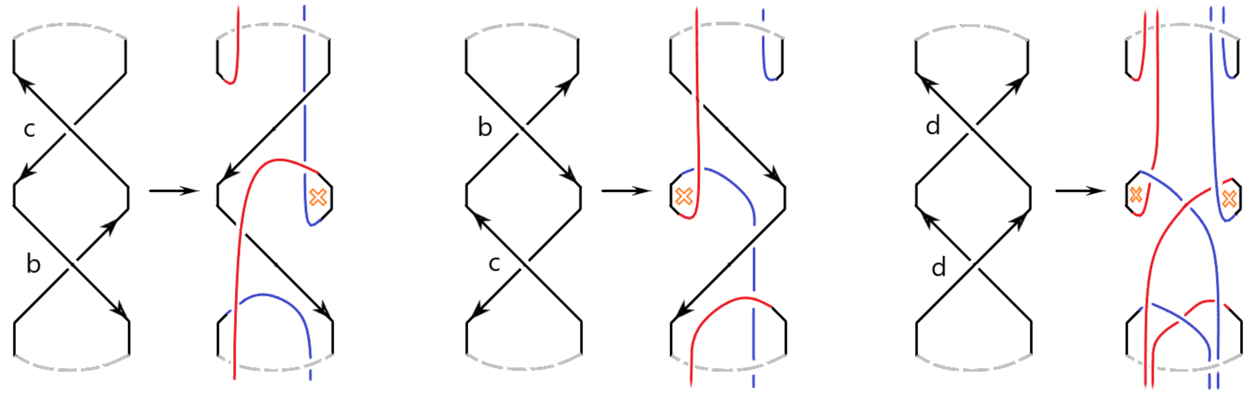

Figure 5.9: Some cases where the Reidemeister I move is needed to bring the braid into standard position.

strands and these intersections are formed with applications of S-moves, since the new strands extend higher than the top plat closure and lower than the bottom plat closure.

For this reason, we have some possibilities occurring, depending on the orientation of the top (resp. bottom) plat closure arc and the possible crossings present right below (resp. above) it.

Let us consider the top part first. Observing that only the odd labelled columns contain the plat closure arcs, we will only focus on these, because we will not add crossings in the top part while performing the S-move along the even columns. We will address the odd column that we are working on with label i. We have two possible orientations for the plat closure arc, from left to right and from right to left, and we will analyze them separately.

With orientation from right to left, it is easy to see that, if there are crossings in columns i or $i+1$, the first that joins the up arc of the closure arc one needs to agree to the orientation: type b or d in column i, type c or d in column $i+1$.

Of course, in the first case, we will need to perform a S-move on the crossing, obtaining the situation depicted in Fig. 5.10a. Considering the number of type c and d crossings as before, it is straightforward to check that in this case the new crossings form the word:

$$T_{L,i} = \sigma_{i+H+K-2}\sigma_{i+H+K-3}\cdots\sigma_{i+1}\sigma_i \tag{5.6}$$

with signs depending on the S-moves. It is important to note that, as we saw in the previous paragraph, we can apply a Reidemeister I move in the top right part to get the braid into a standard position: we would have also a $\sigma_{i+H+K-1}$ but we have removed it.

In the same way, for the $i+1$ case we get the construction in Fig. 5.10b and obtain the expression:

$$T_{L,i+1} = \sigma_{i+H+K-1}\sigma_{i+H+K-2} \dots \sigma_{i+1}\sigma_i \tag{5.7}$$

with signs depending on the S-moves, and no Reidemeister moves.

With orientation from left to right, in the same way as before, we can see that if there are crossings in columns i or $i-1$, the first one joining the up-arc of the closure arc needs to agree to the orientation: type b or d in column $i-1$, type c or d in column i. Analogously, following the construction in Fig. 5.10c-5.10d, we obtain the two expressions:

$$T_{R,i-1} = \sigma_i\sigma_{i+1} \dots \sigma_{i+H+K-2}\sigma_{i+H+K-1} \tag{5.8}$$

$$T_{R,i} = \sigma_i\sigma_{i+1} \dots \sigma_{i+H+K-1}\sigma_{i+H+K-2} \tag{5.9}$$

with signs depending on the S-moves and a Reidemeister I move in the second case, which changes the number of the strings and leads to the final expression.

Now we consider the bottom part. Following the same process, we have the two possible orientations and four possible cases in total for the crossings: Right to left, crossing of type c or d in column $i-1$, Fig. 5.11a; we can check how in column $i-1$ nothing changes from the standard c or d case, but in column i we have

$$B_{L,i-1} = \sigma_{i+H+K-1}\sigma_{i+H+K-2} \dots \sigma_i \tag{5.10}$$

Right to left, crossing of type b or d in column i, Fig. 5.11b; following the picture, we can perform the Reidemeister II move on the left side (since all the crossings are coupled) eliminating the crossings on the left part and then the Reidemeister I move, thus obtaining

$$B_{L,i} = \sigma_{i+H}\sigma_{i+H+1} \dots \sigma_{i+H+K-2} \tag{5.11}$$

with again signs depending on the S-moves.

Left to right, crossing of type c or d in column i, Fig. 5.11c; as before, we perform the Reidemeister II move but on the right side and then the Reidemeister I move, thus obtaining

$$B_{R,i} = \sigma_i\sigma_{i+1} \dots \sigma_{i+H-2} \tag{5.12}$$

with signs depending on the S-moves.

Left to right, crossing of type b or d in column $i+1$, Fig. 5.11d; as before, in column $i+1$ nothing changes from the standard b or d case, adding in column i

$$B_{R,i+1} = \sigma_i\sigma_{i+1} \dots \sigma_{i+H+K-1} \tag{5.13}$$

with signs depending on the S-moves.

Remark 4. Until now we always considered the case of a column with at least one crossing. If we have no crossings in two subsequent columns, then we will have between them a strand which goes straight from top to bottom. If it has an upward orientation then it can be considered as one of the closures in the standard closure, putting it aside.

Moreover, if we have three consecutive empty columns, the first one of which is odd labeled, then we will have an extra trivial component to our link.

Proof of Theorem 5.1.1

We are ready to prove the main theorem of this section:

Proof. Following the procedure of last section, give an orientation to the braid and label each crossing following Fig. 5.3. We now perform the S-move on every b, c, d-type crossing, obtaining

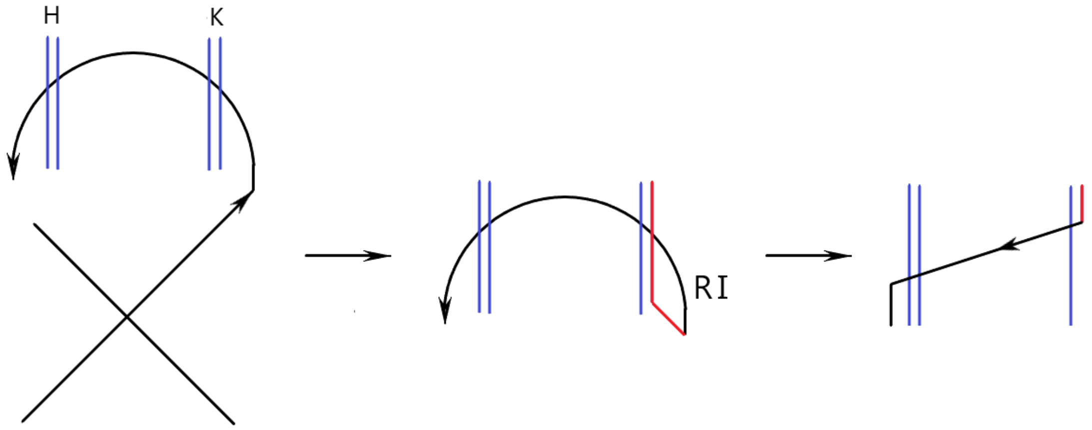

(a) Top part with orientation right to left, first case.

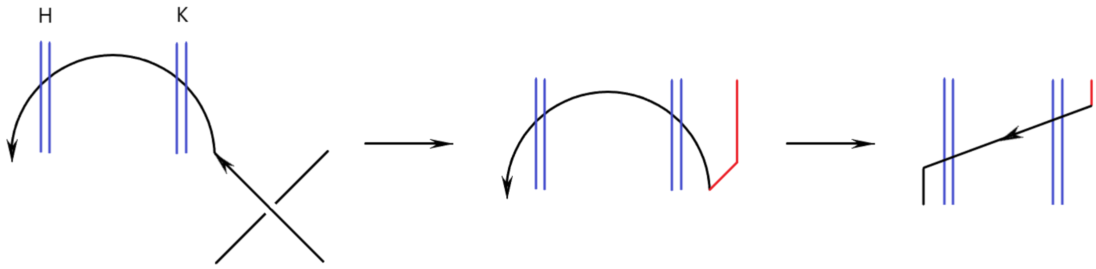

(b) Top part with orientation right to left, second case.

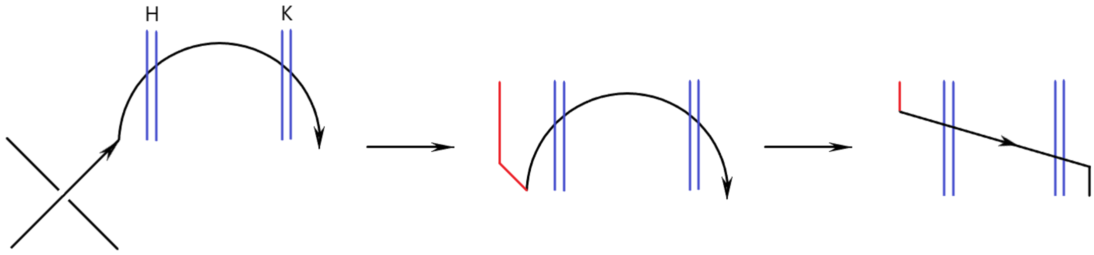

(c) Top part with orientation left to right, first case.

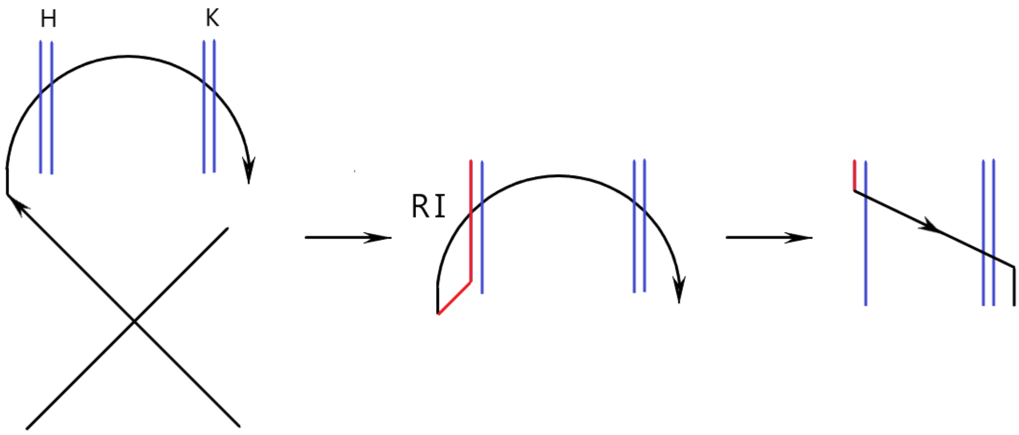

(d) Top part with orientation left to right, second case.

Figure 5.10: Management of the top plat closure arcs.

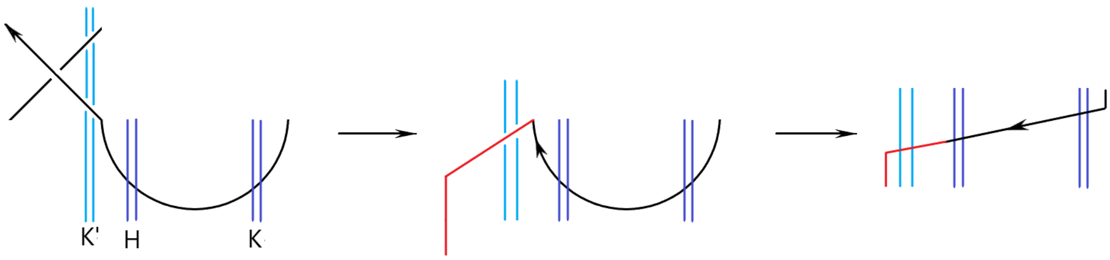

(a) Bottom part with orientation right to left, first case.

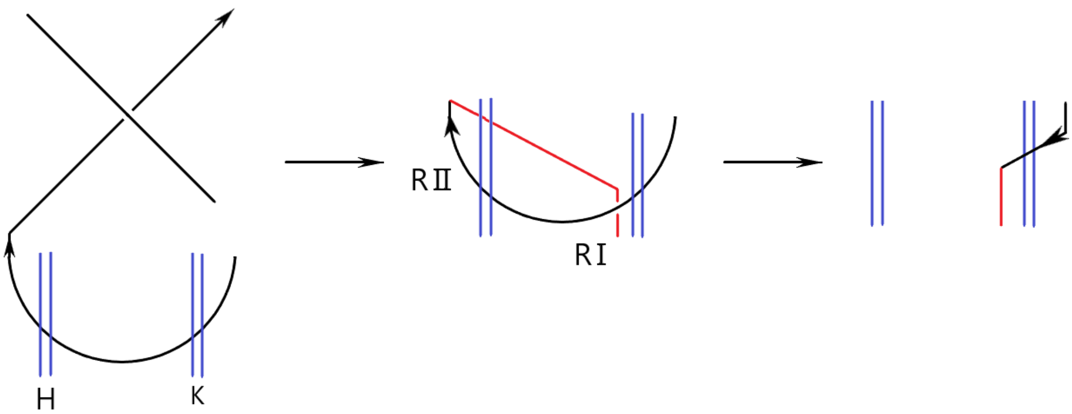

(b) Bottom part with orientation right to left, second case.

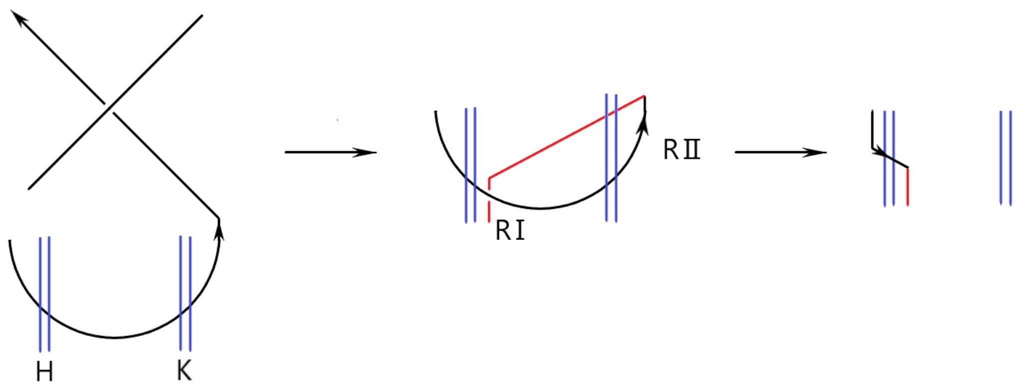

(c) Bottom part with orientation left to right, first case.

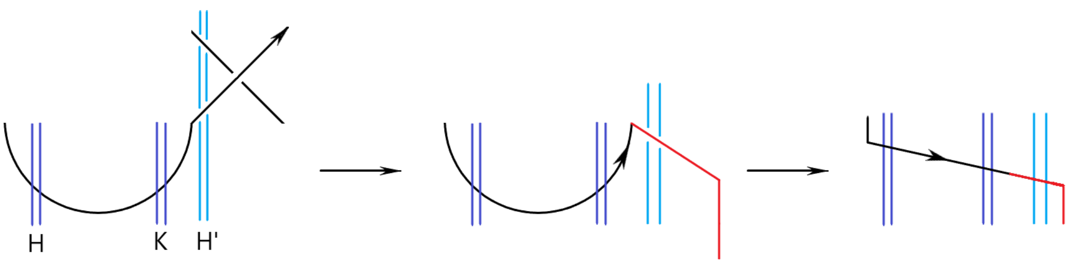

(d) Bottom part with orientation left to right, second case.

Figure 5.11: Management of the bottom plat closure arcs.

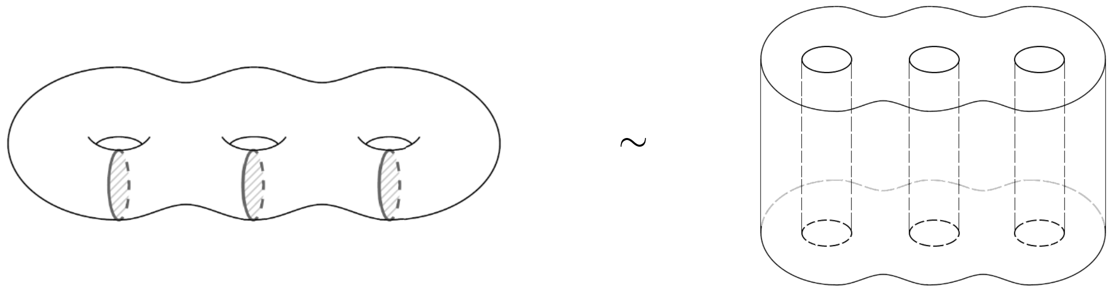

Figure 5.12: Standard handlebody.

only a-type crossings. If we have a total of n_a, n_b, n_c and n_d crossings of a, b, c, d-type, then performing all the S-moves on the crossings of b, c, d-type, we add a total of $n_b + n_c + 2 \cdot n_d$ new strands. If there are trivial cases, where there are no crossings in a column, then move one of the free strands above the braid.

Now all the new strands and the ones coming from the trivial cases lay entirely above or underneath the braid.

Using the result from Lemma 5.1.2, we have as a result that the link represented by the newly generated braid with classical closure is equivalent to L.

Since the operations made are all substitutions on the crossings and are done at most once every crossing, and since we need to check all other crossings on the same column in order to keep track of the type of crossing affected by the S-moves (if the changed arc was an over or under arc), in the worst case scenario the number of controls needed is $N \times (N-1)$, where N is the number of crossings. We can deduce that the computational complexity of the algorithm is quadratic in the number of the crossings. □

5.2 The handlebody case

Let H_g be the standard handlebody of genus g. As seen in the preliminaries and in Section 2.1.2, H_g may be viewed in $\mathbb{R}^3$ as the complement of the identity braid I_g on g indefinitely extended strands. For viewing H_g in S^3 we consider all strands of I_g meeting at the point at infinity. See Fig. 5.12.

Let now L be a link in H_g. Then, using the above representation and fixing I_g point-wise, L

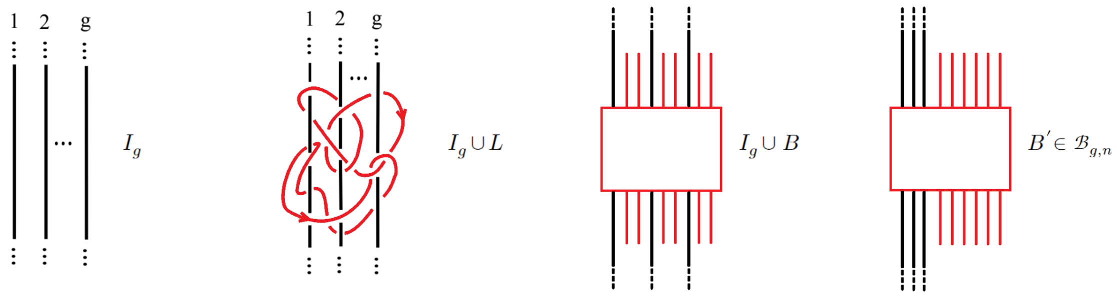

Figure 5.13: Representing H_g in S^3, links in H_g, braids in H_g and elements of $\mathcal{B}_{g,n}$.

may be unambiguously represented by $I_g \cup L$, see Fig. 5.13 for an element of $\mathcal{B}_{g,n}$.

As shown in Section 2.1.2, closing in the standard way the moving part of the braid gives us an oriented mixed link. Note that, in the case of knots and links in H_g, the closing arcs may run entirely over or entirely under the rest of the mixed braid diagram, and different choices are expected to result in different knots or links.

Let $B \in \mathcal{B}_{g,2n}, \beta \in \mathcal{B}_{g,m}$ be two braids representing L via plat closure and standard closure. While it is shown in [34] the braiding algorithm for links represented via standard closure of braids in handlebodies, for the plat closure case we have to adapt the braiding algorithm of [13, 17] for our setting.

Theorem 5.2.1. *Every link L in a genus g handlebody H_g may be braided to a geometric braid in $\mathcal{B}_{g,2n}$, whose plat closure is equivalent to L.*

Proof. Let L be a link in H_g as in the premise, and Σ be a plane cutting H_g and having intersection with all strands of I_g. It is always possible to consider $L \subset N(\Sigma)$, a neighbourhood of Σ. Let $\vec{\Sigma}$ be the unit vector orthogonal to Σ. Now we choose a parametrization $N(\Sigma) = \Sigma \times [0,1]$, such that $L \subset \Sigma \times [0.25, 0.75]$. Consider a polygonal representation of L, with vertices $\{b_0, b_1, \dots, b_n\}$ and no edges parallel to Σ. Following [13, Lemma 2], we have that for any 3 consecutive vertices b_{j-1}, b_j, b_{j+1} of L the line l_j orthogonal to Σ through b_j admits a neighborhood N_j which meets the link only in the edges $[b_{j-1}, b_j]$ and $[b_j, b_{j+i}]$ (see Fig. 5.14).

Then, starting from b_0, for every three points b_{j-1}, b_j, b_{j+1} with

$$([b_{j-1}, b_j] \cdot \vec{\Sigma}) \cdot ([b_j, b_{j+1}] \cdot \vec{\Sigma}) < 0$$

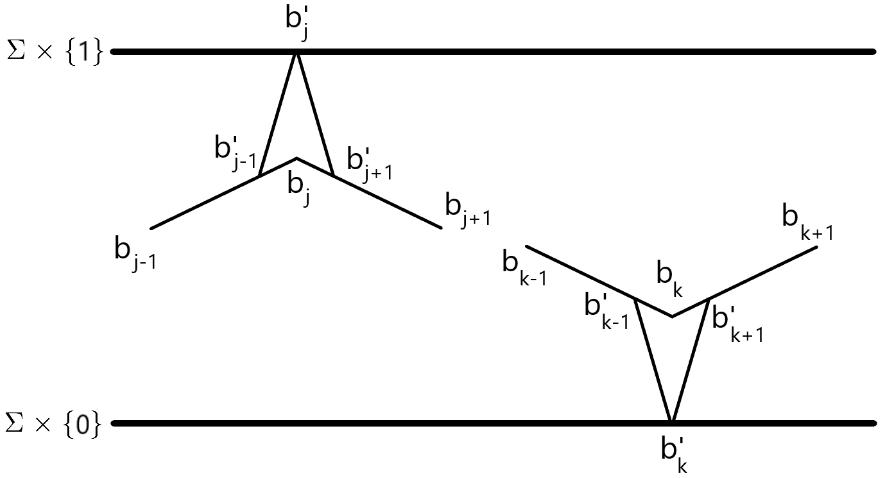

Figure 5.14: The braiding process, reproduced and relabeled from [17].

consider the intersections $[b_{j-1}, b_j] \cap N_j = b'_{j-1}$, $[b_j, b'_{j+1}] \cap N_j = b'_{j+1}$. If $[b_{j-1}, b_j] \cdot \vec{\Sigma} > 0$ (resp. < 0) let $b'_j = l_j \cap \Sigma \times \{1\}$ (resp $b'_j = l_j \cap \Sigma \times \{0\}$). If we replace the edge sequence b_{j-1}, b_j, b_{j+1} with $b_{j-1}, b'_{j-1}, b'_j, b'_{j+1}, b_{j+1}$ the isotopy class of the link does not change, while now the link intersects once $\Sigma \times \{0, 1\}$.

Repeating this operation for every three points satisfying the above condition, we will obtain an equivalent link meeting the planes $\Sigma \times \{0\}$ and $\Sigma \times \{1\}$ in exactly, say, n points, while every other plane $\Sigma \times \{t\}, t \in (0, 1)$ in exactly $2n$ points.

It follows from Artin [5] that such a link determines a well-defined element of $B \in \mathcal{B}_{2n}$, which represents back the link via plat closure on $\Sigma \times \{0, 1\}$.

Now, since we have I_g as the point-wise fixed identity braid on g strands representing the handlebody, if we consider $B \cup I_g$, we get an element of $\mathcal{B}_{g+2n}$. Still, it does not belong to $\mathcal{B}_{g,2n}$ because it is not parted (as in [43]). In order to do so, we recall the *spike move* [13] as follows (see Fig. 5.15): let b_i, b_{i+1}, b_{i+2} be three consecutive points of L such that b_{i+1} is a boundary point and such that the triangle $[b_i, b_{i+1}, b_{i+2}]$ intersects L only on its sides $[b_i, b_{i+1}], [b_{i+1}, b_{i+2}]$, and let b'_{i+1} be a new boundary point on the same boundary component of b_{i+1}; let b'_i, b'_{i+2} be interior points satisfying the conditions $[b_{i+2}, b'_{i+2}, b'_i] \cap L = \{b'_{i+2}\}, [b_i, b'_{i+2}, b'_i] \cap L = \{b'_i\}$ and $[b_i, b'_{i+1}, b'_{i+2}] \cap L = \emptyset$; replacing the edge sequence b_i, b_{i+1}, b_{i+2} with $b_i, b'_i, b'_{i+1}, b'_{i+2}, b_{i+2}$ the isotopy class of the link does not change.

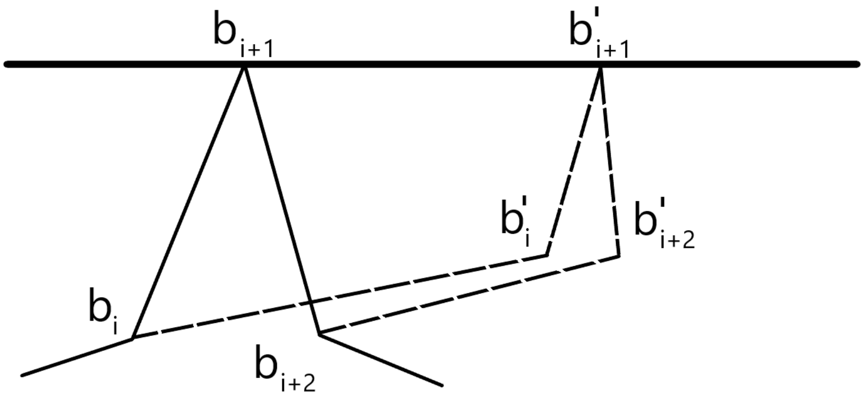

Figure 5.15: An example of spike move.

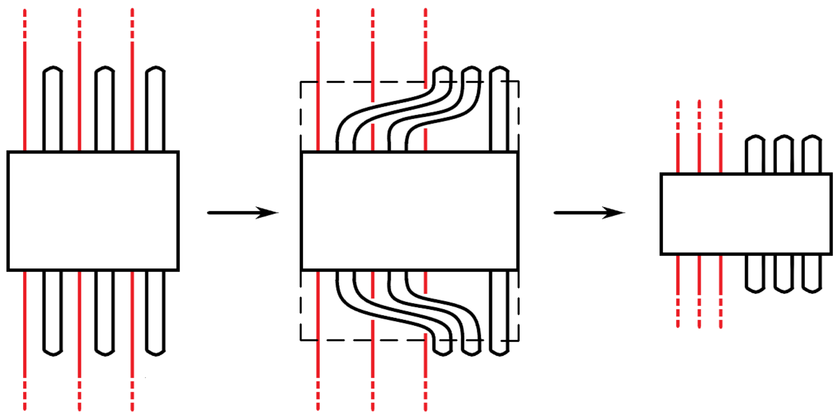

Figure 5.16: The process of parting the braid.

Applying this move to all boundary edges which are on the left of some strings of I_g, we can part the braid letting all the spike braids on the right of all I_g strings being careful to pass these new strands over the strands of I_g (see Fig. 5.16), thus obtaining an element of $\mathcal{B}_{g,2n}$.

□

The operation that let us obtain a representative of the link in both closures, knowing one of the two, is quite similar to the one described in the previous sections, after taking care of the a_i generators of the braids.

We have a_i, σ_i type generators in both representations, via plat or standard closure. For the sake of completeness, it has to be said that the definitions of a_i generators in [17] and [43] are slightly different, see Fig. 5.17 (see also [22], where the transition between the two representations of the mixed braid group is discussed for the case of Heegaard genus $g = 1$). It is still possible

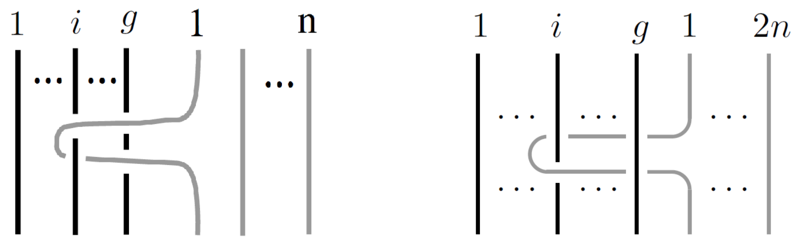

Figure 5.17: The two different definitions of a_i: the case of standard closure on the left [43] and the case of plat closure on the right [17].

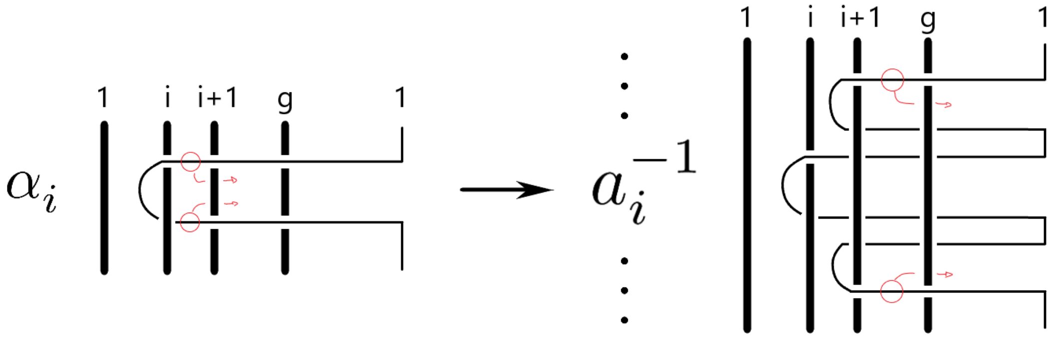

Figure 5.18: Transformation from the α_i to the a_i generator.

to obtain one representation from the other, since there is a equivalence between the first one, say a_i, and the second one, say α_i:

$$\alpha_i^k \iff a_g^{-1} a_{g-1}^{-1} \dots a_{i+1}^{-1} a_i^{-k} a_{i+1} \dots a_{g-1} a_g, \qquad k = \pm 1$$

A geometric interpretation of this equivalence is depicted in Fig. 5.18. From now on, without loss of generality, we will only use a_i to refer to this kind of generators.

The procedure to adopt in both cases (going from standard closure and vice versa) is quite similar to the one that we have already described. For the first one, from standard closure to plat closure of a braid, we follow the same construction of Section 5.1.1: we take the i-th closure arc and we let it pass behind on the right of the i-th strand, becoming the $(2i-1)$-th and $2i$-th strands in the other representation. Since the moving braid can be considered on the right part of the handlebody, this is always possible without interfering with the fixed part of the braid (representing the holes of the handlebody). The algebraic transformation is still Equation 5.1.

The vice versa needs more details. Recall that in this setting the moving braid can be considered on the right part of the handlebody. After giving an orientation to our braid, the situation is very similar to the one that we have in Section 5.1.2, but with a difference: now we can have also an upward or downward oriented a_i generator.

In the braid with standard closure that we will obtain, all a_i generators will be oriented downwards. For this reason, in the braid with plat closure, we have to perform a twist on the a_i's which are oriented upwards, following the construction depicted in Fig. 5.19. Note that after the twist, a_i changes its sign and a d-type crossing is generated into the "0"-th column.

The last thing to do is to perform an S-move for every twist done in this way, say k twists and S-moves in total. When we focus on the result on the "0"-th column, we have: (see Fig. 5.20)

- any not twisted a_i becomes $\sigma_{2k}\sigma_{2k-1}\dots\sigma_{k+1}\sigma_k^{-1}\sigma_{k-1}^{-1}\dots\sigma_1^{-1}a_i\sigma_1\sigma_2\dots\sigma_k\sigma_{k+1}^{-1}\sigma_{k+2}^{-1}\dots\sigma_{2k}^{-1}$
- any twisted a_i becomes $a_i^{-1}\sigma_1\sigma_2\dots\sigma_{k-1}\sigma_{2k}\sigma_{2k-1}\dots\sigma_{k+1}\sigma_k$

Of course, if we have two S-moves one after the other, without any σ_1 in the middle, we will have to perform a Reidemeister I move in order to bring the braid into standard position, as shown in Fig. 5.20.

At this point we can apply, in the remaining part of the braid, the algorithm of Theorem 5.1.1. Note that, since all the substitutions made depend on the number of σ_i, a_i generators and on the type of crossings affected by the S-moves (i.e. the changed arc was an over or under arc), the computational complexity is quadratic, depending on the number of these two generators.

Therefore, the above construction proves the following:

Theorem 5.2.2. *Let H_g be a handlebody of genus g. Given a link $L \subset H_g$ represented by a braid $B \in \mathcal{B}_{g,2n}$ via plat closure, it is possible to generate algorithmically a braid $\beta \in \mathcal{B}_{g,m}$*

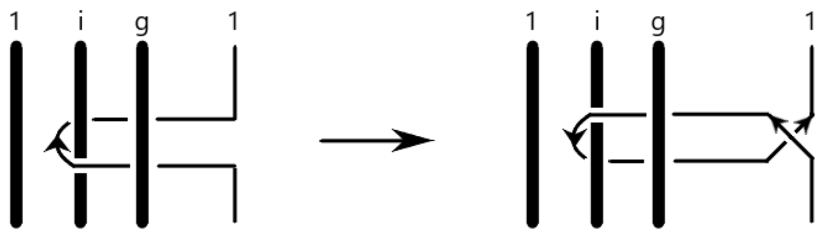

Figure 5.19: Twisting an $a_i^{\pm}$ oriented upward reverses the sign of the exponent and generates a d-type crossing.

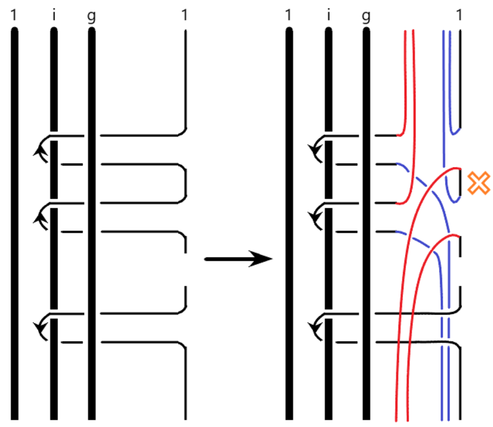

Figure 5.20: The result after all the twists and S-moves performed on the "0"-th column.

which represents, via standard closure, a link equivalent to L and vice versa. The algorithm has a computational complexity of $O(M^2)$ where M is the number of crossings and a_i type generators present in the braid B.

5.3 The thickened surface case

Let now Σ_g be a c.c.o. genus g surface, and consider the surface braid group $\mathcal{B}_{\Sigma_g,n}$ as in Section 2.2.

In this case, we will still represent braids belonging to $\mathcal{B}_{\Sigma_g,n}$ by a braid in $\mathcal{B}_{g+n}$ with the first g strings fixed as in the identity braid, and the last n strands moving. The fixed braid now represents geometrically the holes of Σ_g.

The braiding algorithm for links in thickened surfaces represented via plat closure of braids having an even number of strands is shown in [17]. For standard closure we can prove the

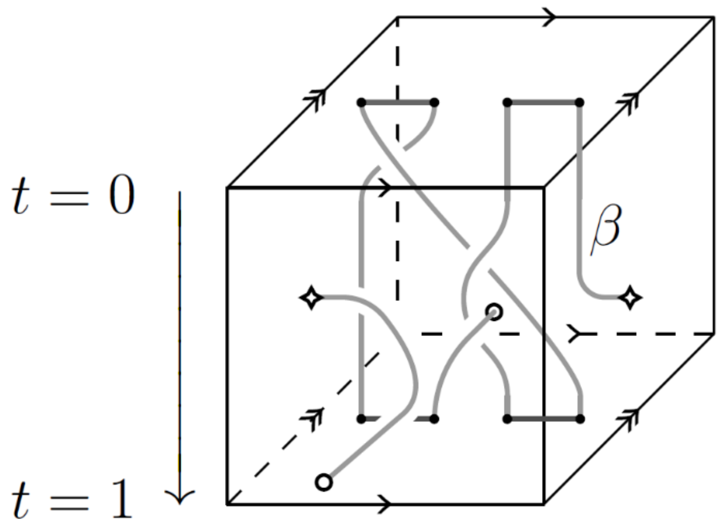

Figure 5.21: An example of braid in a thickened surface of genus one, reproduced from [17].

analogous theorem after showing the existence of a transformation from plat to standard closure.

It is important to note that, given a braid $B \in \mathcal{B}_{\Sigma_g, 2n}$, it is always possible to consider the points in $\mathcal{P}$ in a small disc $A \subset \Sigma_g$ such that all the σ_i generators of the braid B are contained in the intersection between the cylinder $A \times I$ and the braid B. This enables us to use the same definition of S-move as before, since in this case the move is done locally in the cylinder.

For the transformation that, given a braid representing a certain link via plat closure, produces an equivalent one via standard closure, we need to follow the same algorithm as in Section 5.2. After giving an orientation to the braid in plat form, some of the a_i's and b_i's generators could be in upward going strands. If this is the case, as shown previously, we will twist the piece containing the generators as in Figures 5.19 and 5.23. In this way, the generator will change its sign, and a type d-crossing will appear in the "0"-th column. After performing a S-moves for each of these twists, say k twists in total, we will have:

- any not twisted a_i becomes $\sigma_{2k}\sigma_{2k-1} \dots \sigma_{k+1}\sigma_k^{-1}\sigma_{k-1}^{-1} \dots \sigma_1^{-1} a_i \sigma_1\sigma_2 \dots \sigma_k \sigma_{k+1}^{-1}\sigma_{k+2}^{-1} \dots \sigma_{2k}^{-1}$
- any twisted a_i becomes $a_i^{-1}\sigma_1\sigma_2 \dots \sigma_{k-1}\sigma_{2k}\sigma_{2k-1} \dots \sigma_{k+1}\sigma_k$
- any not twisted b_i becomes $\sigma_{2k}\sigma_{2k-1} \dots \sigma_{k+1}\sigma_k^{-1}\sigma_{k-1}^{-1} \dots \sigma_1^{-1} b_i \sigma_1\sigma_2 \dots \sigma_k \sigma_{k+1}^{-1}\sigma_{k+2}^{-1} \dots \sigma_{2k}^{-1}$
- any twisted b_i becomes $b_i^{-1}\sigma_1\sigma_2 \dots \sigma_{k-1}\sigma_{2k}\sigma_{2k-1} \dots \sigma_{k+1}\sigma_k$

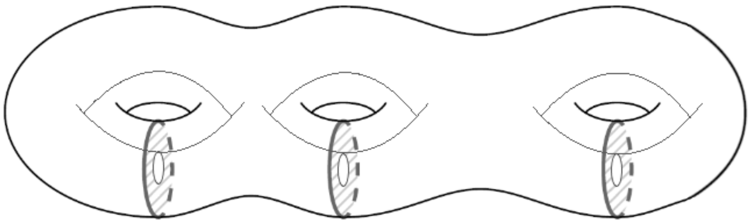

Figure 5.22: An example of thickened Σ_g.

In the same way as before, if we have two S-moves one after the other, without any σ_1 in between, we will have to perform a Reidemeister I move in order to bring the braid into standard position, as shown in Figures 5.24 and 5.20.

In the remaining part of the braid we can apply the algorithm of Theorem 5.1.1. Since all the S-moves are done locally in the cylinder $A \times I$, it is possible to perform the transformation shown in Fig. 5.1 (and also the one depicted in Fig. 5.2), thus obtaining the braid with standard closure from the one with plat closure. Again, note that, since all the substitutions made depend only on the number of σ_i, a_i and b_i generators and on the type of the crossings affected by the S-moves on the same column (i.e. the changed arc was an over or under arc), the computational complexity remains quadratic, but depends on the number of these three types of generators instead.

The previous construction proves the following:

Theorem 5.3.1. *Let Σ_g be a c.c.o. surface of genus g. Given a link L in a tubular neighbourhood $N(\Sigma_g)$ of Σ_g, represented by a braid $B \in \mathcal{B}_{\Sigma_g,2n}$ via plat closure, it is algorithmically possible to generate a braid $\beta \in \mathcal{B}_{\Sigma_g,m}$ which represents, via standard closure, an equivalent link to L. The algorithm has a computational complexity of $O(M^2)$ where M is the number of crossings and a_i and b_i type generators present in the braid B.*

Then, as a corollary, we have proven the Alexander theorem for standard closure of braids:

Corollary 1. Let Σ_g be a genus g surface. Every link $L \subset N(\Sigma_g)$ may be braided to a geometric braid in $\mathcal{B}_{\Sigma_g,n}$, whose standard closure is equivalent to L.

In order to pass from standard closure to plat closure of a braid, we follow the same construction

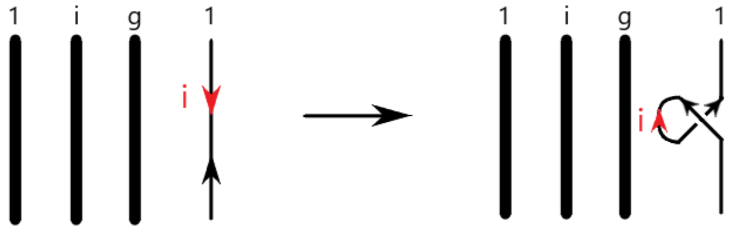

Figure 5.23: Twisting a $b_i^{\pm}$ belonging to an oriented upward strand changes sign and generates a d-type crossing. The black arrow marks the orientation of the strand, while the red one marks the direction of the b_i generator.

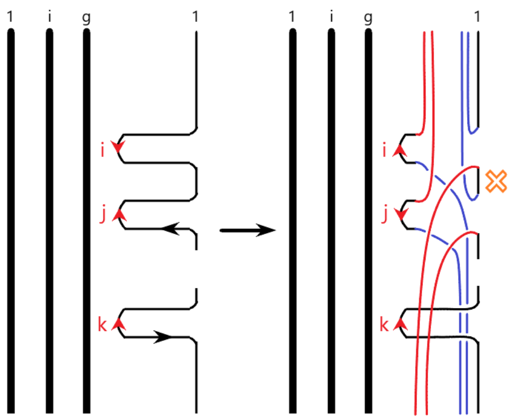

Figure 5.24: The result after all the twists and S-moves performed on the "0"-th column over the b_i generators. Note that the red arrow mark only the direction of the b_i generators.

of Section 5.1.1. Since the moving braid can be considered on the right part of the fixed braid after the parting operation, it is always possible to pass the closure strands past the moving strands without interfering with a_i and b_i generators. The algebraic transformation is still Equation 5.1.

5.4 The C++ Algorithm

In this last section, we describe the algorithm implemented in C++ which realizes the procedures described in the previous sections. The source code can be found on GitHub [1]. The algorithm takes, as input, the word associated to a link described by a braid in plat (resp. standard) closure, then it computes the word associated to an equivalent link represented by a braid via standard (resp. plat) closure.

If the algorithm is asked to compute the plat representation, then it just substitutes each crossing according to Equation 5.1. On the other hand, if the algorithm is asked to compute the standard representation, it gives first an orientation to the plat braid. The pseudo-code implementation is the following:

Algorithm 1 Giving an orientation to the crossings

```
while i ≠ 1 do
    First cycle i ← 1
    for generators ∈ word from left do
        if generator is σ_i or σ_{i−1} then
            i follows the strand
            Add counter to the generator
        end if
    end for
    Change strand once arrived at the bottom closure
    for generators ∈ word from right do
        if generator is σ_i or σ_{i−1} then
            i follows the strand
        end if
    end for
    Change strand once arrived at the top closure
end while
```

The variables are all initialized during the orientation part of the program. Then the main part starts. First of all, if we are not in the case of $\mathbb{R}^3$, we deal with column zero. Every a_i or b_i generator is substituted with the relative word, with respect to its orientation (see Sections 5.2 and 5.3 for details). For every a_i or b_i, we need to check the signs of the other a_i's and b_i's of the same column, in order to compute the right signs for the newly generated σ_i's. For this reason, the computational cost of the algorithm is quadratic in the number of a_i's and b_i's generators.

Then, cycling over every column, the number of type A, B, C and D crossings (see Fig. 5.3) is computed, and their type (over or under crossing) is memorized. Every crossing is then substituted by the appropriate C_a, C_b, C_d or C_d formula, checking for each crossing the signs of the other crossings of the same column, in order to use the right signs for the newly generated σ_i's. For this reason, the computational cost of the algorithm is quadratic in the number of the σ_i generators, too. In this part we also keep track of possible Reidemeister I move necessities. In this eventuality, we will eliminate the extra crossing, obtaining a well-defined braid.

Now, for every odd labeled column the top and bottom part are dealt with, following the rules in Section 5.1.2 and checking which one of the cases depicted in Figures 5.10a, 5.10b, 5.10c, 5.10d and 5.11a, 5.11b, 5.11c, 5.11d occours.

Finally, the algorithm gives as an output the new word associated to the resulting braid, and since every old generator was substituted in some way, the new word pieces are written following the old sequence of generators.

The source files of the program can be found in the GitHub repository at [1].

Bibliography

[1] Repository for computing plat closure from standard closure and vice-versa. `https://github.com/Paolo-Cavicchioli/plat_standard_representation`. C++ source files.

[2] Repository for computing plat slide moves in genus two 3-manifolds. `https://github.com/Paolo-Cavicchioli/6_tuple_representation`. C++ source files.

[3] J.W. Alexander. A lemma on systems of knotted curves. *Proc. Nat. Acad. Sci.*, 9(3):93–95, 1923.

[4] J.W. Alexander. The combinatorial theory of complexes. *Ann. of Math.*, pages 292–320, 1930.

[5] E. Artin. Theory of braids. *Ann. of Math.*, pages 101–126, 1947.

[6] R.P. Bakshi, D. Ibarra, G. Montoya-Vega, J.H. Przytycki, and D. Weeks. On framings of links in 3-manifolds. *Canad. Math. Bull.*, 64(4):752–764, 2021.

[7] P. Bandieri, P. Cristofori, and C. Gagliardi. A census of genus-two 3-manifolds up to 42 coloured tetrahedra. *Discrete Math.*, 310(19):2469–2481, 2010.

[8] C. Bankwitz and H.G. Schumann. Über viergeflechte. In *Abh. Math. Semin. Univ. Hambg.*, volume 10, pages 263–284. Springer, 1934.

[9] P. Bellingeri. On presentations of surface braid groups. *J. Algebra*, 274:543–563, 2004.

[10] P. Bellingeri and A. Cattabriga. Hilden braid groups. *J. Knot Theory Ramifications*, 21(03):1250029, 2012.

[11] S. Bigelow. A homological definition of the Jones polynomial. *Geom. Topol. Monogr*, 4:2941, 2002.

[12] J.S. Birman. Mapping class groups and their relationship to braid groups. *Comm. Pure Appl. Math.*, 22(2):213–238, 1969.

[13] J.S. Birman. On the stable equivalence of plat representations of knots and links. *Canad. J. Math.*, 28(2):264–290, 1976.

[14] M. Boileau, D.J. Collins, and H. Zieschang. Genus 2 Heegaard decompositions of small Seifert manifolds. In *Ann. Inst. Fourier (Grenoble)*, volume 41, pages 1005–1024, 1991.

[15] G. Burde and H. Zieschang. *Knots.* de Gruyter, 2008.

[16] M.R. Casali and L. Grasselli. 2-symmetric crystallizations and 2-fold branched coverings of S^3. *Discrete Math.*, 87(1):9–22, 1991.

[17] A. Cattabriga and B. Gabrovšek. A Markov theorem for generalized plat decomposition. *Ann. Sc. Norm. Super. Pisa Cl. Sci. (5)*, 20(4):1273–1294, 2020.

[18] A. Cattabriga and M. Mulazzani. All strongly-cyclic branched coverings of $(1, 1)$-knots are Dunwoody manifolds. *J. Lond. Math. Soc.*, 70(2), 2004.

[19] A. Cavicchioli, F. Hegenbarth, and A.C. Kim. A geometric study of Sieradski groups. In *Algebra Colloq.*, volume 5, pages 203–217. Institute of Mathematics, Chinese Academy of Sciences, 1998.

[20] J. Cerf. La stratification naturelle des espaces de fonctions différentiables réelles et le théoreme de la pseudo-isotopie. *Publ. Math. Inst. Hautes Études Sci.*, 39:5–173, 1970.

[21] P. Cristofori, M. Mulazzani, and A. Vesnin. Strongly-cyclic branched coverings of knots via $(g, 1)$-decompositions. *Acta Math. Hungar.*, 116(1-2):163–176, 2007.

[22] Ioannis Diamantis. An alternative basis for the kauffman bracket skein module of the solid torus via braids. In *Knots, Low-Dimensional Topology and Applications: Knots in Hellas, International Olympic Academy, Greece, July 2016*, pages 329–345. Springer, 2019.

[23] H. Doll. A generalization of bridge number to links in arbitrary three-manifolds. *Math. Ann.*, 1993.

[24] M.J. Dunwoody. Cyclic presentations and 3-manifolds. In *Proc. Inter. Conf., Groups-Korea*, volume 94, pages 47–55, 1995.

[25] M. Ferri, C. Gagliardi, and L. Grasselli. A graph-theoretical representation of PL-manifolds - a survey on crystallizations. *Aequationes Math.*, 31(1):121–141, 1986.

[26] A.T. Fomenko and S.V. Matveev. *Algorithmic and computer methods for three-manifolds*, volume 425. Springer Science & Business Media, 2013.

[27] C. Gagliardi. Extending the concept of genus to dimension n. *Proc. Amer. Math. Soc.*, 81(3):473–481, 1981.

[28] C. Gagliardi. Regular imbeddings of edge-coloured graphs. *Geom. Dedicata*, 11(4):397–414, 1981.

[29] S. Garnerone, A. Marzuoli, and M. Rasetti. Quantum automata, braid group and link polynomials. *arXiv preprint quant-ph/0601169*, 2006.

[30] S. Garnerone, A. Marzuoli, and M. Rasetti. Quantum geometry and quantum algorithms. *J. Phys. A*, 40(12):3047, 2007.

[31] R.E. Gompf and A.I. Stipsicz. *4-manifolds and Kirby calculus.* Number 20 in Grad. Stud. Math. Amer. Math. Soc., 1999.

[32] L. Grasselli, M. Mulazzani, and R. Nedela. 2-symmetric transformations for 3-manifolds of genus 2. *J. Combin. Theory Ser. B*, 79(2):105–130, 2000.

[33] T. Hahn. International tables for X-ray crystallography. *A. Spacegroup symmetry, Vol. A of International Tables for X-Ray Crystallography, D. Reidel, Berlin*, 1983.

[34] R. Häring-Oldenburg and S. Lambropoulou. Knot theory in handlebodies. *J. Knot Theory Ramifications*, 11(06):921–943, 2002.

[35] P. Heegaard. *Forstudier til en topologisk Teori forde algebraiske Fladers Sammenhæng.* Det Nordiske Forlag, København, 1898.

[36] H. Helling, A.C. Kim, and J.L. Mennicke. A geometric study of Fibonacci groups. *J. Lie Theory*, 8:1–23, 1998.

[37] J. Hempel. *3-Manifolds*, volume 349. J. Amer. Math. Soc., 2004.

[38] H. Hilden. Generators for two groups related to the braid group. *Pacific J. Math.*, 59(2):475–486, 1975.

[39] S.P. Jordan and P. Wocjan. Estimating Jones and HOMFLY polynomials with one clean qubit. *arXiv preprint arXiv:0807.4688*, 2008.

[40] L. Kauffman. From knots to quantum groups (and back). Technical report, Argonne National Lab., IL (USA), 1990.

[41] A.C. Kim, Y. Kim, and A. Vesnin. On a class of cyclically presented groups. In *Proc. Intern. Conf., Groups-Korea*, volume 98, pages 211–220, 2000.

[42] S. Lambropoulou and C.P. Rourke. Markov's theorem in 3-manifolds. *Topology Appl.*, 78(1-2):95–122, 1997.

[43] S. Lambropoulou and C.P. Rourke. Algebraic Markov equivalence for links in three-manifolds. *Compos. Math.*, 142(4):1039–1062, 2006.

[44] W.B.R. Lickorish. A representation of oriented combinatorial 3-manifolds. *Ann. of Math.*, 76(3):531–540, 1962.

[45] A. Markoff. Über die freie äquivalenz der geschlossenen zöpfe. *Sb. Math.*, 1(1):73–78, 1936.

[46] S.V. Matveev. *Algorithmic topology and classification of 3-manifolds*, volume 9. Springer, 2007.

[47] J. Milnor. *Lectures on the h-Cobordism Theorem*, volume 2258. Princeton Univ. Press, 2015.

[48] M. Mulazzani. On periodic Takahashi manifolds. *Tsukuba J. Math.*, 25(2):229–237, 2001.

[49] M. Mulazzani and A. Vesnin. Generalized Takahashi manifolds. *Osaka J. Math.*, 39(3):705–721, 2002.

[50] K. Murasugi and B. Kurpita. *Knot theory and its applications.* Springer, 1996.

[51] M. Pezzana. Sulla struttura topologica delle varieta compatte. *Atti Semin. Mat. Fis. Univ. Modena*, 23(1):269–277, 1974.

[52] V.V. Prasolov and A.B. Sosinski. *Knots, links, braids and 3-manifolds: an introduction to the new invariants in low-dimensional topology*, volume 154. American Mathematical Soc., 1997.

[53] K. Reidemeister. Elementare begründung der knotentheorie. In *Abhandlungen aus dem Mathematischen Seminar der Universität Hamburg*, volume 5, pages 24–32. Springer, 1927.

[54] N. Reshetikhin and V.G. Turaev. Invariants of 3-manifolds via link polynomials and quantum groups. *Invent. Math.*, 103(1):547–597, 1991.

[55] D. Rolfsen. *Knots and links*, volume 346. American Mathematical Soc., 2003.

[56] B. Ruini and F. Spaggiari. On the structure of Takahashi manifolds. *Tsukuba J. Math.*, 22(3):723–739, 1998.

[57] N. Saveliev. Lectures on the topology of 3-manifolds. In *Lectures on the Topology of 3-Manifolds.* de Gruyter, 2011.

[58] M. Scharlemann. Heegaard splittings of compact 3-manifolds. *arXiv preprint math/0007144*, 2000.

[59] A.B. Sossinsky. Preparation theorems for isotopy invariants of links in 3-manifolds. In *Quantum Groups: Proceedings of Workshops held in the Euler International Mathematical Institute, Leningrad, Fall 1990*, pages 354–362. Springer, 2006.

[60] M. Takahashi. On the presentations of the fundamental groups of 3-manifolds. *Tsukuba J. Math.*, 13(1):175–189, 1989.

[61] A.Y. Vesnin and A.C. Kim. Fractional Fibronacci groups and manifolds. *Sib. Math. J.*, 39(4):655–664, 1998.

[62] K.H. Yun. On braid-plat relations in Conway function. *Honam Math. J.*, 33(3):407–418, 2011.